THE EFFECTS OF RANDOM AND RHYTHMIC LOWER LIMB FORCE-TRACKING ON THE HEMODYNAMIC RESPONSE FUNCTION

By PATRICK W. DANS, B.Sc. (HONOURS) PSYCHOLOGY, NEUROSCIENCE, AND BEHAVIOUR

A Thesis Submitted to the School of Graduate Studies in Partial Fulfillment of the Requirements of the Degree Master of Science

McMaster University MASTER OF SCIENCE (2020) Hamilton, Ontario

TITLE: THE EFFECTS OF RANDOM AND RHYTHMIC LOWER LIMB FORCE-TRACKING ON THE HEMODYNAMIC RESPONSE FUNCTION

AUTHOR: Patrick W. Dans, B.Sc. (McMaster University)

SUPERVISOR: Professor Aimee J. Nelson

NUMBER OF PAGES: xi, 127

Abstract

Complexity-modulated tasks elicit differential hemodynamic activations in the primary motor cortex for upper limb motor representations. However, much is yet to be learned regarding lower limb complexity modulation, as most fNIRS complexity modulation studies focus on the upper limb. It is currently unknown whether hemodynamic activations from single-joint lower limb motor tasks are detectable by fNIRS, and further, if fNIRS can detect differences between activations from simple and complex lower limb motor tasks. An fNIRS study was conducted to investigate the effects of an unpredictable, complex force-tracking task vs. a predictable, simple force-tracking task on hemodynamic activations in the TA motor representation. No significant TA motor cortex activations were found for 4/5 participants, with one participant showing a significant activation in one channel. Lack of activation in the TA motor representation was attributed to the depth of the area within the central sulcus. Significant hemodynamic activations were also found in areas assumed to overly STG/SII, and pre-SMA/SMA. These activations were attributed to sensory integration and motor learning, respectively. An fNIRS processing review was also conducted to inform processing decisions in the first experiment and to further fNIRS usage in our lab. Common techniques were identified as low-pass, band-pass, and high-pass filters, smoothing filters, wavelet filters, and the GLM. More appropriate alternative techniques were provided, including short-separation regression, pre-whitening, and spline interpolation with a Savitsky-Golay filter. Future studies may elucidate the lack of activity in the TA motor representation, and will further basic neuroscience regarding fNIRS.

Acknowledgements

I would foremost like to thank my supervisor, Dr. Aimee J. Nelson, for all of her encouragement and feedback through this experience. The advice and help that she provided has pushed me to become a better student. I know that the skills and experience I have acquired through this program will be of great help on my career path. Thank you Aimee, I am very grateful for the opportunity that you gave me.

I would also like to thank my committee, comprised of Dr. Michael Carter and Dr. Audrey Hicks, for their guidance on my thesis project. Your constructive feedback has helped me to do better science.

I am thankful for my colleagues, who offered not only incredible help with data collection and thesis edits, but also friendship that helped make this experience special. I would especially like to thank my undergraduate mentee Tarra D'hoine for her amazing help with data collections. This would not have been possible without her commitment and continuous dedication.

I would like to thank my parents, Raymond and Corina, for their endless support and encouragement through the more difficult points of this experience. Thank you for all of the hugs and delicious meals to keep me going. Your good natures constantly remind me of what I strive to be.

Finally, I would like to thank my friends and girlfriend for their companionship through this experience. They helped me realize that rest and fun can be just as important as work for mental health. Thank you to Tara, Laura, Ashley, Andrew, Ryan, Matt, and Natalie for keeping me sane.

Table of Contents

List of Tables/Figures/Equations

Experiment 1

FNIRS Processing Review

List of Abbreviations

BB – Biceps Brachii

BCP – Bilateral Cerebral Palsy

CAR – Common Average Referencing

CBF – Cerebral Blood Flow

CBSI – Correlation-based Signal Improvement

CBV – Cerebral Blood Volume

CSF – Cerebrospinal Fluid

CWT – Continuous Wavelet Transform

DPF – Differential Pathlength Factor

DWT – Discrete Wavelet Transform

Fe^{2+} – Ferrous Iron

Fe^{3+} – Ferric Iron

FFT – Fast Fourier Transform

FIR – Finite Impulse Response

fMRI – Functional Magnetic Resonance Imaging

fNIRS – Functional Near-Infrared Spectroscopy

GLM – General Linear Model

HbO – Oxygenated Hemoglobin

HbR – Deoxygenated Hemoglobin

HRF – Hemodynamic Response Function

ICA – Independent Component Analysis

IIR – Infinite Impulse Response

M1 – Primary Motor Cortex

MDL – Minimum Description Length

MVF – Maximum Voluntary Force

NIR – Near-infrared

NM – Non-musicians

PCA – Principal Component Analysis

pCG – Precentral Gyrus

PMC – Premotor Cortex

PP – Piano players

PR – Pursuit Rotor

preSMA – Presupplementary Motor Area

RH – Real Hand

RMSE – Root Mean Squared Error

ROI – Region of Interest

SCI – Spinal Cord Injury

SII – Secondary Somatosensory Cortex

SMA – Supplementary Motor Area

SMC – Somatomotor Cortex

SNR – Signal-to-Noise Ratio

SPL – Superior Parietal Lobule

STG – Superior Temporal Gyrus

TA – Tibialis Anterior

TD – Typical Development

TMS – Transcranial Magnetic Stimulation

UCP – Unilateral Cerebral Palsy

VH – Virtual Hand

Chapter 1: Review of the Literature

1.1 History of fNIRS

Functional Near-Infrared Spectroscopy (fNIRS) is a relatively new neuroimaging technique that was discovered by Jobsis (1977), based on the optical method developed by Glenn Millikan in the 1940s (Millikan 1942). Jobsis worked under Britton Chance from 1962 to 1964 at the University of Pennsylvania (Ferrari and Quaresima 2012). After moving on to Duke University in North Carolina (United States), Jobsis was interested in cytochrome-C-oxidase, to further understand the mitochondrial respiratory chain utilizing optical methods (Piantadosi 2007). Instead, Jobsis accidentally discovered that the high transparency of brain tissue in the near-infrared (NIR) range of light allowed for non-invasive detection of hemoglobin oxygenation (Jobsis 1977). This discovery sparked new research into optical methods, and marked the start of the fNIRS field of research.

It was not until 1993 that the first fNIRS studies on human adults were published using single-channel systems with low temporal resolution and poor sensitivity (Chance et al., 1993; Hoshi and Tamura 1993; Kato et al., 1993; Villringer et al., 1994). These first studies were focused on measuring fNIRS signals in the prefrontal and occipital lobes during cognitive and visual task performance, respectively. FNIRS seemed to be promising, however it still required validation. To this end, Kleinschmidt et al. (1996) sought to validate fNIRS utilizing Functional Magnetic Resonance Imaging (fMRI), the better-known technique at the time. Researchers simultaneously measured deoxy-hemoglobin levels using fMRI and fNIRS during a unilateral finger opposition task. They discovered that fNIRS measurements of deoxy-hemoglobin spatially matched the fMRI measurements for activation (Kleinschmidt et al., 1996).

Until this point in time, fNIRS systems were strictly single channel, and thus a combination of different systems was required to use more than one channel for measurement.

However, in 1994 commercially-available multi-channel systems were developed, allowing for multiple fNIRS measurements utilizing a single system (Watanabe et al., 1994). This development allowed for cortical mapping of hemodynamic responses using fNIRS (Ferrari and Quaresima 2012). The first study utilizing the 10 channel Hitachi system was Maki et al. (1995), where fNIRS channel coordinates were compared with MRI data to successfully map fNIRS activity on the cortex for the first time.

1.2 Principles of fNIRS

1.2.1 Basic Principles

FNIRS is a neuroimaging modality that uses light to measure brain activity in real time. This procedure is non-invasive, portable, relatively inexpensive, and can disentangle oxygen consumption and blood flow changes without acquiring blood flow images like in fMRI (Davis et al., 1998; Hoge et al., 1999). As such, it has gained the interest of many researchers for usage during motor and cognitive tasks in a variety of populations (Ferrari and Quaresima 2012). FNIRS utilizes the NIR light range (~700-1000 nm) to exploit the relative transparency of biological tissues (Irani et al., 2007) and indirectly measure concentration changes of oxy- (HbO) and deoxy-hemoglobin (HbR) species through neurovascular coupling.

Neurovascular coupling describes the idea that regional blood flow in the brain is directly related to the firing of neurons within the region (Girouard and Iadecola 2006). Neurons acquire glucose and oxygen in the form of HbO from nearby capillary beds to function (Irani et al., 2007). As such, neuronal firing stimulates the brain to increase local cerebral blood flow (CBF) and cerebral blood volume (CBV). The area is then oversupplied with glucose and oxygen from

the increased CBF, utilizing HbO to do so (Fox et al., 1988). When the neurons stop firing, they stop consuming oxygen, and the flow of HbO to the area is reduced to a baseline level. This pattern of activity is known as the hemodynamic response function (HRF), and has a characteristic shape (see **Figure 1**). Of the two types of hemoglobin, HbO peaks ~5-10 s after stimulation begins (Leff et al., 2011), and remains elevated for the duration of the stimulation period. For HbR, the time to the lowest trough is more variable than that for HbO, and the response may not reach this point until ~15 seconds have passed (Leff et al., 2011). Usually ~12-18 seconds after the stimulation period, the hemodynamic response has settled to baseline values (Santosa et al., 2018).

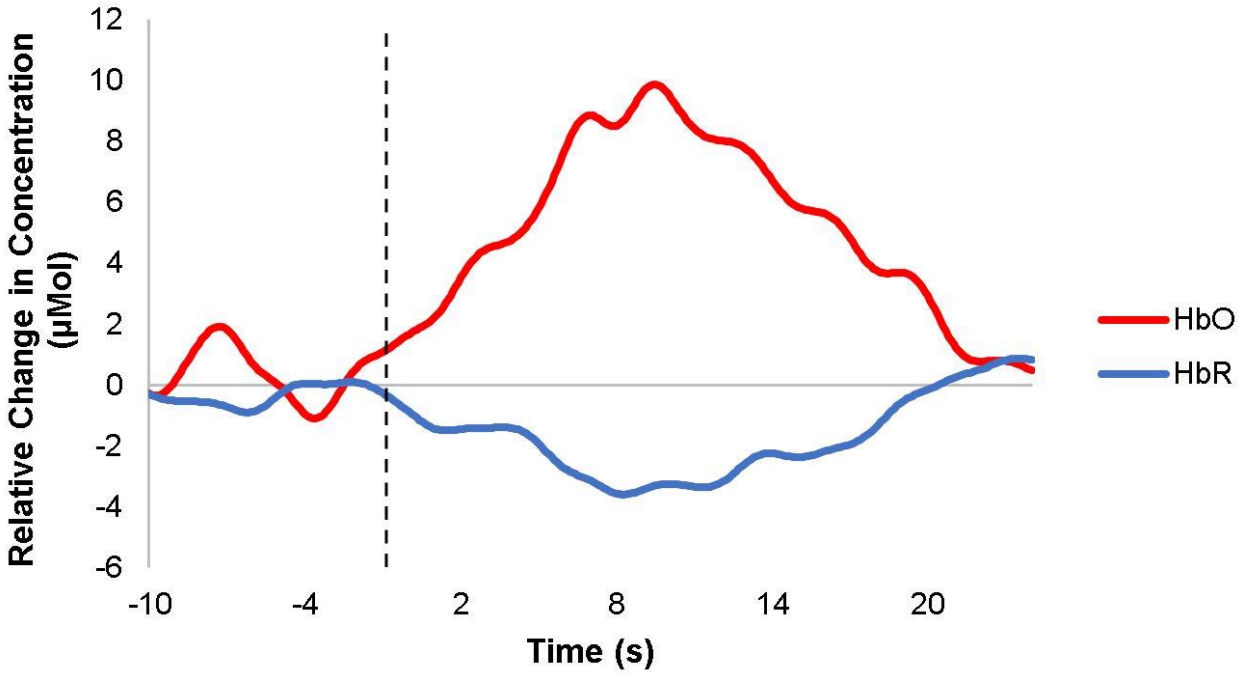

Figure 1: A characteristic hemodynamic response function (HRF). Oxygenated hemoglobin (HbO) is represented by the red line, whereas deoxygenated hemoglobin (HbR) is represented by the blue line. The x-axis is time in seconds, and the y-axis is the relative change in concentration in micromolar. The stimulus producing this response was 10 seconds long, beginning at the zero second mark, indicated by the dashed black line. HbO is observed to peak at ~6-7 seconds, and HbR at ~8-9 seconds. Adapted from Ferrari and Quaresima (2012).

Throughout this time, NIR light is projected through extracerebral tissues (scalp, skull, Cerebrospinal Fluid [CSF]). The light is absorbed, scattered, and reflected along its banana-shaped path (Gratton et al., 1994), and finally exits the head to be detected (see **Figure 2**). Depending on the source-detector separation, NIR light can reach a depth of ~5-8 mm in the cortex (Huppert 2016). Increasing the source-detector distance on the surface of the scalp leads to deeper penetration of light into the brain (Villringer et al., 1993; McCormick et al., 1992). However, the caveat from this is that light intensity decreases beyond detectability after the source-detector distance increases above 5.5-6 cm (Gratton et al., 2006). Detectors become sensitive to hemodynamic activity when source-detector distances are 4 cm or less, and stay sensitive down to ~2 cm (Irani et al., 2007). Due to the nature of fNIRS, the chance for absorption in superficial layers of the head is higher because the light passes through these layers twice – once projecting into the head, and once coming out. This back-reflection geometry makes fNIRS much more sensitive to superficial signals (Gagnon et al., 2011).

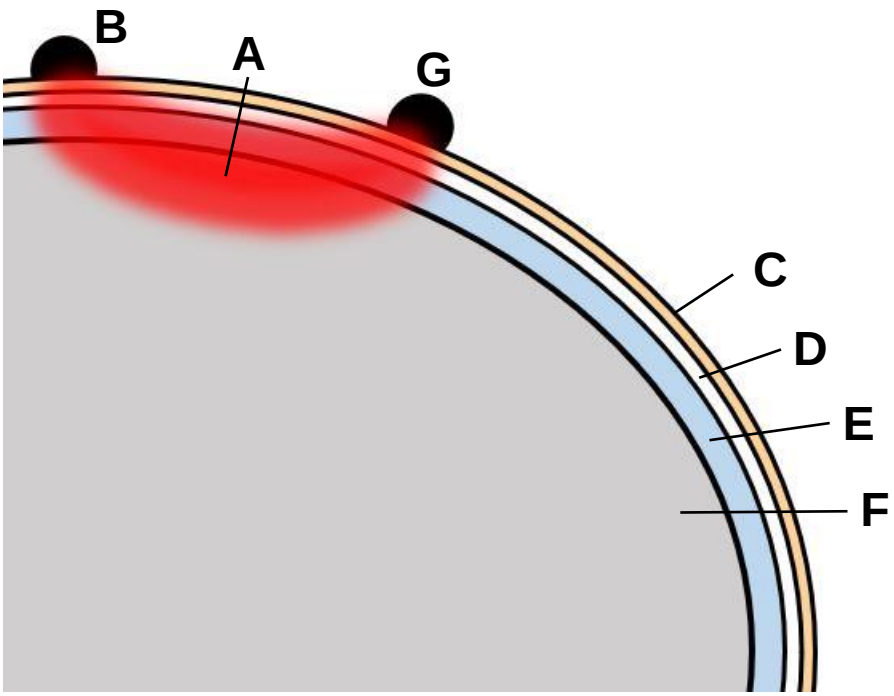

Figure 2: Adapted from Gratton et al. (1994). NIR light is projected along a banana-shaped path (**A**) from the light source (**B**) through scalp (**C**), skull (**D**), cerebrospinal fluid (**E**), and into the cortex (**F**), and is absorbed, scattered, and reflected back out of the head to the detector (**G**).

If the light reaches the cortex, hemoglobin molecules present in the capillaries supplying the neurons of the cortex absorb it. The more hemoglobin molecules that are present in the area at that time, the greater the amount of light that is absorbed, and thus the less light that proceeds to detectors on the surface of the head. The ratio between the projected and detected light is then used to calculate attenuation of light (see **Equation 1**, Delpy et al., 1988). In this equation, the attenuation of light intensity is equal to the negative logarithm of the detected light (I) divided by the projected light (I_0).

$$Attenuation = -\log\left(\frac{I}{I_0}\right) \quad (1)$$

This ratio is equal to the differential pathlength factor (DPF) multiplied by the absorption coefficient for the light (μ_a) and the source-detector distance (d) plus the unknown source-detector geometry coefficient (G, see **Equation 2a**). This law is known as the Modified Beer-Lambert Law, and is the basis for fNIRS (Delpy et al., 1988).

$$Attenuation = -\log\left(\frac{I}{I_0}\right) = DPF\mu_a d + G \quad (2a)$$

The DPF is a coefficient used to correct for the different paths of light due to scatter from biological tissues (Strangman et al., 2003). This coefficient is dependent on wavelength and can be measured with frequency-dependent or time-dependent fNIRS systems. The geometry coefficient represents the loss of light due to scattering (Matcher and Cooper 1994), the amount of which cannot be measured in the most commonly-used continuous-wave fNIRS systems (Ferrari and Quaresima 2012). However, light scatter can be assumed to be constant in the

system, in which case changes in light attenuation are attributed to changes in absorption by hemoglobin species (Pinti et al., 2020). As such, the determination of *absolute* concentration changes in the tissue cannot be made in these systems, as the system cannot parse attenuation due to scatter and absorption separately. Instead, only *relative* concentration changes are able to be determined with these systems.

The absorption coefficient (μ_a) from equation 2a can be expanded, where it is equal to the molar extinction coefficients of HbO and HbR at a particular wavelength (λ) multiplied by their respective changes in concentration ($\Delta[HbO]$ and $\Delta[HbR]$) in the tissue (see **Equation 2b**).

$$= \left[\varepsilon_{HbO}(\lambda)\Delta[HbO] + \varepsilon_{HbR}(\lambda)\Delta[HbR]\right]DPFd \quad (2b)$$

1.2.2 Absorption

Absorption of light is largely dependent upon the inherent physical characteristics of the molecule it is projected on, as well as the wavelength of the light being projected (Jobsis 1977). In the case of fNIRS, the molecular characteristics of hemoglobin, both in oxygenated and deoxygenated forms, determine NIR light absorption. The hemoglobin molecule has four heme groups, each containing porphyrin rings (Perutz 1978; Anson and Mirsky 1930; see **Figure 3A**). The porphyrin rings each contain one ferric iron ion (Fe3+) when not bound to oxygen (see **Figure 3B**). When the ferric iron ion binds to oxygen, it becomes ferrous iron (Fe2+) and is pulled into the plane of the porphyrin ring by oxygen (see **Figure 3C**).

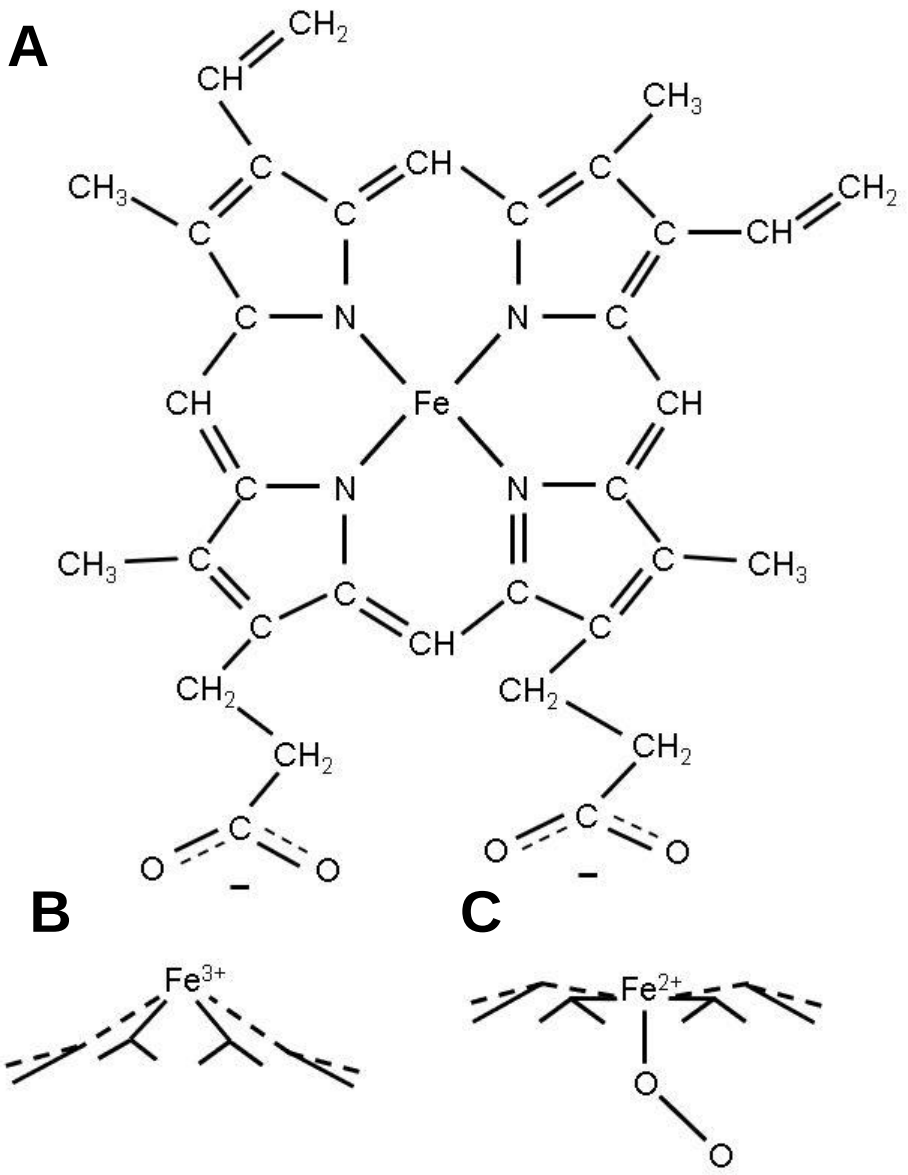

Figure 3: Adapted from Perutz (1978). Figure depicting the chemical composition of the heme group in the hemoglobin molecule. **A**. Top view. A solid black line depicts a single bond, whereas two black lines depicts a double bond. A dashed black line depicts a bond projecting away from the viewer. An iron ion is kept in the middle of the heme group by four nitrogen ions of the porphyrin. **B**. Side view. Connections to ions from the porphyrin ring are depicted by solid black lines. Dashed black lines depict connections projected away from the viewer. The ferric iron ion (Fe^{3+}) is pulled by connection to histidine (not shown) which makes the porphyrin domed. **C**. Side view. Connections to ions from the porphyrin ring are depicted by solid black lines. Dashed black lines depict connections projected away from the viewer. Ferric iron gains an electron from binding to oxygen (O) and becomes ferrous iron (Fe^{2+}). The binding of oxygen to the iron ion pulls it into the plane of the porphyrin.

The shape of the hemoglobin molecule is thus altered by the binding of oxygen, and with it, the absorption characteristics of the molecule. For example, at lower wavelengths of light HbR absorbs a relatively high proportion of light compared to HbO (see **Figure 4**). However, when wavelength increases, HbO absorbs more light in comparison to HbR (Jobsis 1977). Therefore, changes in the concentrations of both molecules can be obtained using two different wavelengths of light.

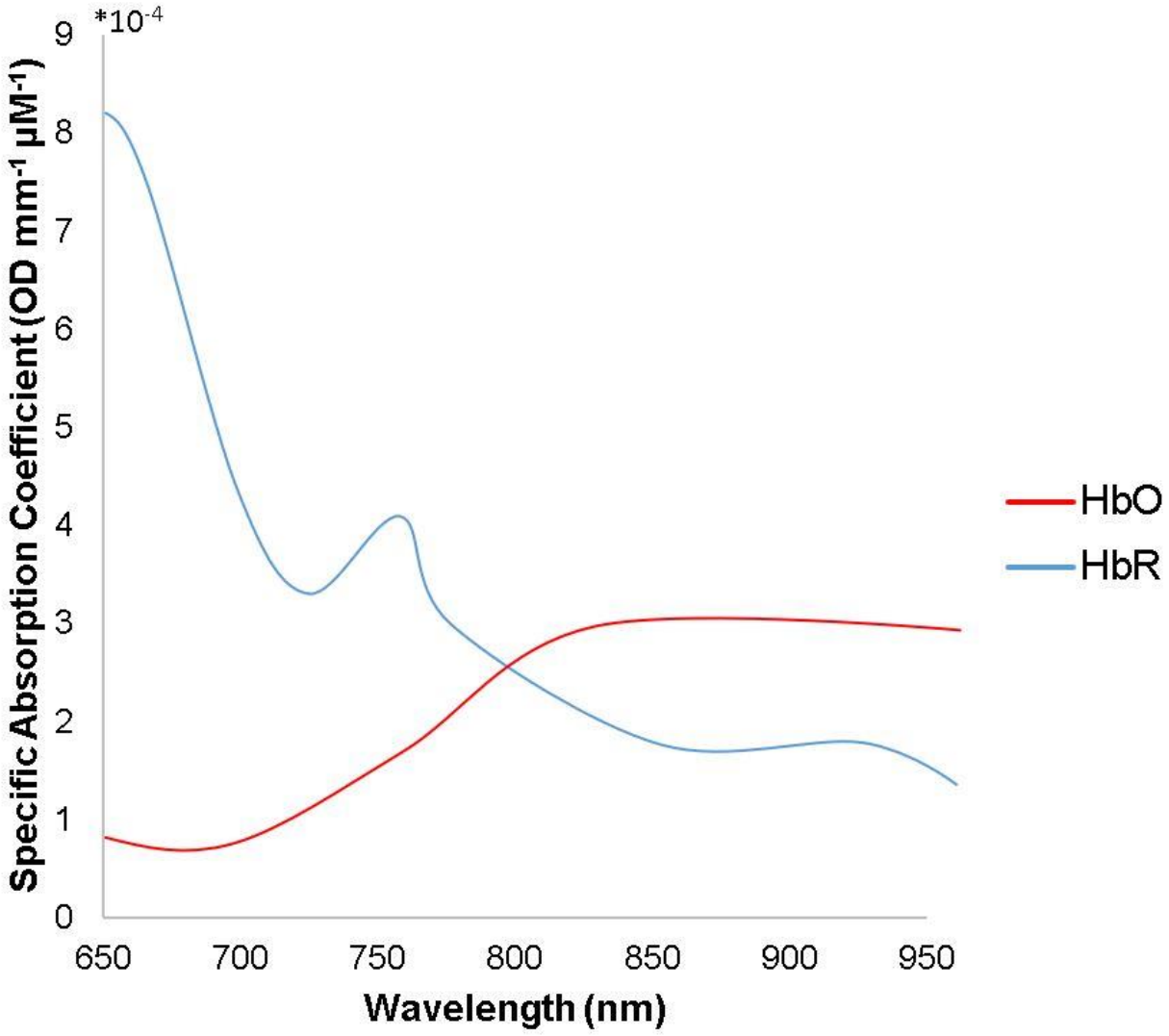

Figure 4: A figure depicting the absorption coefficients for both oxygenated (HbO) and deoxygenated (HbR) hemoglobin species as a function of wavelength. HbO is represented by the

red line, and HbR is represented by the blue line. Generally, as wavelength increases, HbO starts to absorb more light, when at 800 nm it surpasses HbR. Adapted from Irani et al. (2007).

1.2.3 Scattering

NIR light is not only absorbed in biological tissues, but is also highly scattered (Strangman et al., 2003). Light scattering is 100 times more frequent than light absorption and is another factor besides absorption that leads to light attenuation (Delpy and Cope 1997). The main causes of scattering in the head are collagen, keratin, melanin, and lipids located in skin, blood vessels, and soft tissues of the individual (Veesa and Dehghani 2019). Different types of light scatter exist depending on the size difference between the wavelength of light projected and the size of the scattering particle. For example, Mie scattering occurs with light scattered by any size sphere comparable to or larger than the wavelength of light, whereas Rayleigh scattering occurs with particles much smaller than the wavelength of light (Jacques 2013). This scatter affects the pathlength of photons. As a photon is scattered more throughout the tissue, its pathlength increases, and the probability that it will be absorbed increases as well (Pinti et al., 2020). The more scatter, the longer the pathlength, and the more chances for photon absorption. However, due to scatter contributing to light attenuation, many commercially-available fNIRS systems are unable to resolve absolute concentrations of hemoglobin. As such, scatter in these systems is often assumed to be constant, so relative changes in hemoglobin concentrations are obtained instead (Pinti et al., 2020). Scatter is also wavelength-dependent. As the wavelength of light increases, scatter decreases, and vice versa (Jobsis 1977). This fact means that scatter occurs more for HbR than HbO, as HbR is measured at lower wavelengths than HbO. Greater amount of scatter for HbR thus means that less light can be absorbed, the effects of which is seen

in the overall lower signal changes and signal-to-noise ratio (SNR) of HbR when compared to HbO (Cui et al., 2011; Pinti et al., 2020).

1.3 Simple and Complex Motor Tasks in fNIRS

Most fNIRS motor research has focused on responses to upper limb motor tasks, which have been found to elicit robust and reliable hemodynamic responses in primary motor cortex (M1; Plichta et al., 2006, 2007; Sato et al., 2006a; Strangman et al., 2002, 2003, 2006). Specifically, many groups have investigated hemodynamic responses to finger tapping tasks (Chiang et al., 2007; Holper et al., 2009; Kuboyama et al., 2004, 2005; Sato et al., 2006a), and finger opposition tasks (Colier et al., 1997; Franceschini et al., 2003). All of these studies found significant increases in HbO and significant decreases in HbR in channels overlying M1 in response to either simple finger tapping or finger opposition tasks. This research shows that fNIRS can detect hemodynamic responses in the motor cortex from simple motor tasks.

Simple motor tasks, however, can be altered in frequency, intensity, or complexity to modulate the hemodynamic response (Leff et al., 2011). Intensity and frequency-modulated tasks have been explored using fNIRS, but mostly in the upper limb (Leff et al., 2011). Studies involving frequency-modulated tasks have found that movements performed at higher frequencies led to greater increases in HbO concentrations in the primary motor cortex (Obrig et al., 1996; Kuboyama et al., 2004, 2005). Similarly, studies involving intensity-modulated tasks have found that higher-effort movements led to greater motor cortex activation (Kuboyama et al., 2004; Rasmussen et al., 2007; Horovitz and Gore 2003). Complex motor tasks are described as being more difficult than simple tasks (Holper et al., 2009). However, what defines increasing

difficulty of a task is more ambiguous. For example, the number of muscles used to perform a motor task does not necessarily determine the level of difficulty of the task (Verstynen et al., 2005).

Complexity in motor tasks strongly affects the level of activation in bilateral primary motor cortices (M1), and changes patterns of activation in the interconnected cortical areas responsible for planning and correction of movements, and motor learning. Hatakenaka et al. (2007) found that a complex pursuit rotor (PR) task led to significant increases in HbO and significant decreases in HbR in the presupplementary motor, supplementary motor, and primary motor areas (preSMA, SMA, and M1, respectively). This response shifted from preSMA to SMA as participants gained proficiency in the task (Hatakenaka et al., 2007), suggesting that preSMA may be more involved in early stages of motor learning, whereas SMA may be more involved in the later stages. Overall, this study showed that complex motor tasks could elicit cortical hemodynamic activations. Similarly, Holper et al. (2009) investigated the differences between simple and complex upper limb motor tasks. Complex finger tapping in both dominant and non-dominant hands produced significantly larger HbO responses in the contralateral hemisphere to the hand when compared to simple finger tapping (Holper et al., 2009). In summary, not only can fNIRS detect hemodynamic activity from complex motor tasks, these tasks also differ in their activations when compared to simple motor tasks.

However, all of this research involves upper limb tasks. Many lower limb tasks in fNIRS involve walking (de Lima-Pardini et al., 2017; Groff et al., 2019; Herold et al., 2019; Huppert et al., 2013; Jin et al., 2018) or cycling (Asahara and Matsukawa 2018; Asahara et al., 2018; Chacaroun et al., 2019; Lin et al., 2012). However, not many lower limb fNIRS studies include single-joint tasks. As many lower limb tasks involve multiple joints (i.e. walking and cycling),

the information gleaned from these tasks may not translate fully to single-joint tasks. Further, there is a paucity of research involving complexity modulation in lower limb tasks provoking a number of questions. Specifically, can fNIRS detect hemodynamic activations induced by single-joint lower limb tasks in the motor cortices? Further, do these hemodynamic activations differ between simple and complex versions of a lower limb task? This thesis will attempt to address these questions, the answers to which are important for basic neuroscience and the usage of fNIRS for lower limb research.

Chapter 2: Experiment 1 - The Effects of Random and Rhythmic Lower Limb Force-Tracking on the Hemodynamic Response Function

2.1 Introduction

Motor task complexity relates to the difficulty of a motor task (Holper et al., 2009). For example, a finger tapping task in which many fingers are tapped in a specific sequence may be considered more complex than tapping a single digit (Holper et al., 2009). In fMRI work, complex movements differ from simple movements by introducing greater activation globally, while reducing laterality (Rao et al., 1993, Solodkin et al., 2001). However, the study of human movement via fMRI is challenging due to the sensitivity of fMRI to motion artifacts, and the confinement of the machine that limits the performance of large movements such as walking or cycling. Hence, motor tasks in the lower limb such as walking or cycling are not feasible to study using fMRI. Additionally, fMRI is also expensive in comparison to other imaging methods such as fNIRS (Ferrari and Quaresima 2012). To study motor task complexity while overcoming some of the limitations of fMRI, fNIRS could be used instead. Generally, fNIRS is an attractive option for studying complexity modulation as the areas involved in motor actions are considered to be "optically friendly", meaning that NIR light can easily reach the majority of these areas (Leff et al., 2011). However, the degree to which the motor cortex can be measured may depend on the particular muscle group of interest. Further, fNIRS is more resistant to motion artifacts than other neuroimaging modalities (Pinti et al., 2019).

The hemodynamic response recorded by fNIRS can be modulated by the frequency, intensity, or complexity of a motor task (Leff et al., 2011). For example, Holper et al. (2009) investigated the effects of a complex finger tapping task and observed greater changes in M1 oxy-hemoglobin levels when compared to a simple finger opposition task. Additionally, task complexity does not depend on the number of required muscles to induce this greater activation (Verstynen et al., 2005), at least in the upper limb. In this study, fMRI activation differences

presented in the motor cortex between the simple, repetitive finger tapping, and the more complex finger tapping sequences. The complex finger tapping sequences elicited greater M1 activation than simple finger tapping regardless of the number of fingers used in this experiment (Verstynen et al., 2005).

There are different ways of altering task complexity, one of which is the predictability of the motor sequence (Dassonville et al., 1998). Dassonville et al. (1998) showed that their unpredictable finger-tapping task, which was considered to be complex, increased hemodynamic activations in specific areas of the cortex such as the premotor cortex (PMC), superior parietal lobule (SPL), and the SMA. The predictable and unpredictable tasks, however, did not show differential activations in the somatomotor cortex (SMC, Dassonville et al., 1998). In contrast, more recent fNIRS studies have shown differential increases in SMC activity between complex and simple tasks (Holper et al., 2009; Koenraadt et al., 2013). For example, an fNIRS study by Koenraadt et al. (2013) reported significantly higher activations in the SMC for an unpredictable mixed-frequency finger tapping task compared to a predictable single frequency finger tapping task. Further, Holper et al. (2009) showed increased SMC activations for a complex sequenced finger tapping task compared to a simple single-digit tapping task. The discrepancy between studies could be due to a multitude of different reasons. First, the predictability and complexity differences between the finger tapping tasks in Dassonville et al. (1998) may not have been large enough to elicit differential activations between the tasks. Second, the study by Koenraadt et al. (2013) used changes in frequency to make the task unpredictable, which may have been relying on the differential activations usually found in the SMC with changes in frequency (i.e. the "rate effect", Rao et al., 1996), instead of changes in complexity *per se* (Kuboyama et al., 2004, 2005; Obrig et al., 1996). Thus, the rate effect could be the driving factor for the increase in HbO

during the mixed-frequency task. However, the mixed-frequency task (combination of 0.4, 0.8, and 1.4 Hz) induced significantly greater HbO activations than the high frequency task (1.4 Hz), suggesting that the rate effect is not driving the differences (Koenraadt et al., 2013). From these results, it seems that altering the predictability of the motor stimulus may change the complexity of the task.

FNIRS can also be used to measure cortical hemodynamic activity from lower limb motor tasks such as walking and cycling. For example, Kurz et al. (2012) investigated the differences in cortical activity between forward and backward walking tasks with fNIRS. The authors observed greater activity in the SMA, precentral gyrus (pCG), and SPL for the backward walking task than the forward walking task (Kurz et al., 2012). They suggested that the backward walking task could have induced greater activation because it is not a task practiced in daily life for most individuals. Further, they suggest that the absence of peripheral visual stimuli in backward walking makes accurate foot placement more difficult (Kurz et al., 2012). This study was limited in that participants were required to hold on to bars on the sides of the treadmill the entire time they were walking. The data could thus be confounded by providing motor stimuli extraneous to the walking task (i.e. holding onto the bars). Due to the poor spatial resolution of fNIRS (~2-3 cm, Pinti et al., 2020), this extraneous motor stimulus and the associated activity within its representation in the motor cortex could be partially driving the activity in the pCG. Additionally, many muscles are used in the process of walking. Future research could investigate activations from single-muscle complex movements to see if the idea posed by Verstynen (2005) holds true in the lower limb as well.

Beyond the aforementioned study, there is a paucity of research in fNIRS involving lower limb complexity modulation. In general, lower limb fNIRS studies usually focus on walking or

cycling tasks. These studies have reported cortical hemodynamic activity in the prefrontal cortex (Asahara and Matsukawa, 2018; Asahara et al., 2018; Beurskens et al., 2014; Huppert et al., 2013), the premotor cortex (Herold et al., 2019; Lin et al., 2012, 2016), the SMA (Herold et al., 2019; Kurz et al., 2012; Kim et al., 2017; Lin et al., 2012, 2016), the SMC (Kurz et al., 2012; Koenraadt et al., 2012, 2014; Kim et al., 2017; Lin et al., 2012, 2016), and the SPL (Kurz et al., 2012).

The goal of the present study was to investigate the effects of a complexity-modulated lower limb force-tracking task on the amplitude of the hemodynamic response function. In the present study, movement complexity was examined by comparing a complex, unpredictable force-tracking task with a simpler, predictable force-tracking task. For the present study, activity was hypothesized to occur in the medial SMC where the tibialis anterior (TA) motor representation exists. Further, it was of interest to see what other brain areas may be responsive to the motor task. I hypothesized that the force tracking task employing an unpredictable, complex waveform (“Random”) would be more difficult than a task with a predictable, simple waveform (“Rhythmic”) and would thus induce a larger HbO amplitude in the TA representation of M1 in comparison (Holper et al., 2009).

2.2 Methods

2.2.1 Participants

Five healthy participants between the ages of 18-35 years were recruited for this study. To determine the sample size, an *a priori* power analysis to find a moderate effect size was computed with G*Power. The analysis indicated that a minimum of 33 participants were required to reach partial eta-squared of 0.061 for an alpha of 0.05 and power of 0.80. Group-level statistical analyses were not completed for this dataset.

2.2.2 Inclusion/Exclusion Criteria

Participants had no previous or current neurological or psychiatric illnesses. Participants were right-hand dominant as assessed by the Edinburgh Handedness Inventory (Oldfield, 1971), and right-foot dominant as assessed by the Waterloo Footedness Questionnaire (van Melick, Meddeler, Hoogeboom, Nijhuis-van der Sanden, & van Cingel, 2017). They did not possess any musculoskeletal upper and lower limb impairments, or self-reported colour deficiencies, including colourblindness. All participants possessed normal or corrected-to-normal vision.

2.2.3 Apparatus

A visual diagram of experimental setup is shown in **Figure 5**. Participants were seated in an adjustable custom-designed chair with their hands on their lap. Their right foot was positioned in an apparatus that attempted to isolate TA muscle activation and positioned their right knee at a 120-degree angle as measured by a goniometer at the beginning of the experiment. Their left foot

rested on a platform next to the apparatus. The participant's right calf was secured to a slanted platform with foam padding which ensured minimal movement of the leg during the dorsiflexion contraction. The participant's right foot was secured to a floor plate with Velcro straps included in the apparatus. Participants were asked to remove their right shoe to allow for a better fit on the floorplate.

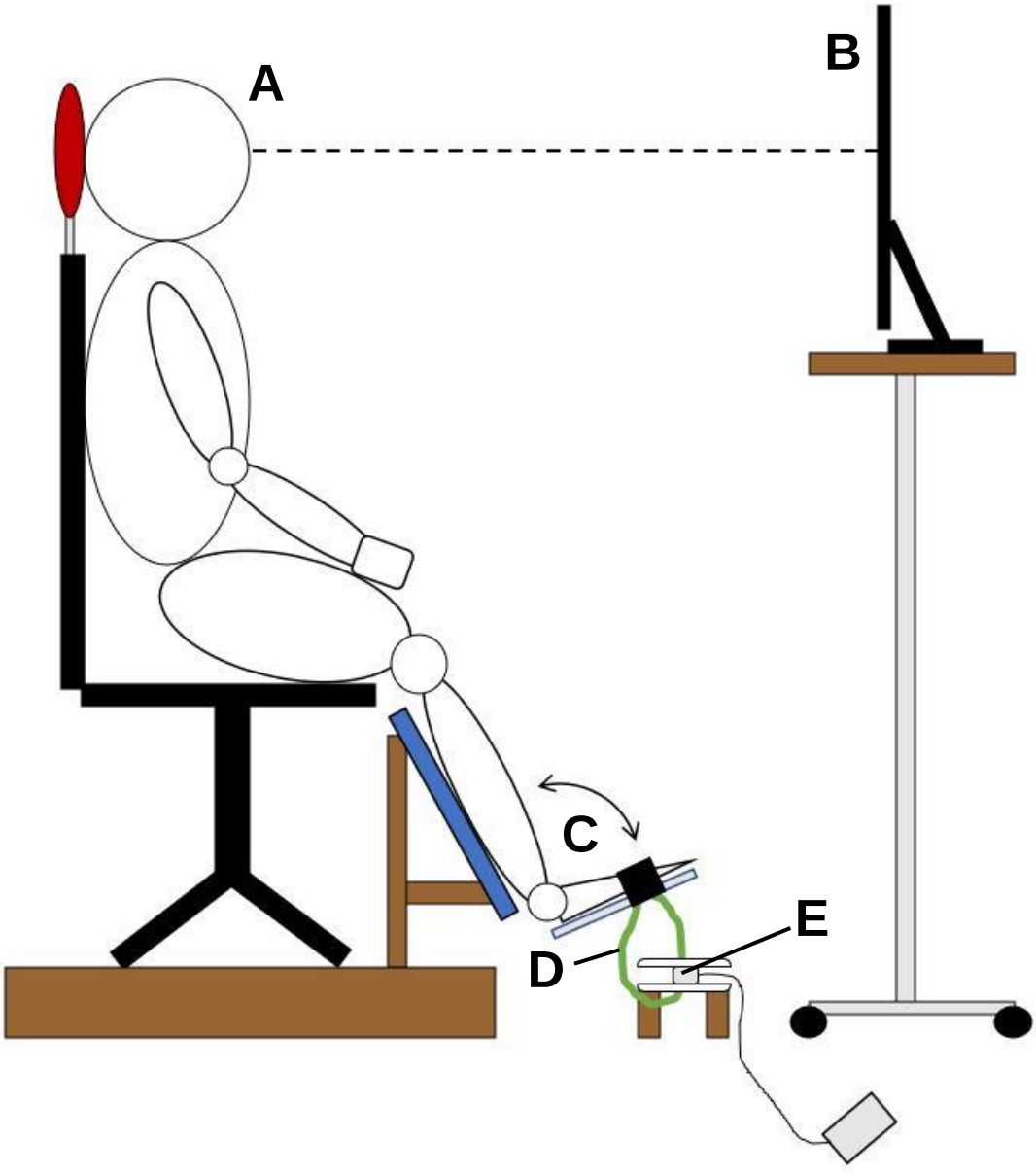

Figure 5: Diagram of experimental setup. A participant is seated (**A**) facing a computer monitor (**B**) and dorsiflexes their right ankle (**C**) to correspond to waveforms depicted on the monitor. The resistance band stretches (**D**) and pulls the 3D-printed casing, which in turn exerts a force on the force transducer (**E**).

A resistance band was secured to the underside of the distal area of the floor plate (see **Figure 6**) to allow for a dorsiflexion contraction. The attending graduate researchers verbally checked with the participant to ensure that the Velcro straps were secure but comfortable. A force transducer was positioned underneath the floorplate to assess the amount of force that the participant produced during the experiment. This force transducer was placed in a custom 3D-printed plastic casing to allow for force translation from the resistance band to the force transducer. This plastic casing consists of two halves: one to hold the force transducer, and the other to apply the load. The lower half of the plastic casing was secured to wooden posts screwed into the apparatus platform, and held the force transducer. This half could translate up and down the unthreaded portions of the screws (see **Figure 7**). The upper half of the casing was secured to the tops of the screws with epoxy resin. When the participant would dorsiflex their right ankle, this would stretch the resistance band. The resistance band, when stretched, applies a load to the lower half of the plastic casing holding the force transducer, pulling this half upwards along the axis of the screws. When the force transducer contacts and is pressed into the upper half of the casing, a load is applied to the force transducer. As the participant pulls harder, more force is applied to the force transducer. Conversely, as the participant relaxes, the force applied to the transducer is lessened in tandem. This device was used to execute the “Random” and “Rhythmic” force tracking tasks. Participants sat facing a computer monitor (Dell 1920x1080 pixel resolution 24”, model G2410) with a screen dimension of 30 x 53 cm. The vertical center of the monitor was aligned with the participant’s mid-line, and the height was adjusted to the

comfort of the participant. The protocol for the force-tracking tasks was implemented and controlled by National Instruments LabVIEW (2017, 32-bit) Software. This software also recorded and saved the force-tracking amplitudes for each trial on a secure computer to assess in later data analysis.

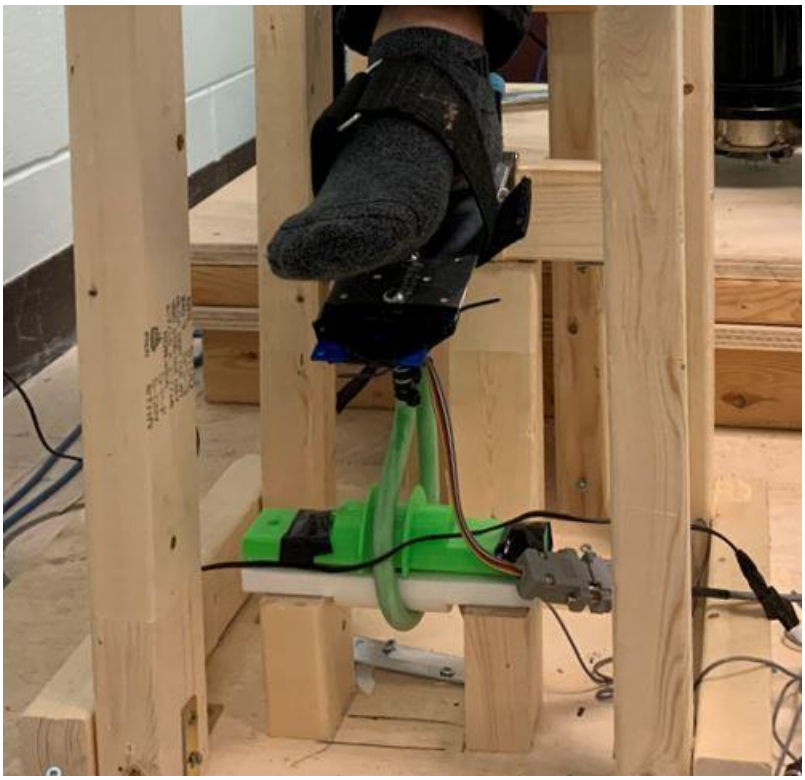

Figure 6: Front view of the force-transducer apparatus. A metal floor plate was connected to a resistance band. The resistance band was wrapped around a 3D-printed case for the force transducer. The participant's right foot was strapped to the floor plate using Velcro. The floor plate is on a hinge which allows the participant to dorsiflex the foot. When the participant pulled up on the floor plate, the resistance band pulled the force transducer case, which then applied a load to the force transducer.

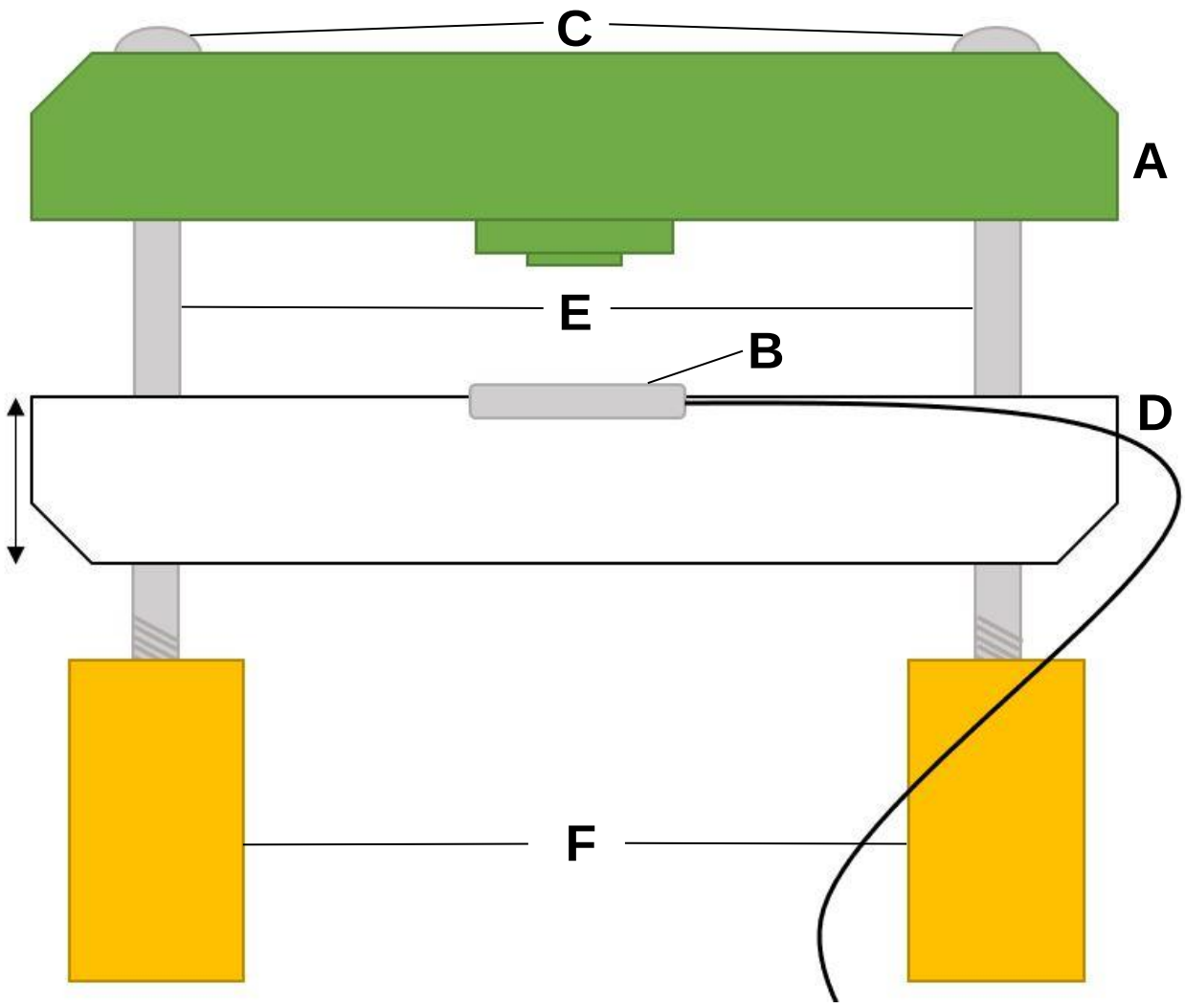

Figure 7: A figure depicting the 3D-printed casing holding the force transducer. The top half of the casing (green, **A**) would apply a load to the force transducer (**B**) when pressed against it, and was secured to the tops of the screws (**C**) using epoxy resin. The lower half of the casing (white, **D**) held the force transducer and could move freely up and down along the unthreaded portions of the screws (**E**), which were screwed into wooden blocks (**F**) at the base of the apparatus.

2.2.4 Maximum Voluntary Force (MVF)

Maximum Voluntary Force (MVF) was acquired from TA muscle. Participants performed 3 maximum force contractions by maximally dorsiflexing their right ankle for 5 seconds with a 2-minute rest interval in between trials. The largest force relative to baseline on

the force-transducer obtained from any of the three trials was defined as MVF. The levels of force corresponding to 20% and 70% MVF were used to calibrate the force transducer for the dorsiflexion tasks (see below). The maximum wave form height was produced with 70% force. This force was chosen to mitigate fatigue throughout the protocol as the participant did not have to exert maximum force to reach the peaks of the waveform. As well, this force limit standardized the level of force exerted across all participants. Additionally, each waveform was standardized so that the average force needed to track each waveform was 45% MVF.

2.2.5 Experimental Timeline

The entire experiment took place over a period of ~1.5-2 hours. Consent took place over 5-10 minutes, where participants were able to ask the attending graduate student any questions they may have about the experiment. Explanation of any experimental procedures always took place before that portion of the experiment. Experiment setup was ~60-75 minutes, including the fNIRS cap, force transducer, and fNIRS recording setup procedures. The fNIRS recording took place over ~20 minutes, throughout which participants performed the three tasks described below.

2.2.6 FNIRS Setup

FNIRS was performed using the Brainsight NIRS device (Rogue Research, Montreal, QC). This machine projects wavelengths of 705nm and 830nm to measure deoxy-hemoglobin and oxy-hemoglobin, respectively. The sources and detectors were placed in a stretchable cap before-hand, after which the participant put on the cap and adjusted the chin strap to comfort.

Optode placement was organized in a lattice arrangement over the head (see **Figure 8**). Source optodes are denoted by S, while detector optodes are denoted by D. Optode pairs will thus be referred to as S#D# where the number sign corresponds to the number of source or detector in the montage. The cap was positioned so that the optode pairs S5D1 and S10D13 were centered over the C3 and C4 respectively (International 10-20 system), corresponding to the bilateral primary motor cortices. Once the cap was positioned, hair was displaced from the area under each optode, and the optode was secured in the cap. A self-adhesive wrap was then placed around the cap on the head to increase optode coupling to the scalp, which was used to improve signal quality. The signal quality was then checked for each channel by looking for the presence of systematic physiological signals. Signal quality was deemed acceptable when clear signals for heartbeat (~1-1.5 Hz), and for Mayer waves (~0.1 Hz) were observed for each channel. Global detector sensitivity was then increased until signal saturation, at which point it was reduced ~2-5 V to allow for modulations in the signal during recording. Individual detector sensitivities were then adjusted so that each signal matched the channel with the highest signal strength as closely as possible.

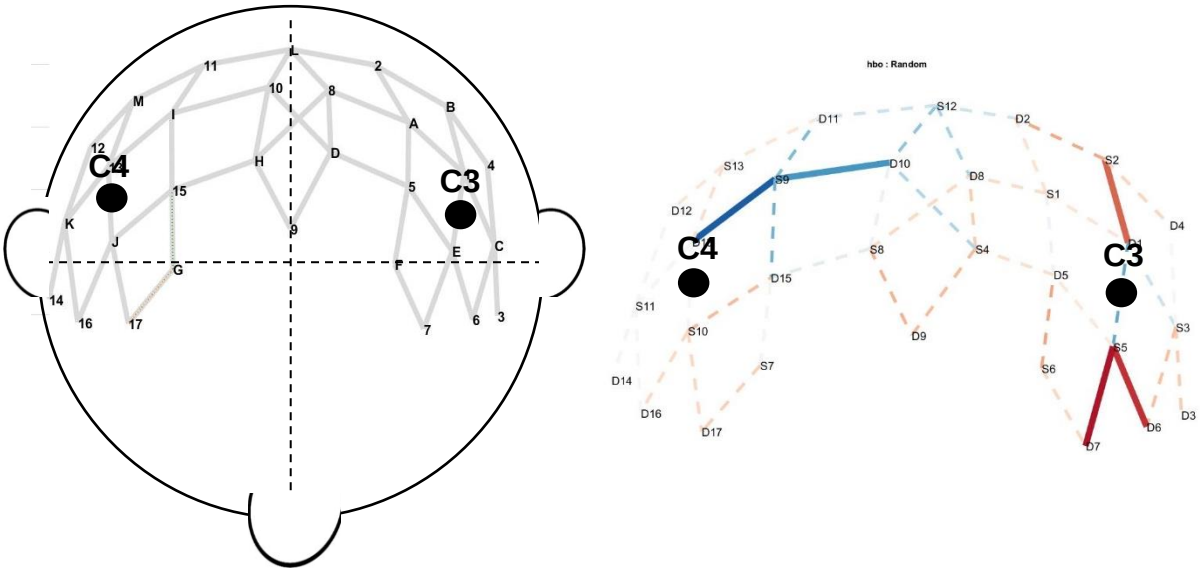

Figure 8: A representation depicting the optode montage. **A**. The montage represented on the participant's head. A source is represented by a letter. A detector is represented by a number. The grey lines in between sources (letters) and detectors (numbers) represent channels. Two channels will be centered over C3 and C4 (primary motor cortices). **B.** The montage as it looks in the fNIRS processing software.

2.2.7 Protocol for Acquisition of Experimental Trial

First, a baseline measure was performed. Participants were seated comfortably with their arms and legs relaxed and their eyes closed, breathing normally. Participants were asked to relax for 5 minutes to ensure that any pre-existing hemodynamic changes due to previous activities were reduced to their baselines. Once the 5 minutes had passed, the fNIRS recording was initiated with a 2-minute baseline measurement while the participants were at rest. Participants were instructed to keep as still as possible to not introduce motion artifacts into the data. Prior to the commencement of each trial, a 10 second baseline measure was taken to compare to each task period. Following the conclusion of a trial, a variable 30-50 second rest period allowed for hemodynamic activity to return to baseline values and prevented time-locking of physiological noise to the task. The secondary purpose of the rest period was to mitigate potential fatigue that participants may experience from repeated force productions during the task. The combination of baseline and rest periods amounted to a variable 40-60 seconds between trials. During baseline and rest periods, a centrally-positioned white fixation cross appeared on the screen. Participants were instructed beforehand to relax and fixate on the cross when it appeared. Trial timing was not divulged to participants, so as to mitigate the effects of trial anticipation on hemodynamic activity.

2.2.8 Tasks

Three tasks were compared in the present study. Each task was presented for a 10 second duration and the order of task presentations was randomized for each participant. No participant had the same order of tasks as another. Tasks consisted of **A**. Dorsiflexion of the ankle during random waveform force-tracking ("Random") **B**. Dorsiflexion during rhythmic waveform force-tracking ("Rhythmic"), and **C**. Rest without task demands (no stimulation; "Rest"). Importantly, the mean force produced during tasks A and B were matched to ensure that the intensity of force production was not the cause of any difference in hemodynamic activation between tasks. Task A consisted of random waveform force-tracking with dorsiflexion of the right ankle, where a pseudorandom sinusoid with unpredictable amplitude and peak timing was tracked for each trial. Task B consisted of rhythmic waveform force-tracking task in which a rhythmic sine wave with predictable timing and amplitude for each peak was tracked for each trial. All waveforms were comprised of 10 peaks and troughs, to ensure that the frequencies of the waveforms were similar and did not modulate the hemodynamic response. The order of tasks was pseudo-randomized to prevent order effects. For example, task A may have been followed by task B or task C, but not by another task A (see **Figure 9**). Each task was repeated 10 times, for a total of 30 task presentations. A full description for each task is provided below.

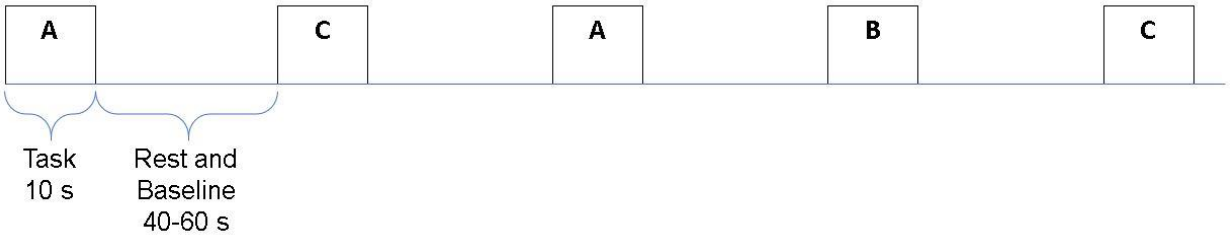

Figure 9: A figure depicting the pseudo-randomization of tasks during the fNIRS recording. Tasks were randomized so that one type of task may not occur concurrently. For example, above,

task ordering is **A C A B C**, however, the ordering **A A C B C** is not possible due to the concurrent presentation of task A. Tasks were 10 seconds long, with rest and baseline periods of 30-50 seconds and 10 seconds respectively, in between task presentations. There were 10 presentations of each task, for a total of 30 task presentations.

2.2.8.1 Task A: In this task, participants controlled a cursor and followed the path of a pre-generated waveform on a screen. This pre-generated waveform was a random sinusoid with varying amplitude and timing of peaks and troughs (see **Figure 10**) that was selected from a set of 10 based on the pseudo-randomization for that participant. Each of these waveforms was used once in a given collection – only the order of presentation changed. No waveform was repeated for the same participant. The waveforms used were considered to be complex as they are unpredictable, and thus would require more motor planning and finer motor control than a simpler sinusoid to track accurately. Force tracking was elicited through contracting the right TA muscle. As the force was tracked in real time, an increase caused the cursor to rise and a decrease caused the cursor to fall. The waveforms oscillated within 20% and 70% MVF for the participant. Performance on the task was assessed using the root mean squared error (RMSE) of the difference between the participant's cursor and the pre-generated waveform.

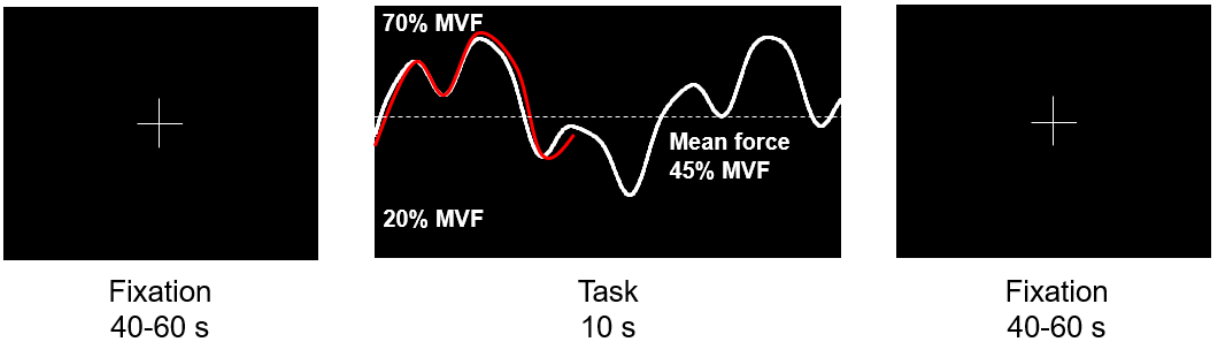

Figure 10: A representation of task A. Participants fixated on a white fixation cross before the task. The task then commenced, and continued for 10 seconds. During the task, the participant controlled the cursor (**red**) to try to follow the pre-generated waveform (**white**). The waveform was a random sinusoid that moved unpredictably in timing and amplitude. The mean force

produced corresponded to 45% MVF. As well, the waveform was set so that it is within the range of 20% to 70% MVF. The participant would modify the height of the cursor by pulling more (upward) or less (downward) with their right foot. Performance on the task was assessed using RMSE of the distance between the cursor and the waveform.

2.2.8.2 Task B: In this task, participants controlled a cursor and followed the path of a pre-generated waveform on a screen (see **Figure 11**). This pre-generated waveform was a sinusoid with consistent timing and amplitude throughout the 10 second task duration. Force tracking was elicited through contracting the right TA muscle. As with task A, the waveforms oscillated within 20% and 70% MVF for the participant. Task A and B waveforms were matched for mean amount of force. This was to ensure that the intensity of force production did not modulate the fNIRS response. Additionally, all waveforms were comprised of 10 peaks and troughs to ensure that the frequencies of the waveforms were similar and did not modulate the hemodynamic response. The same waveform was presented each time to ensure that the complexity of the task was not affected by changing the shape of the waveform. Performance on the task was assessed using RMSE of the difference between the participant's cursor and the pre-generated waveform.

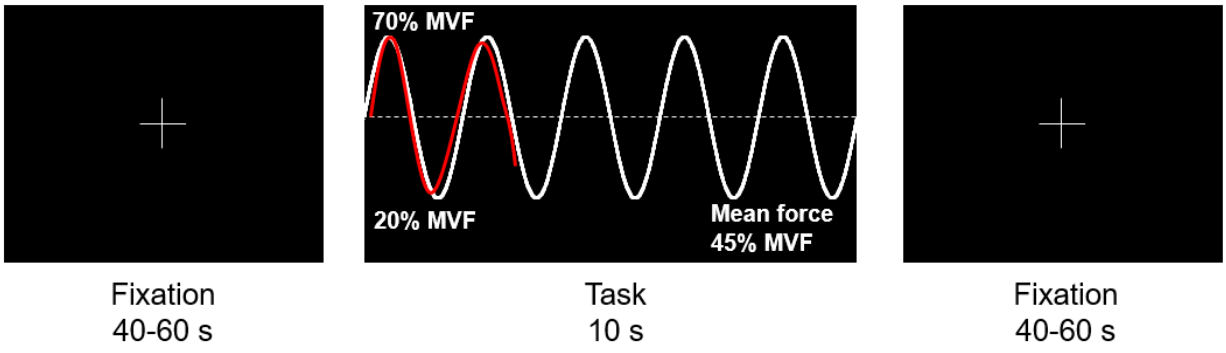

Figure 11: A figure depicting task B. Participants fixated on a cross before the task. The task then began, and continued for 10 seconds. During the task, the participant controlled the cursor (**red**) to follow the pre-generated waveform (**white**). The waveform was predictable in timing and amplitude. The participant modified the height of the cursor by pulling more (upward) or less (downward) with their right foot. The sine wave oscillated between 20% and 70% MVF,

with a mean force produced of 45% MVF. Performance was assessed using root mean squared error (RMSE) of the distance between the cursor and the waveform.

2.2.8.3 Task C: This task was a rest task with no task demands. The screen presented for this task was the same as those presented for rest and baseline (see **Figure 12**). As such, participants were unaware of the timing of this task to avoid anticipation effects on hemodynamic activity. This task is important as it allowed a baseline measure of hemodynamic activity that was compared to other tasks to ensure that the hemodynamic activity was significantly different.

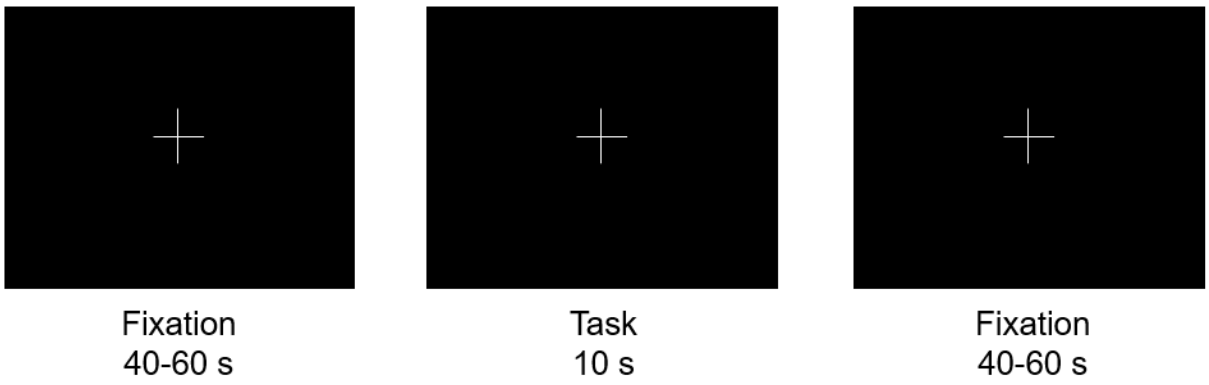

Figure 12: A figure depicting task C. Participants fixated on a cross before the task. The task then began, and continued for 10 seconds. During the task, the participant watched the fixation cross and refrained from making any movements.

2.2.9 FNIRS Data Processing

FNIRS data was processed using NIRS Brain AnalyzIR Toolbox in MATLAB (Santosa et al., 2019). FNIRS signals were first downsampled to 4 Hz to reduce serial correlations. The raw light intensity signals were then converted to changes in Optical Density, and a Principal Component Analysis (PCA) filter was applied to reduce global spatial trends in the data, removing 2 components. The global spatial trends include low-frequency drift, as well as

fluctuations due to heart rate, respiration, and Mayer waves. Although I was going to use short-separation channel regression to reduce physiological noise (Saager and Berger 2005), the fNIRS machine used in this study did not have the capability to record from short-separation channels, hence the PCA filter was used. The PCA filter was chosen because some sources of physiological noise (i.e., respiration and Mayer waves) can have frequency overlap with the hemodynamic response. Hence other techniques that rely on differences in frequency content to distinguish between cortical signal and noise are unable to remove it. Relative changes in hemoglobin concentrations were then calculated using the Modified Beer Lambert Law (Delpy et al., 1988). The fNIRS data was modelled with a General Linear Model (GLM) with a design matrix corresponding to the canonical HRF, and with an autoregressive prewhitening procedure to reduce the effects of serial correlations (Huppert 2016). The GLM assumes a linear combination of elements, including those from the predictors and different types of noise. The GLM was solved with an Iteratively-Reweighted Least Squares procedure, which removed outliers from whitened data that were assumed to correspond to motion artifacts.

2.2.10 Statistical Analysis

T-tests were used to compare average baseline and task period values for each channel across task (Random, Rhythmic, and Rest) for oxygenated hemoglobin (HbO) using the NIRS Brain AnalyzIR Toolbox software in Matlab. HbO was used for analysis as previous research has found that the retest reliability, SNR, and stability of HbO signals are higher than those for HbR (Plichta et al., 2006; Cui et al., 2011; Miyai et al., 2001; Strangman et al., 2002). The specific region of interest (ROI) that was investigated in this study was the bilateral TA representation of the motor cortex. This ROI was chosen because of the specific activation of the right TA muscle

in each of the tasks. To this end, four channels were selected in the midsection of the fNIRS montage that corresponded to this ROI: **S4D8**, **S4D10**, **S8D8**, and **S8D10**. It was expected that fNIRS signal would arise in one or more of these channels. Due to the poor spatial resolution of fNIRS (2-3 cm, Pinti et al., 2020) and potential differences in individual anatomy, no one channel was singled out as the expected channel for hemodynamic activation. In addition, channels with significant differences ($p<0.05$) between baseline and task period amplitudes were investigated further for specific activation patterns. Mean RMSE values were calculated for each participant across the "Random" and "Rhythmic" tasks, however due to the low sample size, these were not statistically analyzed.

2.3 Results

2.3.1 TA Motor

The primary area for investigation in this study was the motor cortex representation for TA. Four channels were selected that overlaid the TA motor representation in the participants. These channels were **S4D8**, **S4D10**, **S8D8**, and **S8D10** in the center of the montage, as indicated by the blue box in **Figure 13**. Average baseline values were compared to task amplitudes for all three tasks in each individual participant. The figures displayed below are average responses over the 10 trials for each task. $P<0.05$ was used as the statistical threshold for significance. The "0" on the x-axis of each graph represents the start time for the trial. One significant channel (S8D8) was found for one participant (P10) in the "Rhythmic" task (see **Figure 16**). All other channels/tasks were non-significant for participants. Considering the absence of activity in most participants, the hypothesis regarding activation in M1 from TA activity could not be addressed.

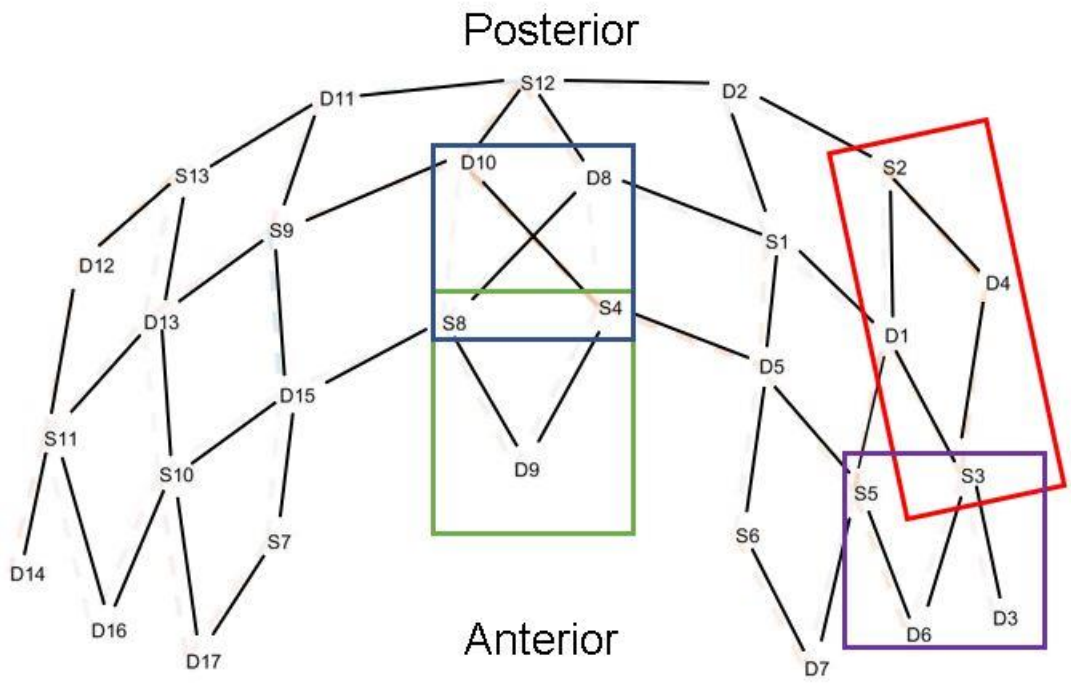

Figure 13: Figure depicting ROIs for the experiment. The blue box surrounds the medial channels overlying the TA motor representation. The red box surrounds the lateral channels overlying the left Somatomotor cortex. The green and purple boxes surround channels thought to overly Frontal and Temporal cortices, respectively.

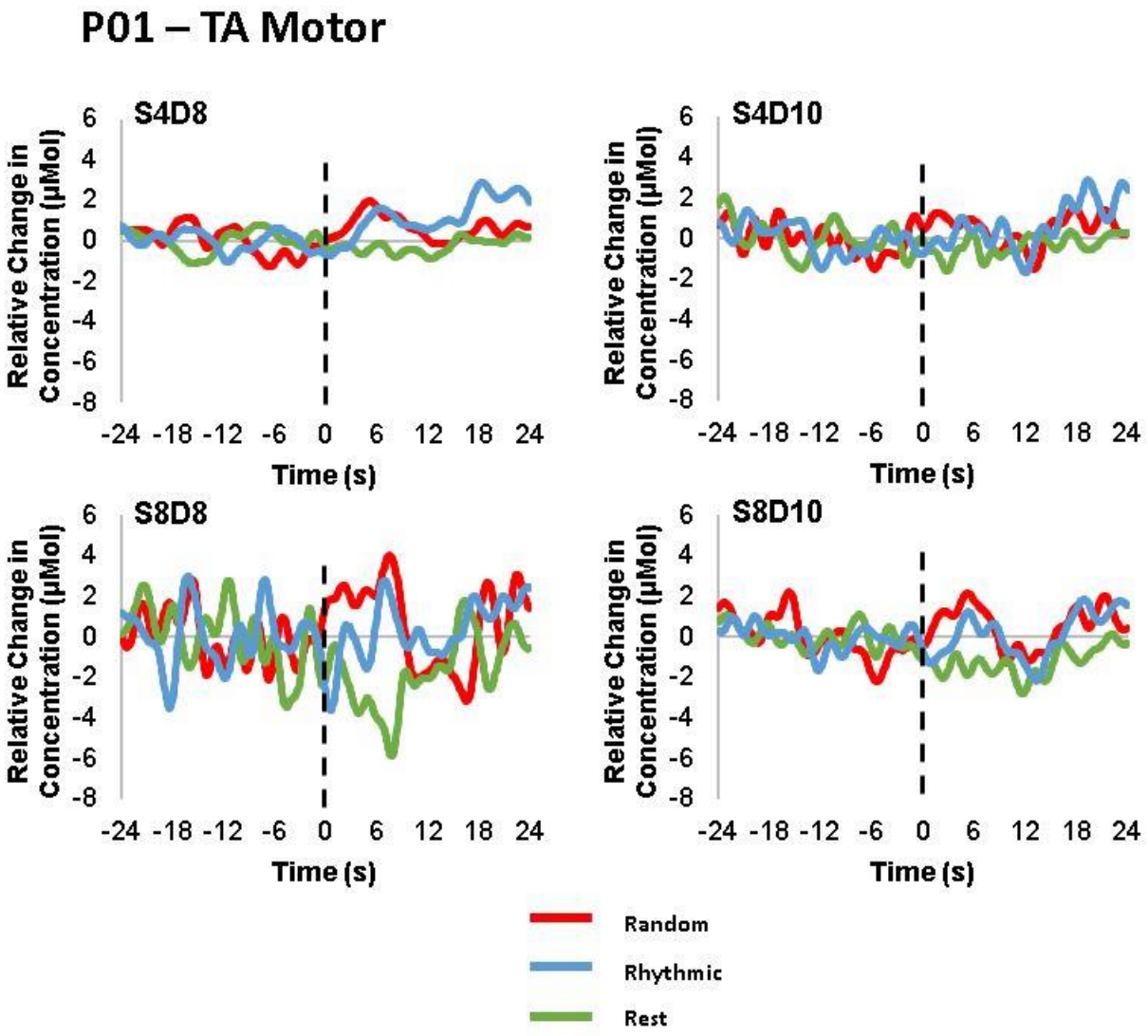

Figure 14: Figure depicting HbO activation detected in channels overlying the TA motor representation for P01. X axis is time in seconds, with negative numbers representing the baseline period. The dashed line above Time = 0 s represents the start of the task. Tasks were 10 seconds long. Y axis is the relative change in HbO concentration in micromolar. The HbO activation in the "Random" task is represented by a red line, "Rhythmic" by a blue line, and "Rest" by a green line. (*) represents a significant increase in HbO amplitude from baseline, whereas (†) represents a significant decrease in HbO amplitude from baseline. All graphs in the figure are scaled to the same size to accurately compare activations. Channels S4D8 and S8D8 looked like they may have had some activation for both the "Random" and "Rhythmic" tasks, however no channels reached statistical significance.

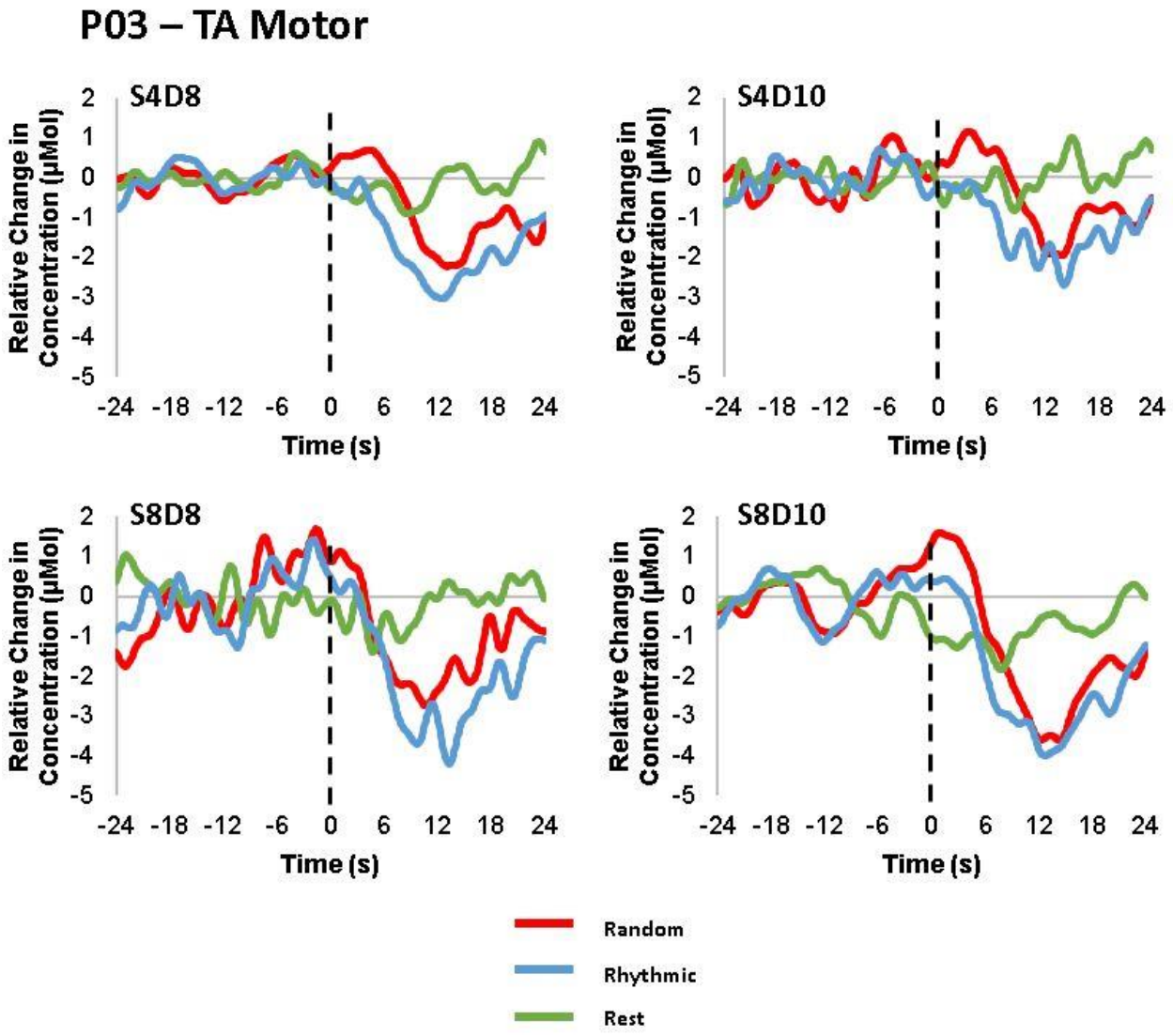

Figure 15: Figure depicting HbO activation detected in channels overlying the TA motor representation for P03. X axis is time in seconds, with negative numbers representing the baseline period. The dashed line above Time = 0 s represents the start of the task. Tasks were 10 seconds long. Y axis is the relative change in HbO concentration in micromolar. The HbO activation in the "Random" task is represented by a red line, "Rhythmic" by a blue line, and "Rest" by a green line. (*) represents a significant increase in HbO amplitude from baseline, whereas (†) represents a significant decrease in HbO amplitude from baseline. All graphs in the figure are scaled to the same size to accurately compare activations. Large decreases in HbO were seen in every channel after ~6 seconds. No channels reached statistical significance.

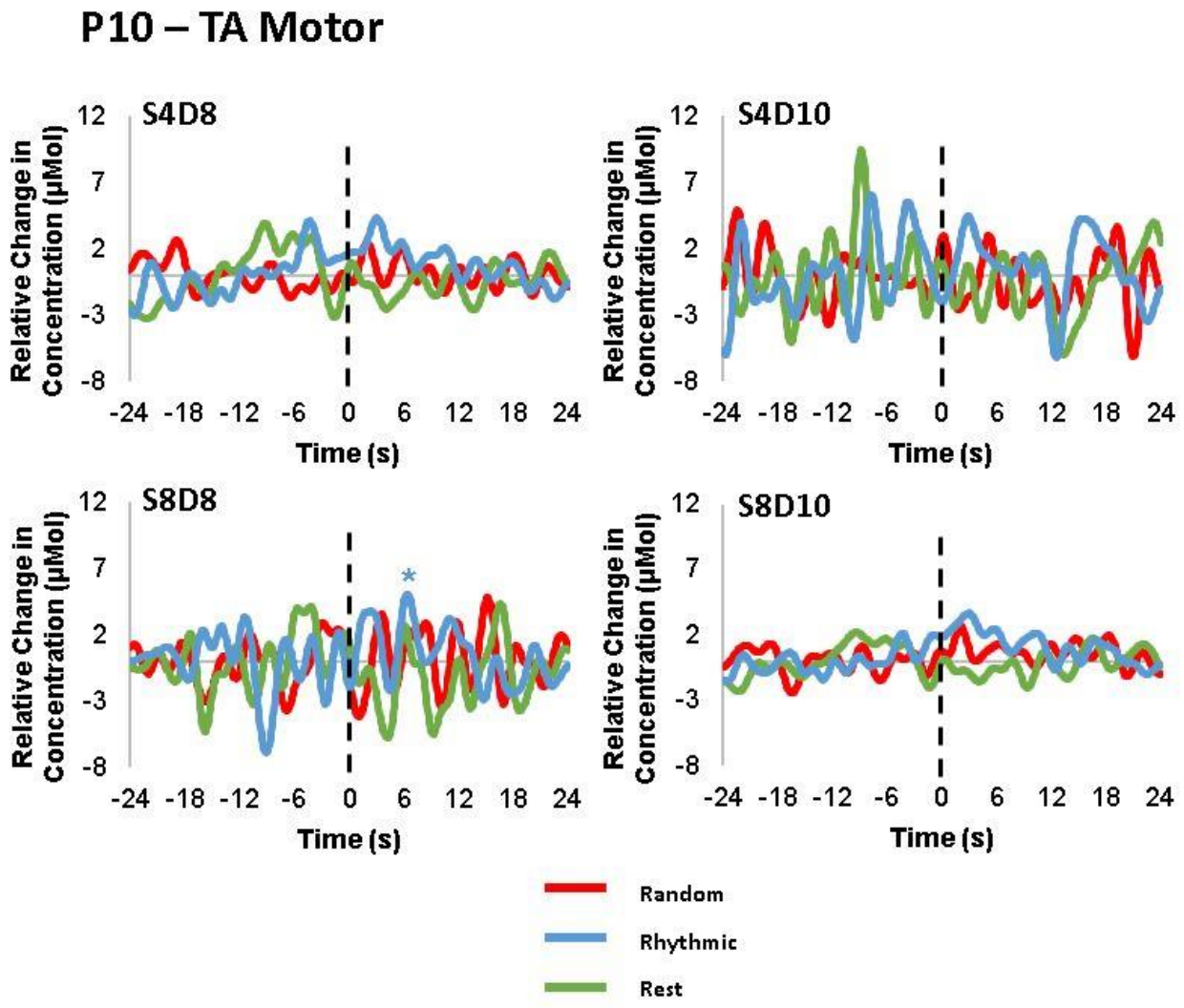

Figure 16: Figure depicting HbO activation detected in channels overlying the TA motor representation for P10. X axis is time in seconds, with negative numbers representing the baseline period. The dashed line above Time = 0 s represents the start of the task. Tasks were 10 seconds long. Y axis is the relative change in HbO concentration in micromolar. The HbO activation in the "Random" task is represented by a red line, "Rhythmic" by a blue line, and "Rest" by a green line. (*) represents a significant increase in HbO amplitude from baseline, whereas (†) represents a significant decrease in HbO amplitude from baseline. All graphs in the figure are scaled to the same size to accurately compare activations. Channel S8D8 reached statistical significance in the "Rhythmic" task, however this result could be due to excessive noise in the channel. No other channel reached statistical significance.

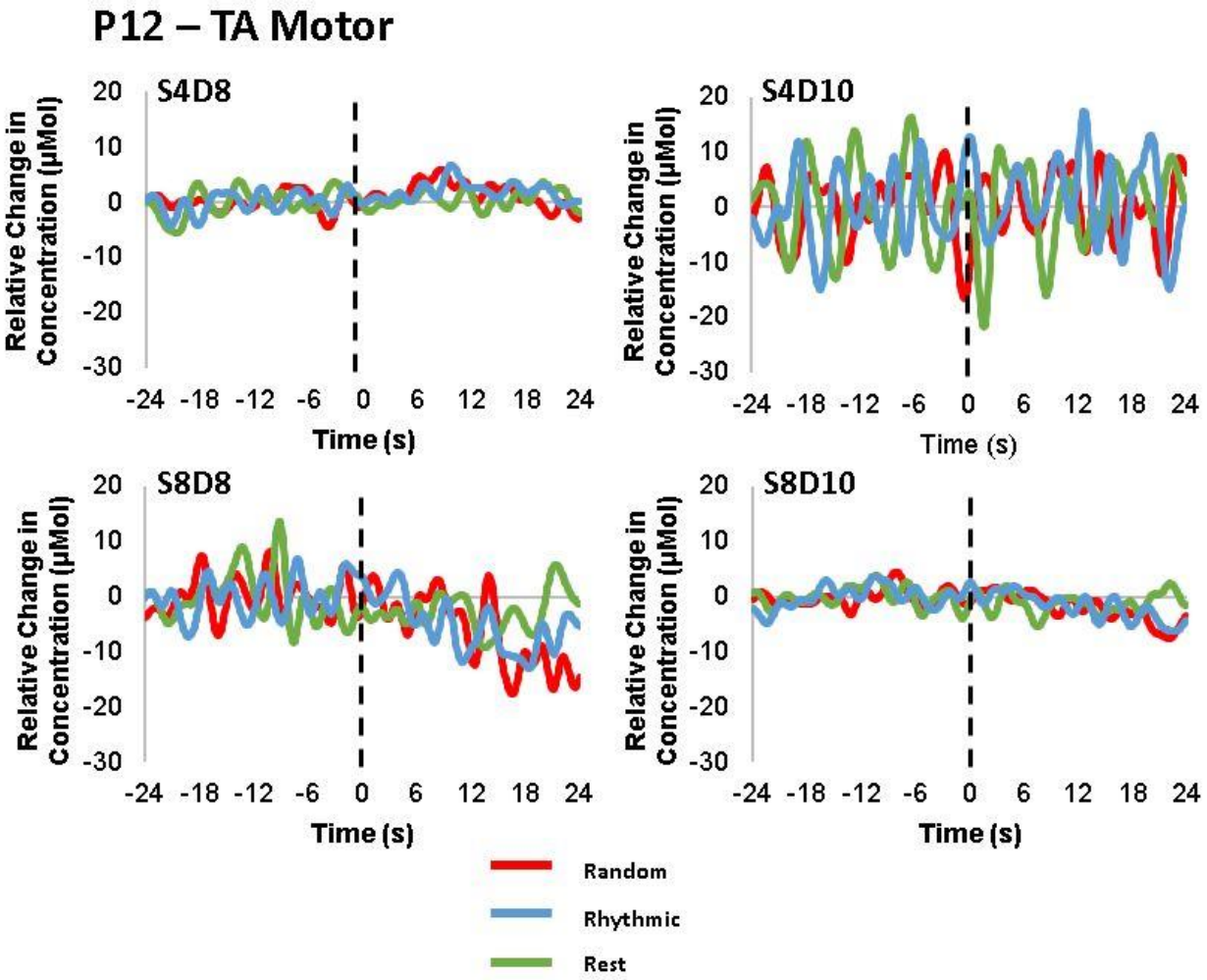

Figure 17: Figure depicting HbO activation detected in channels overlying the TA motor representation for P12. X axis is time in seconds, with negative numbers representing the baseline period. The dashed line above Time = 0 s represents the start of the task. Tasks were 10 seconds long. Y axis is the relative change in HbO concentration in micromolar. The HbO activation in the "Random" task is represented by a red line, "Rhythmic" by a blue line, and "Rest" by a green line. (*) represents a significant increase in HbO amplitude from baseline, whereas (†) represents a significant decrease in HbO amplitude from baseline. All graphs in the figure are scaled to the same size to accurately compare activations. Channels S4D10 and S8D8 seem to have large random fluctuations, which may indicate excessive noise in those channels. Channel S4D8 may have had some activation in the "Random" and "Rhythmic" tasks, but not enough to reach significance. No channels reached statistical significance.

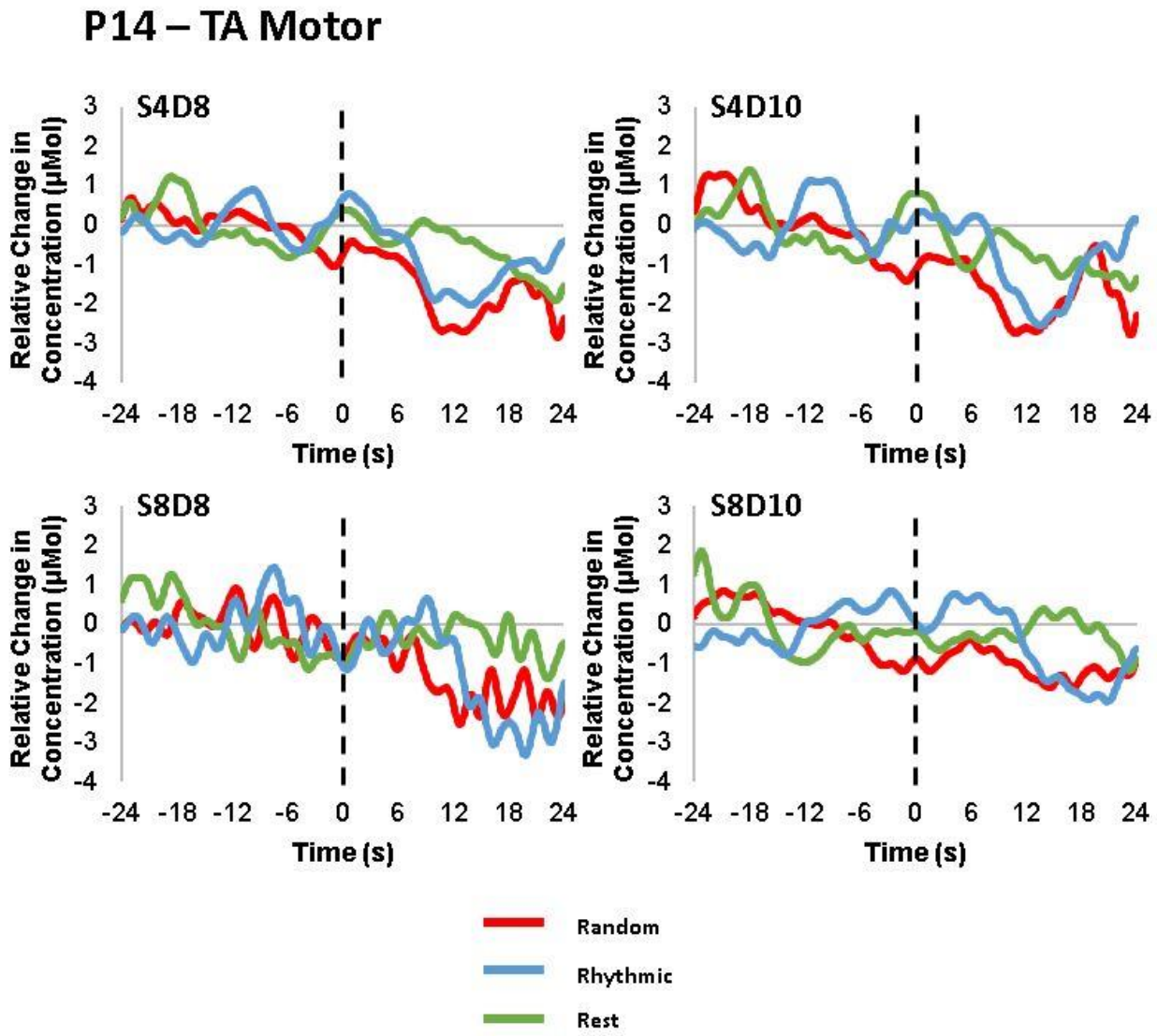

Figure 18: Figure depicting HbO activation detected in channels overlying the TA motor representation for P14. X axis is time in seconds, with negative numbers representing the baseline period. The dashed line above Time = 0 s represents the start of the task. Tasks were 10 seconds long. Y axis is the relative change in HbO concentration in micromolar. The HbO activation in the "Random" task is represented by a red line, "Rhythmic" by a blue line, and "Rest" by a green line. (*) represents a significant increase in HbO amplitude from baseline, whereas (†) represents a significant decrease in HbO amplitude from baseline. All graphs in the figure are scaled to the same size to accurately compare activations. All channels seem to have a downward trend, potentially indicating baseline drift. Additionally, signals in all channels seem to be very oscillatory, potentially indicating the presence of systematic physiological noise in the data. No channels reached statistical significance.

2.3.2 Other Areas Demonstrating Significance

2.3.2.1 Somatomotor Area

One area that showed significant channels in addition to the TA motor representation region was the area labelled "Somatomotor". Four channels were selected that overlaid the Somatomotor area in participants, represented by the red box in **Figure 13**. These channels were **S2D1**, **S2D4**, **S3D1**, and **S3D4** in the left hemisphere of the montage. Average baseline values were compared to task amplitudes for all three tasks in each individual participant. The figures displayed below are average responses over the 10 trials for each task. $P<0.05$ was used as the statistical threshold for significance. The "0" on the x-axis of each graph represents the start time for the trial. Significant channels were found for all participants in various channels.

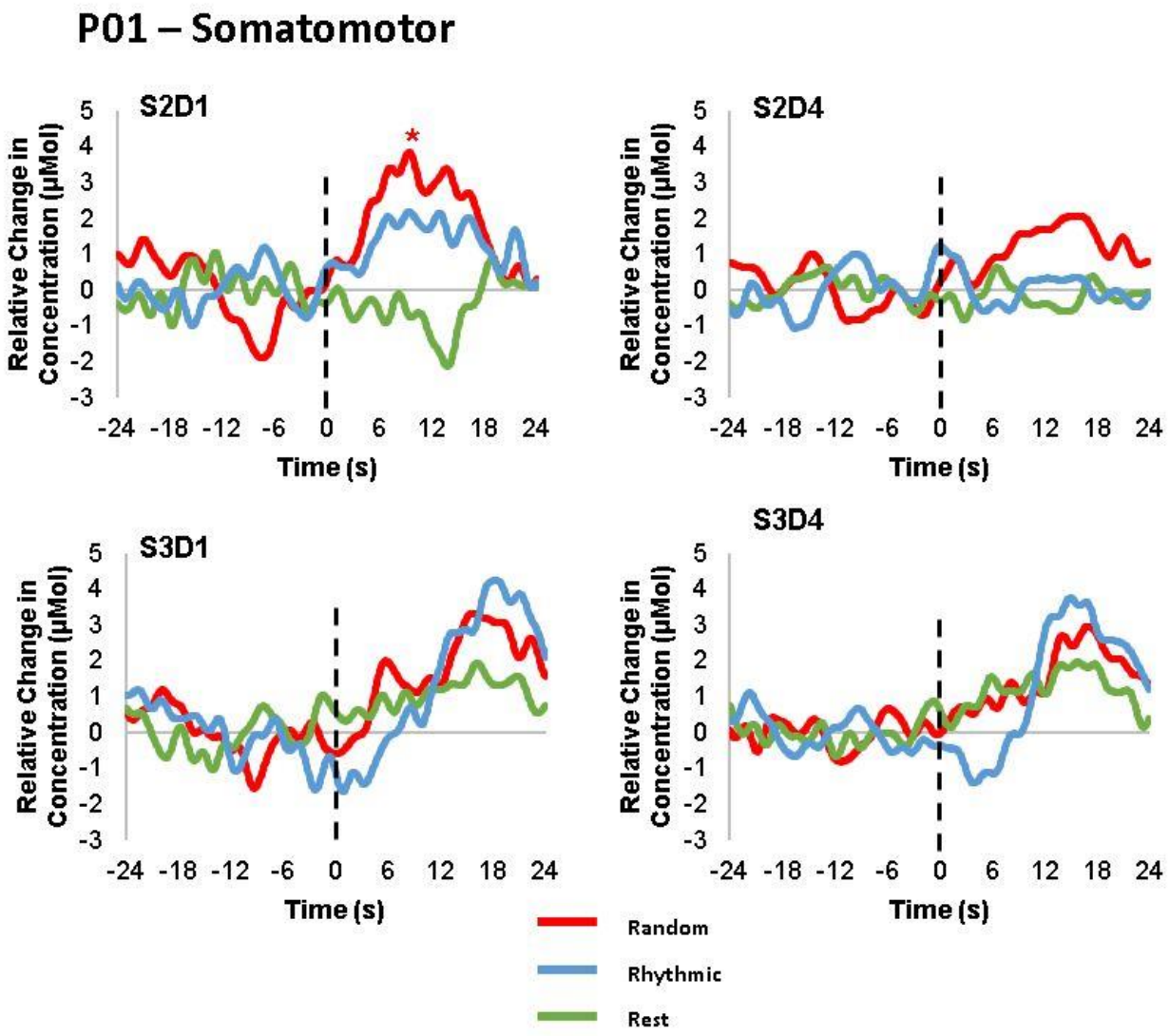

Figure 19: Figure depicting HbO activation detected in channels overlying the Somatomotor representation for P01. X axis is time in seconds, with negative numbers representing the baseline period. The dashed line above Time = 0 s represents the start of the task. Tasks were 10 seconds long. Y axis is the relative change in HbO concentration in micromolar. The HbO activation in the "Random" task is represented by a red line, "Rhythmic" by a blue line, and "Rest" by a green line. (*) represents a significant increase in HbO amplitude from baseline, whereas (†) represents a significant decrease in HbO amplitude from baseline. All graphs in the figure are scaled to the same size to accurately compare activations. Channel S2D1 reached statistical significance in the "Random" task. Channels S3D1 and S3D4 seem to have some activation in both the "Random" and the "Rhythmic" tasks, however the "Rest" task also seems to show some activation, indicating that the other activations could be spurious. No other channel reached statistical significance.

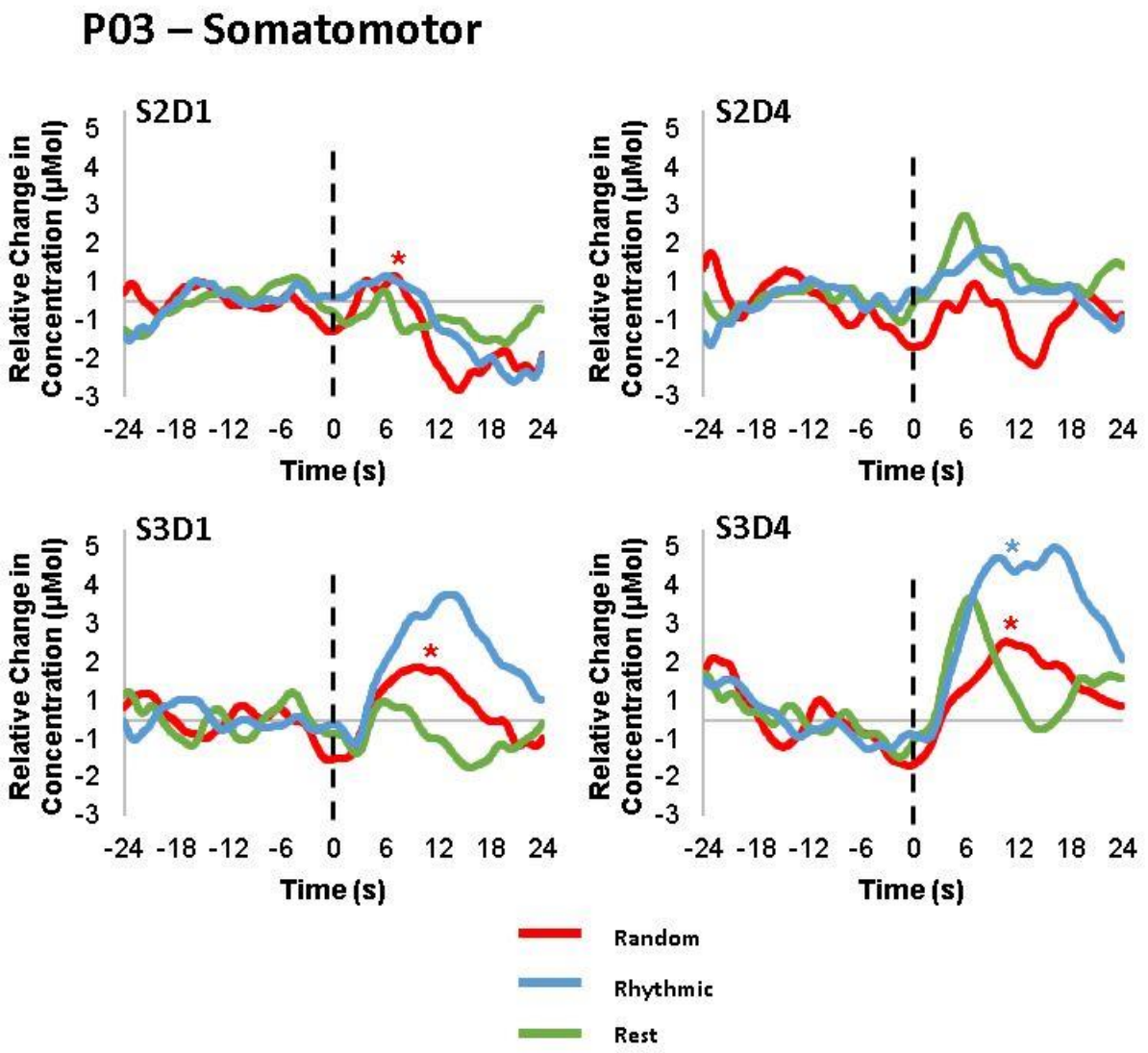

Figure 20: Figure depicting HbO activation detected in channels overlying the Somatomotor representation for P03. X axis is time in seconds, with negative numbers representing the baseline period. The dashed line above Time = 0 s represents the start of the task. Tasks were 10 seconds long. Y axis is the relative change in HbO concentration in micromolar. The HbO activation in the "Random" task is represented by a red line, "Rhythmic" by a blue line, and "Rest" by a green line. (*) represents a significant increase in HbO amplitude from baseline, whereas (†) represents a significant decrease in HbO amplitude from baseline. All graphs in the figure are scaled to the same size to accurately compare activations. Channels S2D1, S3D1, and S3D4 reached statistical significance for the "Random" task, and channel S3D4 for the "Rhythmic" task as well. Channel S2D4 did not reach statistical significance.

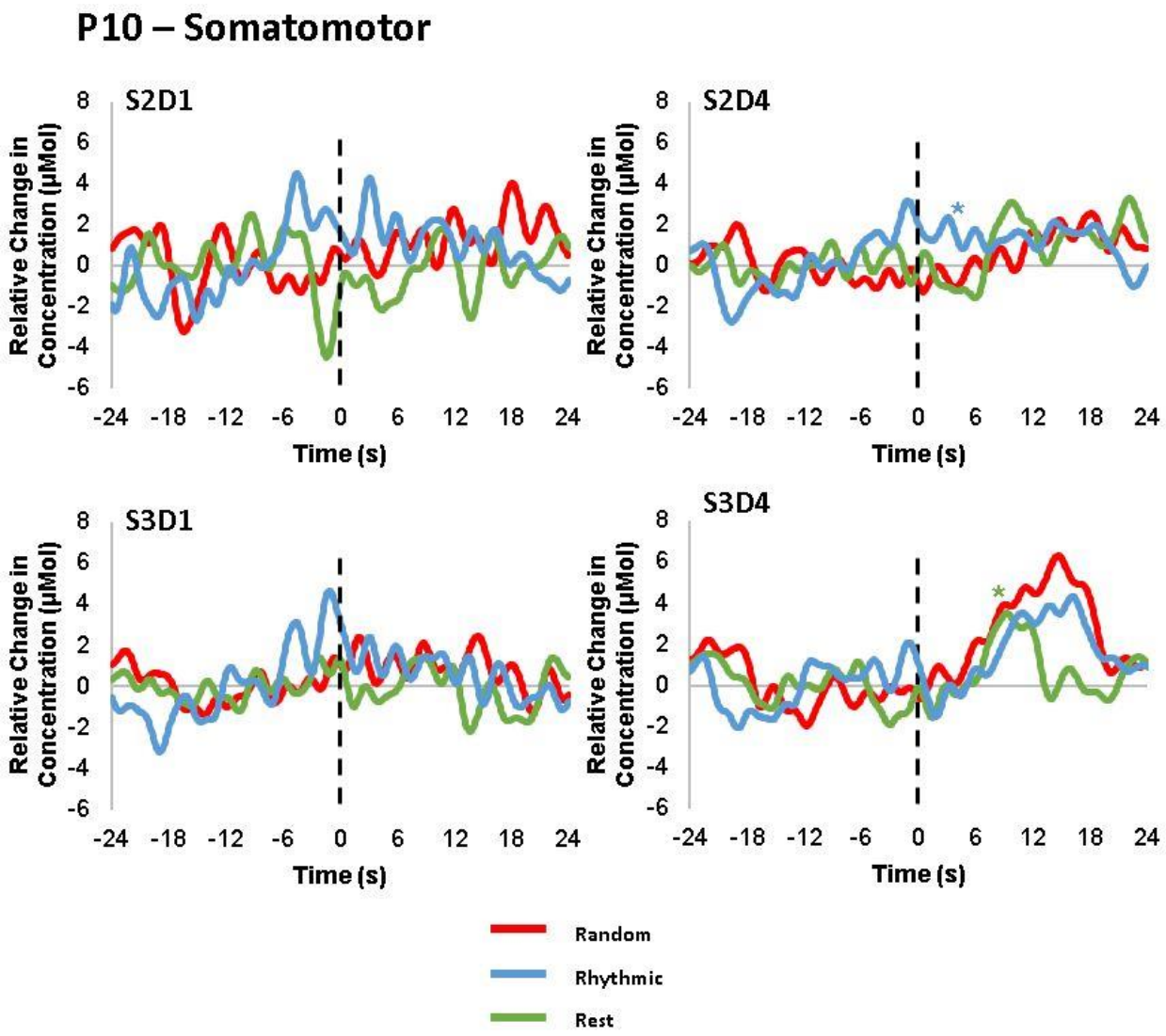

Figure 21: Figure depicting HbO activation detected in channels overlying the Somatomotor representation for P10. X axis is time in seconds, with negative numbers representing the baseline period. The dashed line above Time = 0 s represents the start of the task. Tasks were 10 seconds long. Y axis is the relative change in HbO concentration in micromolar. The HbO activation in the "Random" task is represented by a red line, "Rhythmic" by a blue line, and "Rest" by a green line. (*) represents a significant increase in HbO amplitude from baseline, whereas (†) represents a significant decrease in HbO amplitude from baseline. All graphs in the figure are scaled to the same size to accurately compare activations. Channels S2D4 and S3D4 reached statistical significance for the "Rhythmic" and "Rest" tasks, respectively. In S3D4, the fact that the "Rest" task increases alongside the "Random" and "Rhythmic" tasks potentially indicates that these activations are spurious. No other channels reached statistical significance.

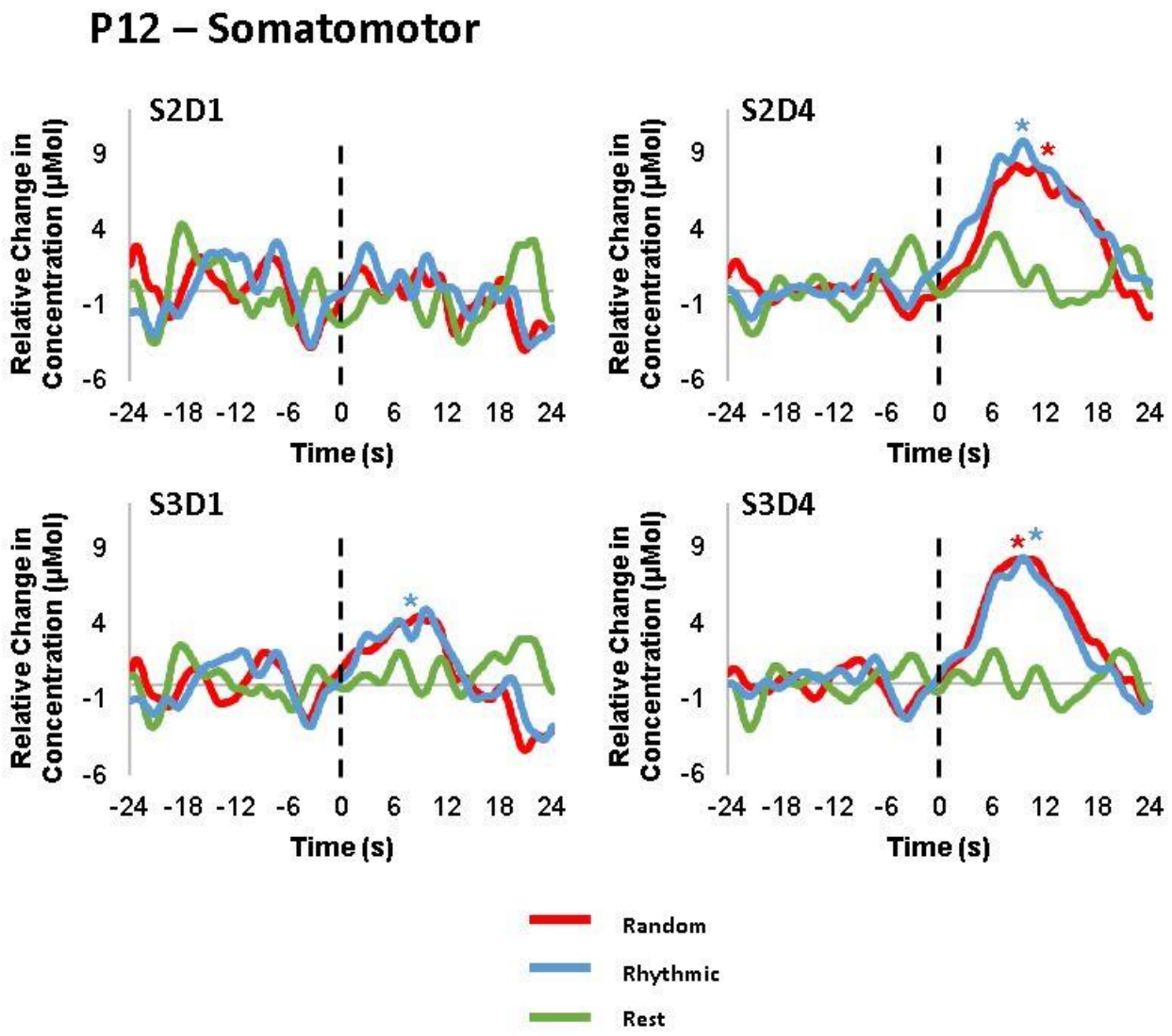

Figure 22: Figure depicting HbO activation detected in channels overlying the Somatomotor representation for P12. X axis is time in seconds, with negative numbers representing the baseline period. The dashed line above Time = 0 s represents the start of the task. Tasks were 10 seconds long. Y axis is the relative change in HbO concentration in micromolar. The HbO activation in the "Random" task is represented by a red line, "Rhythmic" by a blue line, and "Rest" by a green line. (*) represents a significant increase in HbO amplitude from baseline, whereas (†) represents a significant decrease in HbO amplitude from baseline. All graphs in the figure are scaled to the same size to accurately compare activations. Channels S2D4, S3D1, and S3D4 reached statistical significance for the "Rhythmic" task. Channels S2D4 and S3D4 also reached statistical significance for the "Random" task. The activation patterns and amplitudes seemed to be very similar across the "Random" and "Rhythmic" tasks in all channels. Channel S2D1 did not reach statistical significance.

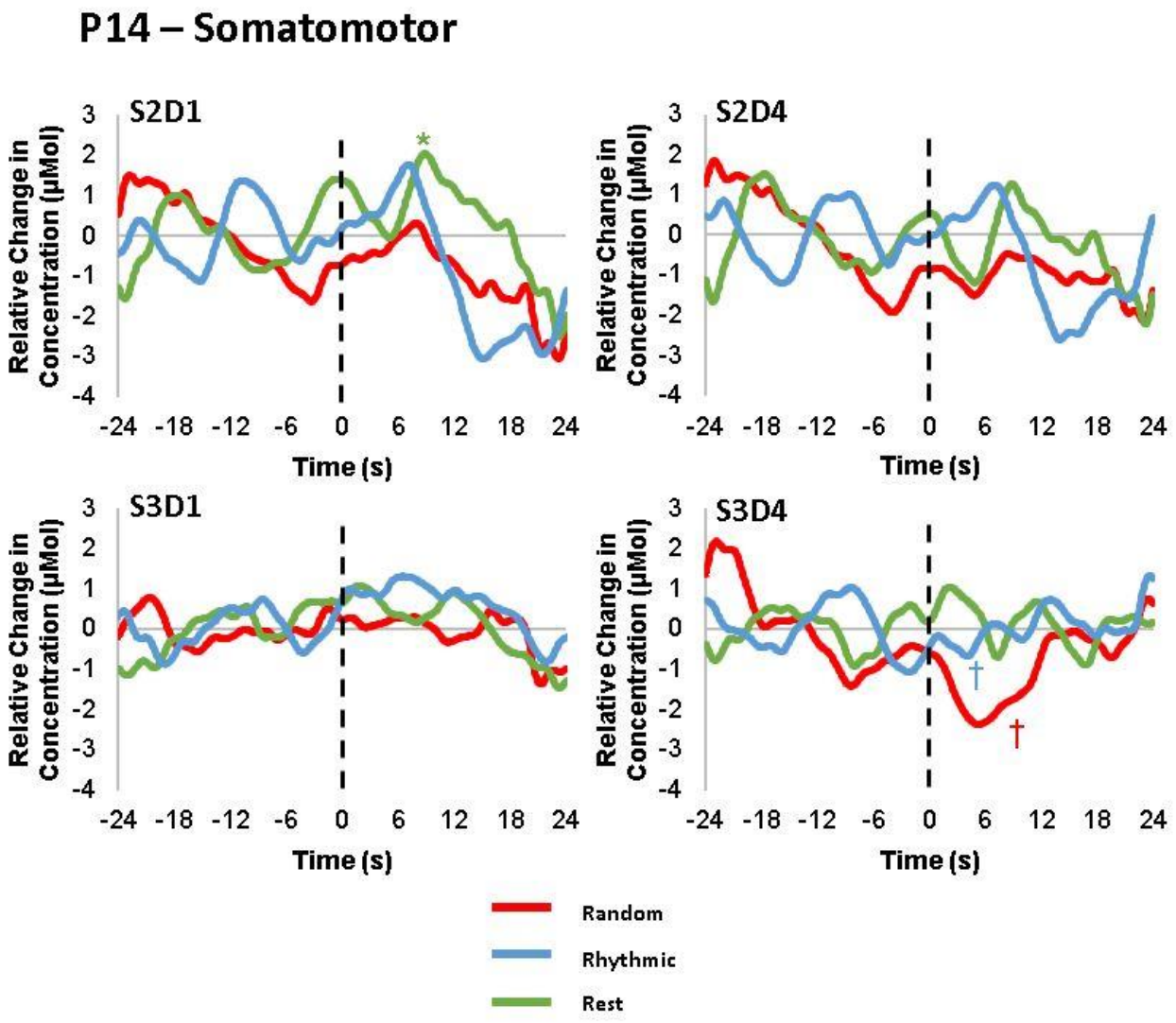

Figure 23: Figure depicting HbO activation detected in channels overlying the Somatomotor representation for P14. X axis is time in seconds, with negative numbers representing the baseline period. The dashed line above Time = 0 s represents the start of the task. Tasks were 10 seconds long. Y axis is the relative change in HbO concentration in micromolar. The HbO activation in the "Random" task is represented by a red line, "Rhythmic" by a blue line, and "Rest" by a green line. (*) represents a significant increase in HbO amplitude from baseline, whereas (†) represents a significant decrease in HbO amplitude from baseline. All graphs in the figure are scaled to the same size to accurately compare activations. Channel S2D1 reached statistical significance for the "Rest" task, and S3D4 for the "Random" and "Rhythmic tasks. However, activations in S3D4 were consistently in the negative direction, potentially indicating excessive noise in the channel. Additionally, each channel demonstrated oscillatory activity for each task, potentially indicating that any activations were spurious. No other channels reached statistical significance.

2.3.2.2 Frontal Cortex

Another area that showed significant channels in addition to the TA motor representation region was the Frontal cortex. Channels **S4D9** and **S8D9** were assumed to overly the Frontal cortex in participants, and are represented by the green box in **Figure 13**. Average baseline values were compared to task amplitudes for all three tasks in each individual participant. The figures displayed below are average responses over the 10 trials for each task. $P<0.05$ was used as the statistical threshold for significance. The "0" on the x-axis of each graph represents the start time for the trial. The two channels demonstrated significance in P10 for both the "Random" and "Rhythmic" tasks (see **Figure 24**). All other channels/tasks were non-significant for participants.

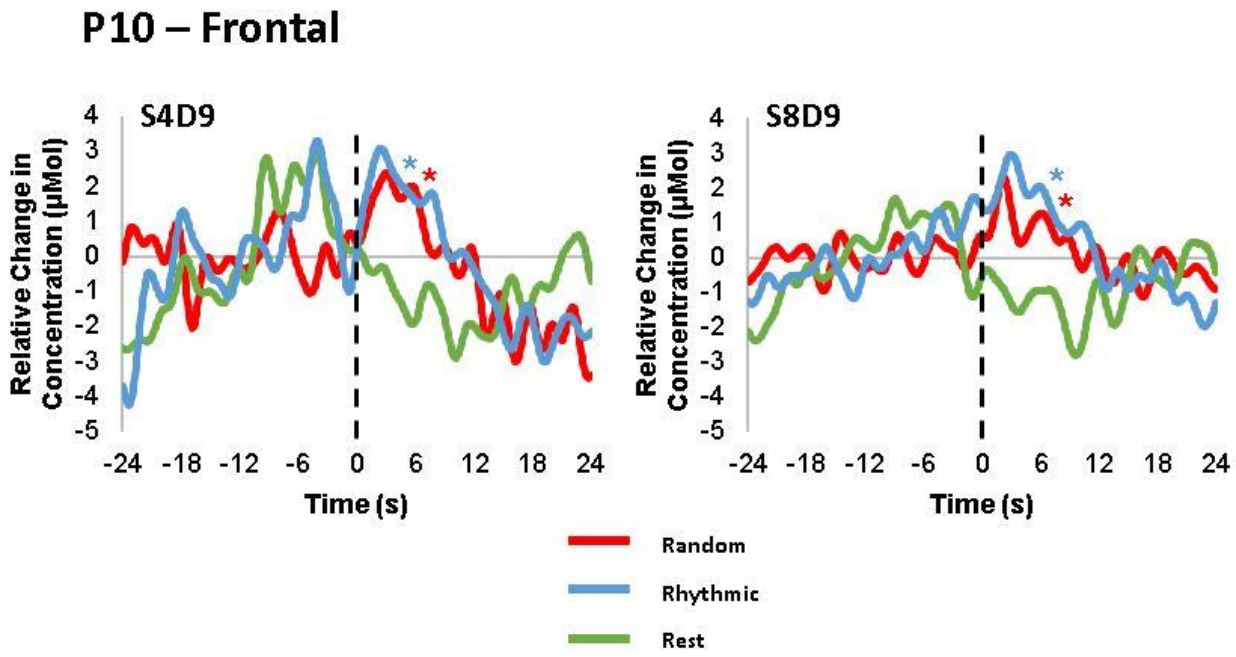

Figure 24: Figure depicting HbO activation detected in channels overlying the Frontal representation for P10. X axis is time in seconds, with negative numbers representing the baseline period. The dashed line above Time = 0 s represents the start of the task. Tasks were 10 seconds long. Y axis is the relative change in HbO concentration in micromolar. The HbO activation in the "Random" task is represented by a red line, "Rhythmic" by a blue line, and

"Rest" by a green line. (*) represents a significant increase in HbO amplitude from baseline, whereas (†) represents a significant decrease in HbO amplitude from baseline. All graphs in the figure are scaled to the same size to accurately compare activations. Both S4D9 and S8D9 reached statistical significance for both the "Random" and the "Rhythmic" tasks. However, the large pre-task activation in S4D9 for the "Rhythmic" task potentially indicates that this particular activation could be spurious.

2.3.2.3 Temporal Cortex

A final area that showed significant channels in addition to the TA motor representation region was the Temporal cortex. Channels **S3D3** and **S5D6** were assumed to overly the Temporal cortex in the left hemisphere, and are represented by the purple box in **Figure 13**. Average baseline values were compared to task amplitudes for all three tasks in each individual participant. The figures displayed below are average responses over the 10 trials for each task. $P<0.05$ was used as the statistical threshold for significance. The "0" on the x-axis of each graph represents the start time for the trial. Channel S5D6 was active in P01 for both the "Random" and "Rhythmic" tasks, whereas channel S3D3 was active in P03 for the "Random" task. All other channels/tasks were non-significant for participants.

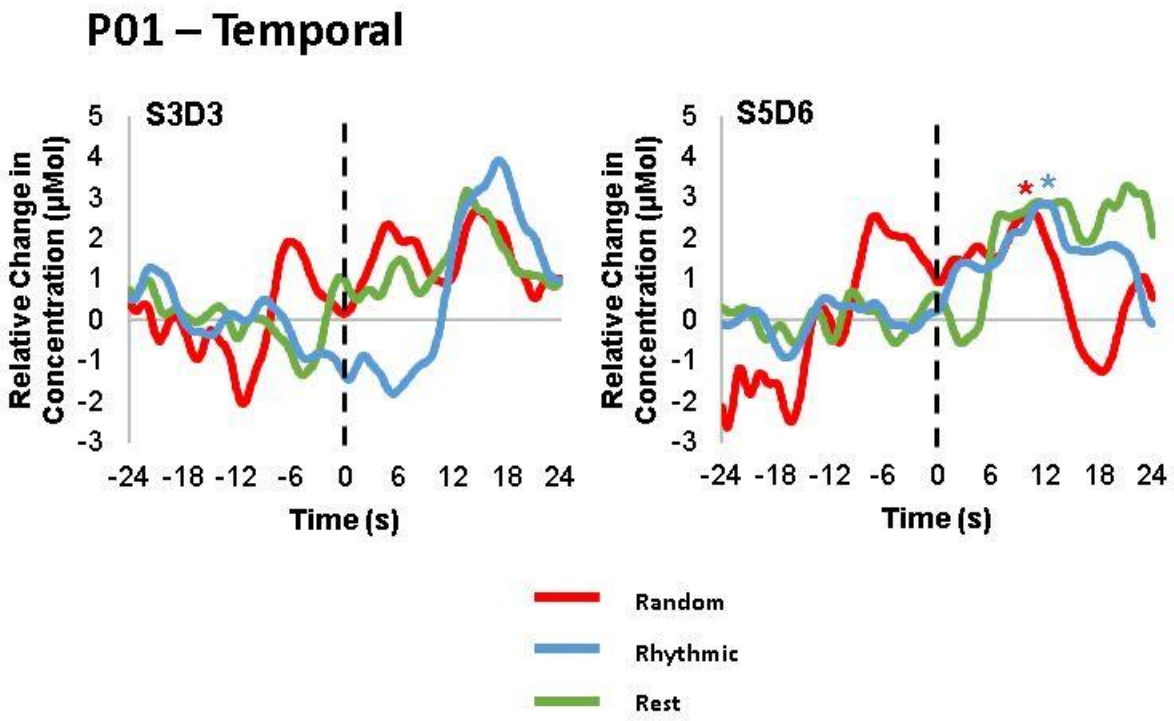

Figure 25: Figure depicting HbO activation detected in channels overlying the Temporal representation for P01. X axis is time in seconds, with negative numbers representing the baseline period. The dashed line above Time = 0 s represents the start of the task. Tasks were 10 seconds long. Y axis is the relative change in HbO concentration in micromolar. The HbO activation in the "Random" task is represented by a red line, "Rhythmic" by a blue line, and "Rest" by a green line. (*) represents a significant increase in HbO amplitude from baseline, whereas (†) represents a significant decrease in HbO amplitude from baseline. All graphs in the figure are scaled to the same size to accurately compare activations. Channel S5D6 reached statistical significance for the "Random" and the "Rhythmic" tasks. However, the large activation during the "Rest" task and the large pre-task activation for the "Random" task potentially indicate that these activations are spurious. The other channel did not reach statistical significance.

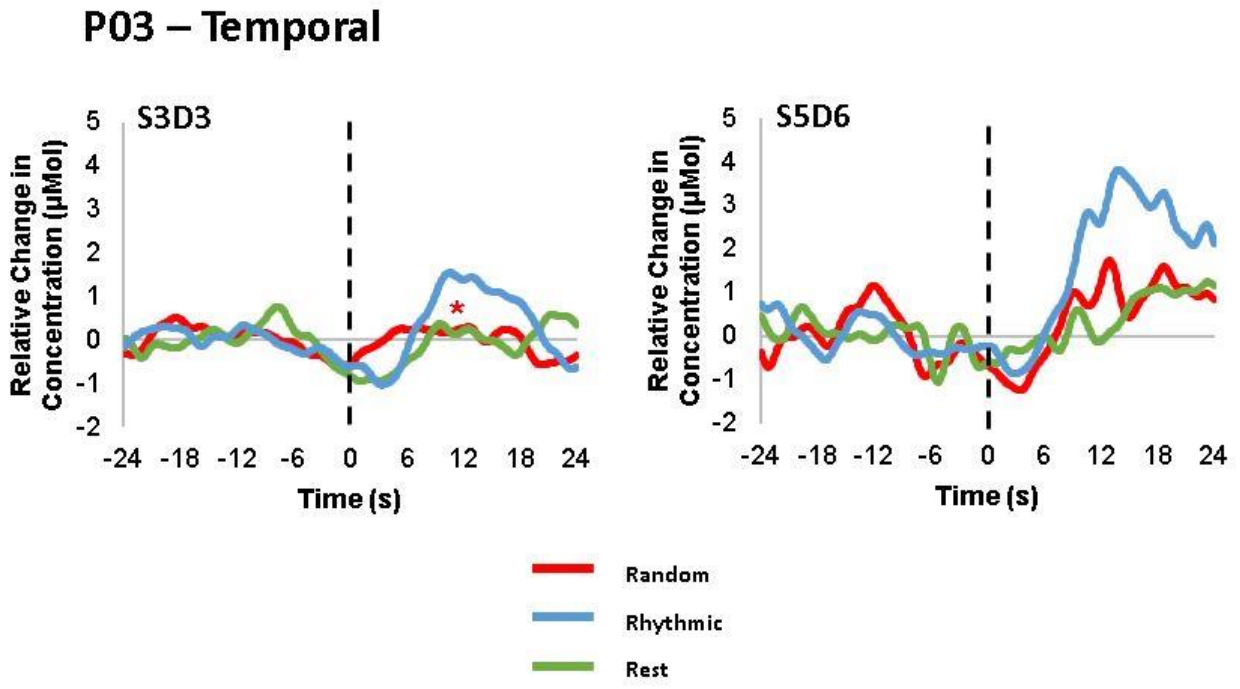

Figure 26: Figure depicting HbO activation detected in channels overlying the Temporal representation for P03. X axis is time in seconds, with negative numbers representing the baseline period. The dashed line above Time = 0 s represents the start of the task. Tasks were 10 seconds long. Y axis is the relative change in HbO concentration in micromolar. The HbO activation in the "Random" task is represented by a red line, "Rhythmic" by a blue line, and "Rest" by a green line. (*) represents a significant increase in HbO amplitude from baseline, whereas (†) represents a significant decrease in HbO amplitude from baseline. All graphs in the figure are scaled to the same size to accurately compare activations. Channel S3D3 reached statistical significance for the "Random" task, however this activation seems to be at the same amplitude as the pre-task baseline. Additionally, other activations seem to be higher, however they also seem to be peaking later than the task period, and thus may be spurious activations. The other channel did not reach statistical significance.

2.3.3 Behavioural Results

Behavioural performance on both force-tracking tasks was assessed using RMSE values expressed as % MVF. Mean RMSE values and their standard deviations are presented in **Table 1**. Force-tracking signals were truncated by 1 second at the beginning of each trial so that

seconds 1-9 were used in the calculation of RMSE. This was done to avoid errors from delays in starting the task. No trends emerged from the RMSE data. I expected that RMSE values would be larger in the "Random" task than in the "Rhythmic" task. The "Random" task was hypothesized to be more difficult for the participants to complete due to the varying amplitude and timing of peaks and troughs in each waveform. With a full dataset, this result could have been statistically analyzed and would have provided more information on the RMSE.

Participant Number	P01	P03	P10	P12	P14
RMSE average - Random	10.11 (± 2.89)	28.83 (± 18.76)	17.78 (± 4.74)	13.34 (± 4.78)	11.16 (± 3.17)
RMSE average - Rhythmic	15.04 (± 3.78)	46.34 (± 31.91)	17.02 (± 3.30)	11.49 (± 3.17)	15.20 (± 8.87)

Table 1: Table depicting average RMSE values (% MVF) across tasks for participants.

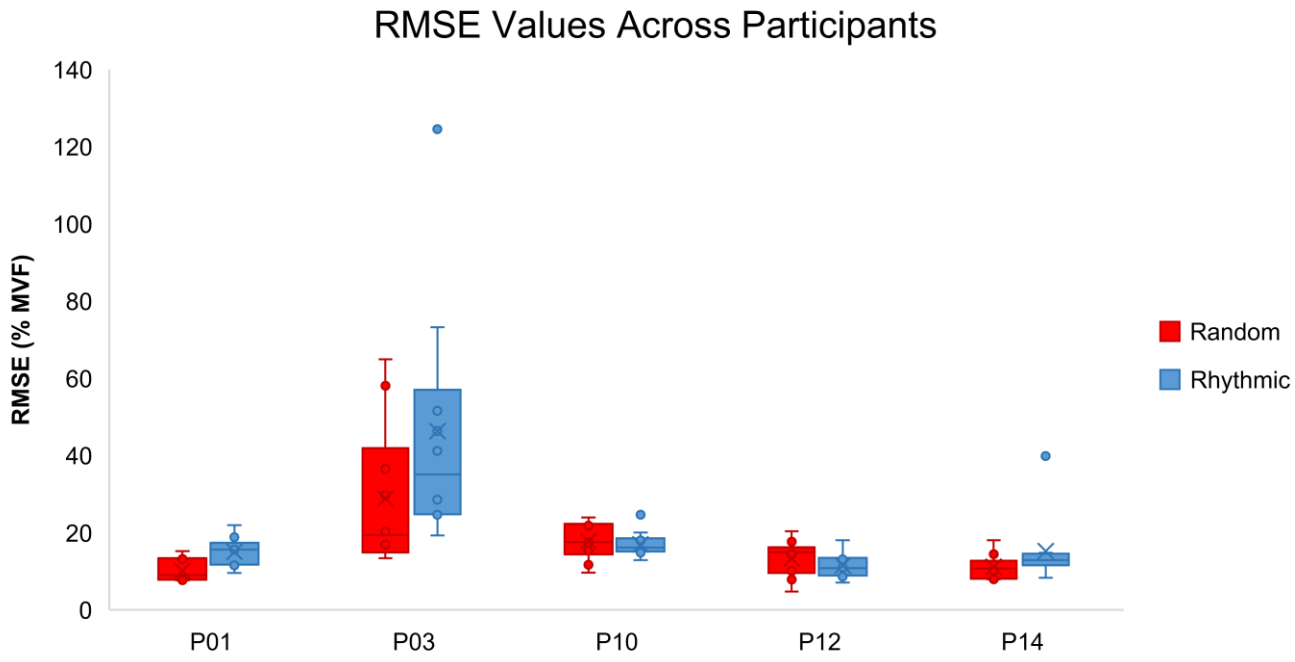

Figure 27: Figure depicting a box and whisker plot of RMSE values across participants and tasks. X's on the graph represent mean values. Within participants, error rates are very similar across tasks, suggesting that the tasks were equally difficult (complex).

2.4 Discussion

The present study explored cortical hemodynamic responses to a lower limb force-tracking task in healthy individuals. Although the study was incomplete, preliminary findings provide interesting information regarding the feasibility of performing lower limb fNIRS for a motor task involving a single joint. Additionally, the results of the present study indicate activity in similar cortical regions to previous work, suggesting that activations in the present study may reflect similar cortical mechanisms. Below, the preliminary findings and their possible biological origins are discussed.

2.4.1 Why was there no activation from TA motor representation?

No significant increases were found for HbO in channels overlying the TA motor representation excepting one in the present study. There could be multiple reasons why other channels failed to reach statistical significance. First, methodological issues like inadequate optode coupling to the top of the scalp could have introduced extraneous noise and decimated the SNR for the channels. However, each channel was double-checked to limit the amount of hair under the optodes before the experiment started. Additionally, the head was wrapped with a bandage to improve optode coupling to the scalp. Despite the wrap, pressure may have been disproportionate across channels due to the head shape of individual participants. Further, the task may have been ineffective in activating the TA motor region due to the transient task period (10 seconds). However, some lower limb fNIRS studies have reported task periods of as little as two seconds, while reporting significant HbO activations (De Lima-Pardini et al., 2017; Huppert et al., 2013).

Second, it is possible that fNIRS was unable to record signals from the area simply due to depth of the area within the longitudinal fissure in most participants. Light projected by fNIRS is only able to measure signals from 5-8 mm into the cortex (Huppert 2016), which may not be deep enough to reach the TA motor representation. These deeper areas also have lower contrast-to-noise ratios (Huppert et al., 2013), which may affect researchers' ability to see signals from these regions. However, other fNIRS studies such as Pittaccio et al. (2013) and Koenraadt et al. (2012) reported activation in the medial motor cortices during similar lower limb tasks to the present study. Pittaccio et al. (2013) showed some fNIRS activation in the medial motor region during passive and active ankle dorsiflexion, however these results were not analyzed statistically and thus the level of activation may not be statistically significant. Koenraadt et al. (2012) showed significant fNIRS activation in a rhythmic ankle dorsiflexion-plantarflexion movement over the motor cortex, however this result could be due to the activation of multiple muscles, the motor representations of which may be closer to the scalp than others. Therefore, it is difficult to say whether a motor task dominated by the action of TA muscle can induce activations within the depths of the central sulcus that can be detected by fNIRS in healthy individuals. In line with this, the TA motor representation is not the same in all individuals. For example, a Transcranial Magnetic Stimulation (TMS) motor-mapping study by Vaalto et al. (2013) found that TA motor representations for trained figure skaters were significantly larger in the dominant hemisphere than TA motor representations in age-matched controls. Similarly, Streletz et al. (1995) found that biceps brachii (BB) motor maps were significantly greater in area and produced larger responses in patients with acute complete cervical spinal cord injury (SCI) compared to healthy controls. If the TA motor representation is similar to the motor representation for BB, the TA motor representation may be greater in area and produce larger

responses in SCI patients. However, complete SCI prevents these patients from participating in the task, as there is no residual function. Instead, incomplete SCI patients, while presenting similar changes to complete SCI, still retain function in the affected limbs. Specifically, Freund et al. (2011) assessed 10 SCI patients (2 complete, 8 incomplete; cervical SCI) in regards to fMRI activations in motor representations of affected limbs. They found that a handgrip task elicited greater fMRI activations in the motor representation for the hand when compared to controls (Freund et al., 2011). This effect was augmented in tandem with reduced spinal cord area. This study demonstrates that in incomplete SCI, some motor areas with residual function have greater levels of activation. This phenomenon, if also present in lower limb motor areas, may allow for more expansive studies of the lower limb in SCI patients. This increased level of activation is also present in other clinical populations. In fact, a recent fNIRS study by Sukal-Moulton et al. (2020) investigated different activations between young adults with typical development (TD), unilateral cerebral palsy (UCP), or bilateral cerebral palsy (BCP) during an ankle dorsiflexion task. The authors found that only the BCP group had significant channels for the ankle dorsiflexion task, and not the TD or UCP groups (Sukal-Moulton et al., 2020). Additionally, the UCP and BCP groups had more global activity than the TD group (Sukal-Moulton et al., 2020). Thus, TA motor representations may only produce detectable responses to fNIRS in specific populations, such as those with SCI. Future studies should investigate activations from TA motor tasks in both clinical and healthy populations to elucidate this issue.

2.4.2 Why was there activity in Somatomotor Area?

One area that produced statistically significant channels was the area labelled "Somatomotor". The channels in this area were **S2D1**, **S2D4**, **S3D1**, and **S3D4**. These channels

produced statistically significant increases in HbO activation during the “Random” and “Rhythmic” tasks for four out of five participants. These increases could be related to multiple functions from the underlying brain regions. For example, these channels could be relaying activations from the superior temporal gyrus (STG), which is responsible for sensory integration. In a lower limb fNIRS study, Tachibana et al. (2011) found statistically significant activations in channels overlying this area when participants played a dance video game. The authors suggested that multiple sensory cues such as the arrows on the screen and the music from the game required sensory integration for the participant to accurately dance in the game (Tachibana et al., 2011). In the present study, participants also needed to integrate information from multiple sources. The visual cue of the waveform, the proprioceptive cue from the position of the foot, and the somatosensory cue from the resistance band all contribute to the accuracy of the participant in the force-tracking task. These cues may have been integrated into a cohesive unit that was then sent downstream to the motor cortex to affect behaviour (Tachibana et al., 2011).

Alternatively, fNIRS activations in these channels could reflect secondary somatosensory cortex (SII) activation. In a recent fMRI study, the authors reported significant activations in SII while participants attended to either a virtual hand (VH) or to their real hand (RH) during repeated grasping motions, with higher activations in the RH condition (Limanowski and Friston 2020). The authors suggested that this increased activity in SII could be related to proprioceptive attention to the hand; in other words, attending to the unseen body part. This idea of proprioceptive attention is in line with previous hypotheses of motor attention (Rushworth et al., 2001). In the present study, participants could be directing proprioceptive attention to their foot in the apparatus to connect that location with the location of the cursor on the screen.

Consequently, both areas SII and STG could be active, due to the requirement of sensory integration to complete the task.

2.4.3 Why was there activity in Frontal Area?

A third area that showed significant HbO activations in one participant (P10) was labelled as "Frontal". The channels in this area were **S4D9** and **S8D9**. These channels produced statistically significant HbO increases for both the "Random" and "Rhythmic" tasks. Due to their proximity to Cz, these channels could possibly be overlying the preSMA and/or the SMA in P10. The preSMA and SMA areas are thought to be important for the learning of new motor skills (Hund-Georgiadis and von Cramon 1998; Hatakenaka et al., 2007). For example, in Hund-Georgiadis and von Cramon (1998), the authors found significant fMRI activations in the SMA throughout a complex finger tapping task. Specifically, the authors compared fMRI activations between piano players (PP) and non-musicians (NM) throughout their learning of a complex finger tapping task. The NM group had significantly higher SMA activations than the PP group throughout most of the training. Additionally, SMA activations decreased in both groups as the training progressed. From these results, the authors suggest that the SMA is involved in motor learning (Hund-Georgiadis and von Cramon 1998). Similarly, a more recent fNIRS study by Hatakenaka et al. (2007) found increased activations in the preSMA and SMA as participants were trained on a PR task. The authors in this study also concluded that preSMA and SMA were likely involved in the motor learning process due to decreasing activations in both areas as training progressed (Hatakenaka et al., 2007).

In the present study, only one participant (P10) showed significant activations in these channels, however other participants did not. One potential reason for this may be anatomical differences between that participant and others. The head size of P10 was smaller compared to other participants' head sizes. Thus, the montage may have reached these more frontal areas in comparison to someone with a larger head size. Another potential reason, though unlikely, is that other participants learned the task faster, and thus had lower overall activations in these areas that, when averaged over the different trials, did not lead to significant activations. However, this theory cannot be tested as error rates cannot be compared statistically across so few participants.

2.4.4 Why was there activity in Temporal area?

The fourth area that showed significant activations in channels was labelled "Temporal" due to its anterior and lateral position on the montage. The channels in this area were **S3D3** and **S5D6**. Two participants (P01, P03) had significant increases in HbO for these channels in the "Random" and "Rhythmic" tasks. However, the patterns of activation in some of these channels imply that they were spurious activations. For example, in **Figure 25** channel S5D6, all three tasks ("Random", "Rhythmic", and "Rest") seemed to increase around the same period, suggesting that they could be due to global physiological or motion artifacts. Additionally, **Figure 26** showed a significant activation in channel S3D3 for the "Random" task, however from visual inspection there seemed to be no increase, especially in comparison to the "Rhythmic" task from the same channel. In channel S5D6 of the same figure, there were much larger activations that appeared to be non-significant, however these activations seemed to peak later in time (~12 s after task begins) than is usual (~5-10 s, Leff et al., 2011).

2.4.5 Complexity Modulation

There was limited evidence of hemodynamic complexity modulation for the present study. In most participants, HbO activations were similar for the "Random" and "Rhythmic" tasks across most channels. One explanation for this result is that the tasks were too similar. Both the "Random" and "Rhythmic" tasks were ~0.5 Hz frequency, and the mean amount of force produced in each task remained at 45% MVF. Simply the timing and amplitude of the peaks and troughs of the waveforms differed. In this sense, perhaps such changes were minute and did not increase the difficulty of the task enough to change the hemodynamic response. However, the fact that the channels overlying the TA motor representation did not produce significant increases in HbO in either case prevents further investigation, as differences in activations between the tasks would be expected to arise in that region (Holper et al., 2009; Koenraadt et al., 2012). Further, considering the small sample size, an effect may be present but may not be visible without a larger sample. Within participants, statistical contrasts revealed no statistical differences between all channels in these areas. If the area labelled Somatomotor truly lay over areas STG and/or SII, a lack of differences in activation between the "Random" and "Rhythmic" force-tracking conditions may simply reflect the fact that the same amount of sensory integration is required for both tasks. This notion may be likely, as the only difference between the tasks was between the waveforms themselves, while the basic methodology for force-tracking remained similar.

In the Frontal channels, significant activations in a single participant were also similar between tasks. If the Frontal channels truly lie over preSMA/SMA areas, similar activations may indicate similar difficulty between tasks. However, as reported by Hatakenaka et al. (2007), activations in these areas change as the participant learns the motor task. Consequently, it may be

more accurate to observe the activations across time for each task instead of as an average activation level.

2.5 Conclusions

These preliminary data suggest that fNIRS is not capable of detecting hemodynamic activation from the TA motor representation, and thus may not be capable of detecting complexity-modulated responses in this area. Further, force-tracking may induce hemodynamic activation in STG/SII, and preSMA/SMA in regards to sensory integration and motor learning, respectively. No further conclusions can be drawn in regards to the present data due to small sample size. Future studies may conduct similar studies with lower limb force-tracking to disambiguate hemodynamic activity and its biological origin.

Chapter 3: FNIRS Processing - The Uses and Considerations Regarding Processing Techniques

3.1 Introduction

FNIRS is often paired with tasks involving human movement due to the relatively superficial location of the motor cortex (Leff et al., 2011). As such, a large number of papers have been published utilizing fNIRS to study experimental paradigms related to human movement. Consequently, fNIRS methodologies have become increasingly varied in regards to recording and processing of fNIRS data.

FNIRS data contains noise from different sources including those from physiological, instrumental, and motion. These different noise sources can enshroud the cortical signal and prevent researchers from observing the effects of their tasks. Consequently, revealing a tangible cortical signal requires pre-processing of the collected fNIRS data to remove this extraneous noise. Many different pre-processing techniques exist; however, some perform better in certain situations than others. As a result, the implementation of sensible pre-processing is of cardinal importance for the accurate detection of task-related cortical hemodynamic events.

The fNIRS literature reveals a wide range of processing methods (see section ***3.3 Processing Techniques and their Uses***). The variety and lack of information in pre-processing methods creates challenges for new fNIRS users. The purpose of this chapter is to identify common fNIRS pre-processing methodologies that are specific to the motor control field. Subsequently, the techniques identified as the most common will be discussed in terms of their uses, considerations for utilization, and methodology.

3.2 Literature Review

3.2.1 Literature Search Criteria and Data Extraction

The following PubMed headings were used in a PubMed literature search: *((((((((NIR) OR NIRS) OR fNIRS) OR fNIR) OR functional near-infrared spectroscopy) OR functional near-infrared spectroscopic) OR optical imaging system) OR optical topography) AND ((((((((motor) OR motor control) OR motor behaviour) OR motor behavior) OR motor function) OR motor coordination) OR motor activity) OR motor ability) AND ((((((((((((((upper limb) OR lower limb) OR gait) OR locomotion) OR balance) OR ambulation) OR cycling) OR walking) OR standing) OR obstacle) OR dorsiflexion) OR plantarflexion) OR finger opposition) OR finger tapping) OR squeezing) OR grasping) OR manipulation) AND ("2010/01/01"[PDAT] : "2020/12/31"[PDAT])*. Additionally, the NCBI filter function was used to narrow the search based on the date of the study (1st January 2010 to 1st June of 2020). Studies were also limited to those written in English and performed on humans. The following information was independently collected from each study by two graduate trainees (P.D., S.F.): first author, year of publication, fNIRS hardware used, processing software used, experimental task, fNIRS optode montage, participant demographics, sample size, processing approach, and the presence or absence of figures reporting of processed hemodynamic responses.

3.2.2 Inclusion/Exclusion Criteria

In order to have been included in this review, studies had to meet the following criteria: a) Studies must be peer-reviewed articles, b) studies must employ an ON/OFF task paradigm

which alternates between task and rest periods, c) studies must employ fNIRS in relation to, in combination with, or separate from other neuroimaging techniques on the cortex of the brain, d) studies must investigate healthy populations, e) studies must report processing techniques for fNIRS data, and f) studies must be performed in human participants.

These criteria were used to determine the inclusions at each stage of the review process (see **Figure 1**).

3.2.3 Study Selection

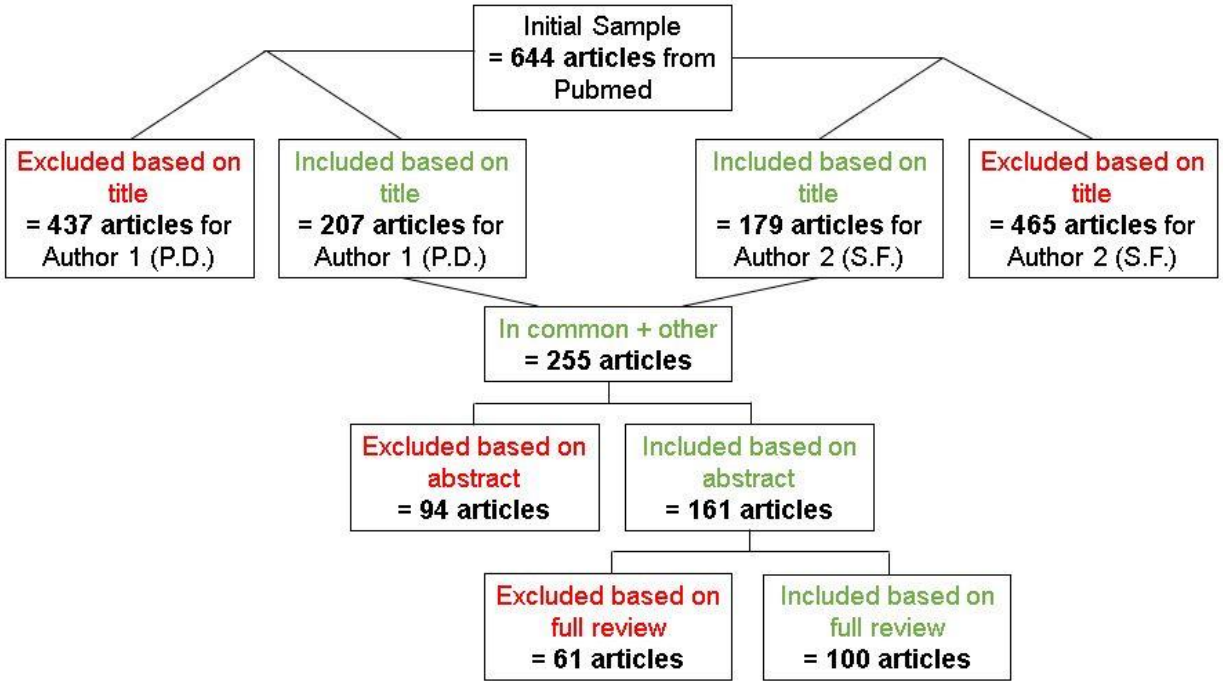

Figure 1: Figure depicting the study selection process for the review.

3.2.4 Results of the Literature Review

Article information (i.e. authors, processing, montage, etc.) from the final sample of 100 articles is included in **Appendix A**. Otherwise, processing technique usage from the final sample

is included in **Table 2** below. Studies are categorized by processing techniques employed – as such, many studies appear more than once in the table, as more than one technique was usually utilized when pre-processing fNIRS data. The techniques utilized by more than 10 studies were considered to be the most common. Therefore, the most common techniques in the motor control field were identified to be band-pass, low-pass, and high-pass filters, smoothing algorithms (moving average, Gaussian, Savitzky-Golay), wavelet filtering, and the general linear model (GLM).

Table 2: Processing Technique Usage

Processing Techniques	Used by
Band-pass, Low-pass, and High-pass filtering	Anwar et al. 2013; Banville et al. 2017; Batula et al. 2017a, 2017b; Brigadoi et al. 2012; Bruno et al. 2018; Buccino et al. 2016; Chen et al. 2017; Choi et al. 2019; Crivelli et al. 2018; de Lima-Pardini et al. 2017; Derosiere et al. 2014; Dresler et al. 2011; Ferrari et al. 2014; Fu et al. 2017; Funane et al. 2014; Gagnon et al. 2012; Groff et al. 2019; Harrison et al. 2018; Heinze et al. 2019; Herold et al. 2017, 2019; Holper and Wolf 2010, 2011; Holper et al. 2010, 2012, 2014; Holtzer et al. 2011, 2017, 2019; Hong and Naseer 2016; Hu et al. 2013; Khan et al. 2018; Kobashi et al. 2012; Koenraadt et al. 2012, 2013, and 2014; Koren et al. 2019; Kurz et al. 2012; Lachert et al. 2017; Lin et al. 2012, 2016; Lu et al. 2013, 2015, 2017; Lucas et al. 2019; Maidan et al. 2018; Mandrick et al. 2013; Mehnert et al. 2013; Mehta and Rhee 2017; Mirelman et al. 2014, 2017; Muthalib et al. 2016, 2018; Naseer and Hong 2013; Pfurtscheller et al. 2011; Pittaccio et al. 2013; Propper et al. 2017; Rosner and Barlow 2016; Seidel et al. 2017, 2019; Shibuya 2011; Shibuya et al. 2014; Shin et al. 2014; Stuart et al. 2019; Tempest et al. 2019; Vasta et al. 2017; Waldert et al. 2012; Willis et al. 2019; Wolf et al. 2011; Woorons et al. 2019; Wriessnegger et al. 2017, 2018; Yin et al. 2015; Yu et al. 2014
Smoothing (moving average, Savitzky-Golay filter, Gaussian weighted filter)	Amemiya et al. 2010; Anwar et al. 2013; Chacaroun et al. 2019; Funane et al. 2014; Gagnon et al. 2012; Holper and Wolf 2010; Jang et al. 2014; Koehler et al. 2012; Kim et al. 2017; Lachert et al. 2017; Sagari et al. 2015; Shin et al. 2014;

	Wriessnegger et al. 2018; Yeo et al. 2013; Yokoyama et al. 2019
Visual inspection	Beurskens et al. 2014; Holtzer et al. 2017, 2019; Lucas et al. 2019; Muthalib et al. 2018; Pittaccio et al. 2013; Shibuya et al. 2014; Vasta et al. 2017; Wriessnegger et al. 2017, 2018
Downsampling	De Lima-Pardini et al. 2017; Holper and Wolf 2011; Holper et al. 2010, 2012, 2014; Ishii et al. 2018; Kobashi et al. 2012; Yin et al. 2015; Zimmermann et al. 2013
Wavelet filtering	Beurskens et al. 2014; Bruno et al. 2018; Herold et al. 2019; Jang et al. 2014; Jin et al. 2018; Kim et al. 2017; Koren et al. 2019; Maidan et al. 2018; Mehta and Rhee 2017; Mirelman et al. 2014, 2017; Moro et al. 2016; Muthalib et al. 2015; Schurholz et al. 2012; Seidel et al. 2019; Stuart et al. 2019; Tempest et al. 2019; Yeo et al. 2013
PCA Filter	Harrison et al. 2018; Holtzer et al. 2011; Kurz et al. 2012; Lin et al. 2012; Lu et al. 2015
Independent Component Analysis (ICA) Filter	Holtzer et al. 2011
General Linear Model (GLM)	Bruno et al. 2018; de Lima-Pardini et al. 2017; Dresler et al. 2011; Gagnon et al. 2012; Hu et al. 2013; Huppert et al. 2013; Jang et al. 2014; Karim et al. 2012; Kim et al. 2017; Lu et al. 2013; Mehnert et al. 2013; Moro et al. 2016; Muthalib et al. 2015; Pittaccio et al. 2013; Rosso et al. 2017; Seidel et al. 2017, 2019; Tempest et al. 2019; Yu et al. 2014
Kalman filtering	Gagnon et al. 2012; Khan et al. 2018
Standard Deviation Cutoff	Beurskens et al. 2014; Rosner and Barlow 2016
Inverse Z-score	Zimmermann et al. 2013
Linear Interpolation	Fu et al. 2017; Lachert et al. 2017; Mehnert et al. 2013; Metzger et al. 2017; Yin et al. 2015
Spline Interpolation	Beurskens et al. 2014; Holper et al. 2012, 2014; Kobashi et al. 2012; Koren et al. 2019
Common Average Referencing (CAR)	Batula et al. 2017a, 2017b; Shibuya et al. 2016
Correlation-Based Signal Improvement (CBSI)	Batula et al. 2017b; Maidan et al. 2018; Metzger et al. 2017; Mirelman et al. 2017; Shin et al. 2014

Prewhitening	Huppert et al. 2013; Karim et al. 2012
Precoloring	Beurskens et al. 2014; De Lima-Pardini et al. 2017; Schurholz et al. 2012
Bayesian modelling	Brigadoi et al. 2012
Short-Separation Channel Regression	Gagnon et al. 2012; Koenraadt et al. 2014; Moro et al. 2016; Seidel et al. 2019

3.3 Processing Techniques and their Uses

3.3.1 General Filter Considerations

There are two general types of filters: Infinite Impulse Response (IIR), and Finite Impulse Response (FIR) filters. The mathematical equations for these two types of filters differ in their filter coefficients, which are calculated as the ratio between the sampling frequency of the system and the cutoff frequency of the filter (Winter 2009).

The FIR filter type has filter coefficients that are comprised of entirely inputs, whereas the IIR filter has filter coefficients that are comprised of both inputs and previous outputs of the filter. In this sense, the output of the IIR filter can be *recursive*, because it depends on both inputs and previous outputs (Winter 2009). FIR filters also have a linear phase, meaning that there is no phase distortion of the signal. IIR filters, however, have phase distortion, in that different frequencies have different levels of phase shift. This distortion can be avoided by using a zero-phase filter (Pinti et al., 2019). Pinti et al. (2019) suggest using a high-order (>1000) FIR filter in place of an IIR filter due to the problem of phase distortion. Additionally, because FIR filters always have a finite output for a finite input, they are considered inherently stable. IIR filters may not be stable, as the output could be finite or infinite (Ifeachor and Jervis 2002; Pinti et al., 2019).

Filter order is another important characteristic. The higher the order of a filter, the greater the slope of the filter at the cutoff frequency (see **Figure 2**; Winter 2009). In the filter's equation, the number of filter coefficients represents the filter order, which becomes greater as more coefficients are added. Consequently, filters with greater filter orders require more time to compute (Winter 2009). FIR filters need to be implemented with greater orders than IIR filters to get similar results (Pinti et al., 2019). Consequently, this also means that computers using FIR filters require a greater amount of time to compute the output of the filter, due to the greater number of terms in the equation.

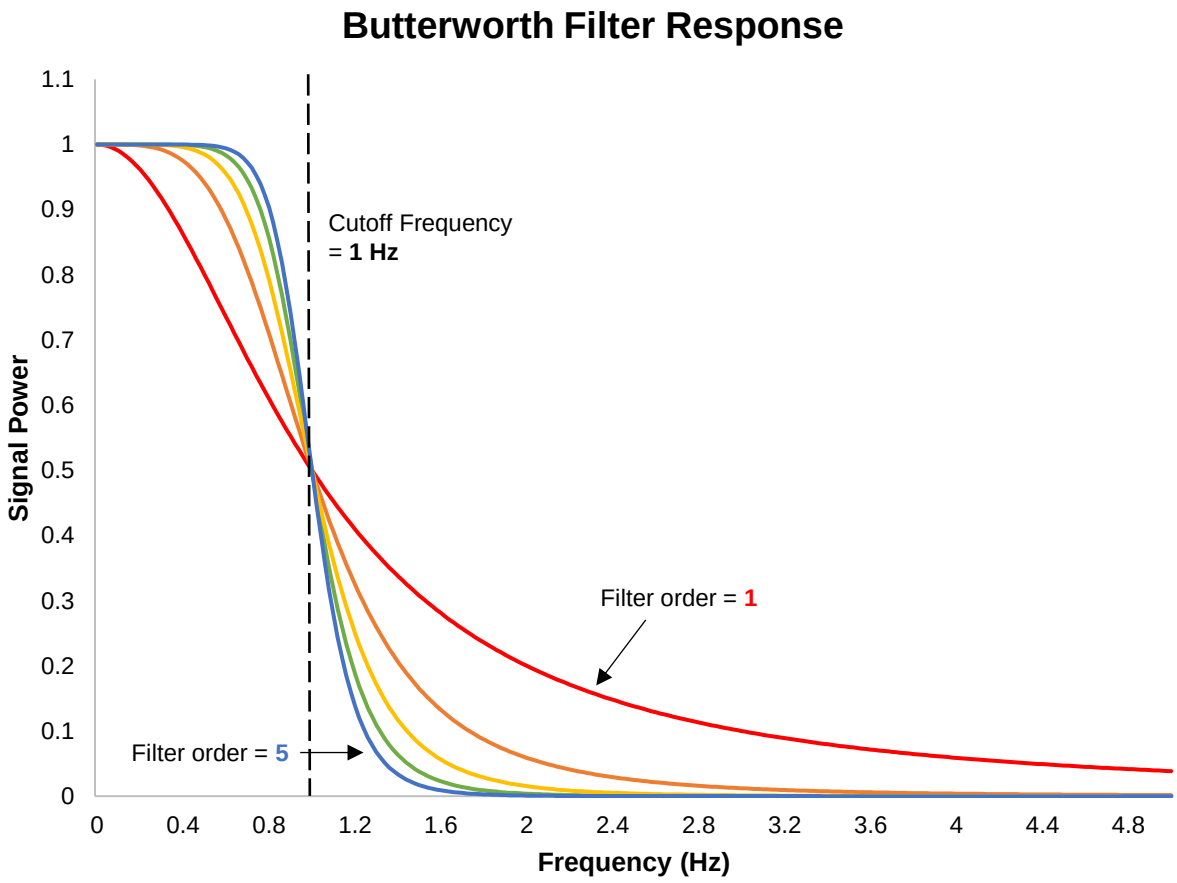

Figure 2: Figure depicting the magnitude-response of a low-pass Butterworth-type filter with a cutoff frequency of 1 Hz. Different colours represent different orders of filter. Red has a filter order of 1, orange has a filter order of 2, yellow has a filter order of 3, green has a filter order of

4, and blue has a filter order of 5. Higher order filters have steeper curves, and thus attenuate signals to greater degrees than lower order filters, except at the cutoff frequency. As signals increase in frequency, they are attenuated more, the degree to which is decided by filter design.

3.3.2 Low-pass, High-pass, and Band-pass Filters

A low-pass filter passes signals with a frequency lower than a selected cutoff frequency, and attenuates signals with frequencies higher than the cutoff frequency (Winter 2009). Similarly, a high-pass filter passes frequencies higher than a cutoff while attenuating lower ones. The band-pass filter passes frequencies within a certain band, while outside the band, frequencies are attenuated. In all of these filters, the passband describes the range of frequencies passed through the filter, whereas the stopband describes the range of frequencies that are attenuated.

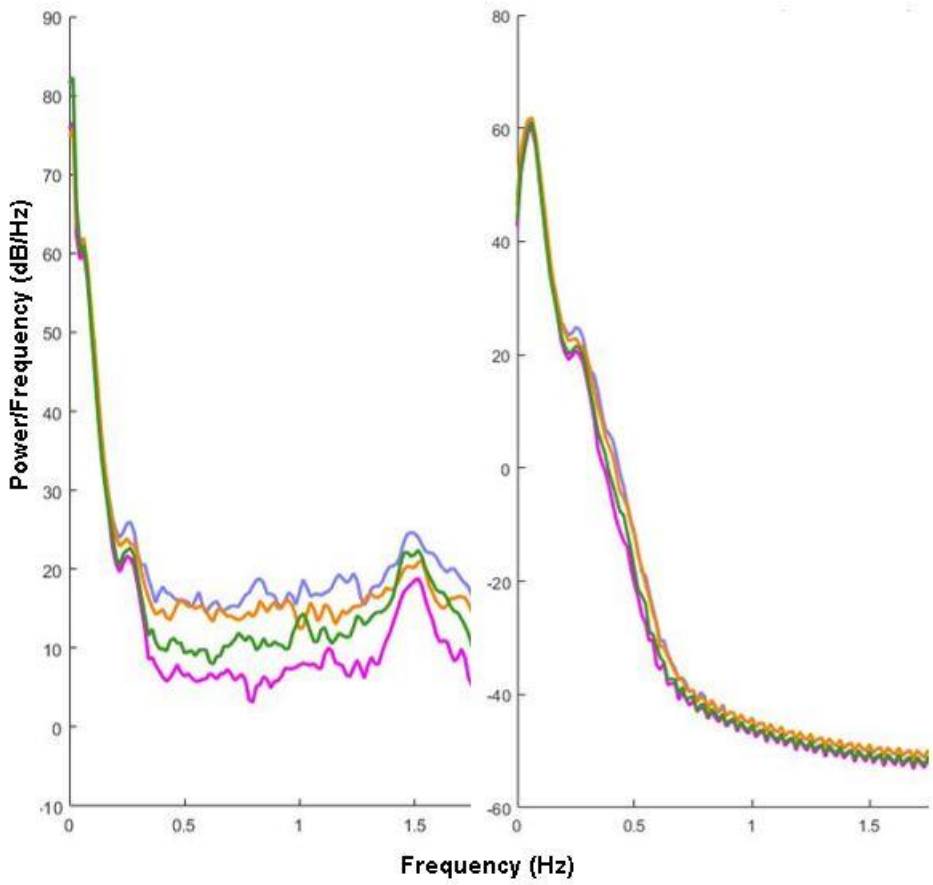

Figure 3: A comparison between FFTs of unprocessed oxygenated hemoglobin concentration data (**A**) and band-pass filtered data (**B**, 0.1-0.4 Hz, 3rd order IIR Butterworth filter). The x-axis represents frequency in Hz, and the y-axis represents power/frequency in dB/Hz. As can be seen, the higher frequencies in **A** (~1.5 Hz, presumably related to HR) are significantly reduced in power when the bandpass filter is applied (**B**). What is less noticeable but still of note is the reduction in power of very low-frequency oscillations (~0.01 Hz) from nearly 82 dB/Hz to ~42 db/Hz (**B**).

These techniques are used in fNIRS to attenuate high and low-frequency physiological and instrumental noise which are usually attributed to heart rate, respiration rate, extraneous light, and baseline drift. The low-pass filter is used to attenuate very high frequency noise arising from the environment such as extraneous light, and physiological noise such as heart rate and respiration. The high-pass filter is used to attenuate very low frequency oscillations, specifically those from baseline drift, which can arise from the gradual movement of the optodes on the scalp. The band-pass filter is a simple combination of a low-pass and high-pass filter, in that it passes a certain band of frequencies, and attenuates the frequencies located outside of the band, which are typically all of the sources of noise listed above.

To implement these filtering techniques, the type of filter, filter order, and cutoff frequency (or frequencies) must be chosen. There are many different subtypes of these filters, the most common being the different IIR filters such as Butterworth, Chebyshev Types I and II, and the Elliptic filters, as well as the FIR filter (Naseer and Hong 2015). **Butterworth** filters are designed to be maximally-flat-magnitude-response filters, in that frequencies in both the passband and the stopband experience the least distortion possible (Ifeachor and Jervis 2002). **Chebyshev Type I** filters are designed so that frequencies after the cutoff frequency are much more sharply attenuated and monotonic (flat), but this comes with the cost of the passband frequencies becoming slightly distorted (Ifeachor and Jervis 2002). **Chebyshev Type II** filters are designed in the opposite way to Type I, such that the passband is as monotonic (flat) as

possible, which then introduces distortion into the stopband (Ifeachor and Jervis 2002). **Elliptic** filters have "equiripple", or equal distortions in both the passband and the stopband, however, these filters also have the highest rate of attenuation of the different filters for the same order (Ifeachor and Jervis 2002).

When using these filters, differences in physiology between populations and individuals may necessitate the adjustment of filter parameters. For example, athletes have lower resting heart rate than non-athletes (Barak et al., 2011). In the case of a low-pass filter, the researcher would have to potentially lower the cutoff frequency to account for the lower resting heart rate of the athlete. For the higher resting heart rate of the non-athlete, the researcher could potentially use a higher cutoff frequency for the low-pass filter. Additionally, the type of task used can affect decisions as well. For example, heart rate and respiration rate increase during exercise vs. non-exercise motor tasks (Turner and Carroll 1985). Therefore, implementing a filter with a "one-size-fits-all" cutoff frequency is not ideal. In consideration of these factors, applying a fast Fourier transform (FFT) to an fNIRS dataset will allow the researcher to visually inspect the data and determine the spectral location of noises for a particular dataset. In light of these considerations, general recommendations exist for filter parameters. Naseer and Hong (2015) for example, recommend a passband of 0.1~0.4 Hz to remove most physiological and instrumental noises from fNIRS data if the task period is 10 seconds in length. Many other passbands have been used by fNIRS researchers (ex. 0.01-0.2 Hz, Heinze et al., 2019; 0.01-0.5 Hz, Anwar et al., 2013) but no explanations are given for the parameters beyond the basic reasons for usage of a filter.

These filters are quick and easy to implement, and are included in most fNIRS processing programs such as HOMER2 (Huppert et al., 2009). As well, filtering techniques like these can be

useful since the frequencies related to physiology are usually known (Naseer and Hong 2015). However, some researchers disagree with this notion and instead suggest that frequency characteristics can vary across time, location on the head, and participant (Duan et al., 2018). Additionally, some types of simple filters produce “ripples”, which affect the signal amplitudes of certain frequencies in the passband and/or the stopband (Ifeachor and Jervis 2002). As a result, some cortical data may be distorted, or some frequencies in the stopband may not be attenuated. Another related aspect of these filters is that frequencies in the stopband are not completely removed, but instead are only attenuated (Naseer and Hong 2015), still allowing some noise to pass through the filter. Even if noise does not penetrate the filter due to incomplete attenuation, some physiological noise (i.e. Mayer waves, resulting from changes in blood pressure) can overlap in frequency with the cortical signal (Duan et al., 2018), rendering the filter unable to completely remove noise while preserving signal. As such, other processing techniques have been created to better distinguish physiological noises from the cortical signal of interest, such as short-separation channel regression. Finally, with improper use of these filters, the cortical response may be affected. For example, if the cutoff frequency is set to remove noise in the range of the hemodynamic response (~0.15 Hz for a 10 s task; Ferrari and Quaresima 2012), the user risks affecting a portion of the response itself, either by attenuation or amplification of certain frequencies (Duan et al., 2018).

In sum, low-pass, band-pass, and high-pass filters are all simple noise-filtering techniques that are employed to attenuate high and/or low frequency noise in fNIRS. Many different types and subtypes of these filters exist, which may distort noise or data depending on the type. Types of filter (IIR or FIR) can also differ in their time requirement for computation, which may affect

decisions for usage in online scenarios. Individual physiological differences can also affect usage of these techniques, particularly regarding the cutoff frequency.

3.3.3 GLM

The GLM is a method of statistical modelling for fNIRS data. It has previously been used to model the fMRI BOLD response (Monti 2011), and has thus been adopted due to the similarity between the hemodynamic responses from the two types of systems. The GLM utilizes predictors to describe the largest sources of variability within the fNIRS data (Monti 2011). For example, the researcher would input their task timings into the model, along with the predictor that describes the hemodynamic response, either through estimation or assumption of the shape of the hemodynamic response function. Some studies model the hemodynamic response with a linear combination of gamma functions as a predictor (ex. de Lima-Pardini et al., 2017, Dresler et al., 2011, Jang et al., 2014, etc.) assuming the shape of the hemodynamic response function. Other studies use a deconvolution procedure (ex. Moro et al., 2016), which estimates the hemodynamic response with a series of gaussian functions spaced in increments along the task period.

In its simplest form, the GLM is represented by a linear equation (see **Equation 1**), in which the amplitude of the hemodynamic response in one channel (Y) is equal to the predictor (X) multiplied by the "weight" of that predictor (β) plus the error term (ε).

$$Y = X\beta + \varepsilon \quad (1)$$

Predictors are given weight in the model in regard to how much that predictor contributes to the variability of the signal. In other words, if the researcher's estimate/assumption of the

shape of the hemodynamic response is correct, then that estimate will be given a higher weight by the model. The error term in the equation represents all noise in the recording, consisting of physiological, instrumental, and motion noise.

The GLM has assumptions regarding the data and the noise in the system. These assumptions are as follows (Monti 2011):

1. Task responses are non-stochastic (non-random), and are the same across trials of the same task.
2. Noise is independently and identically distributed, with a mean of zero and with some amount of variance around that point.
    a. Noise is homoscedastic, meaning there is noise from only one distribution in the data.
    b. Noise is not serially correlated, meaning that past noise does not affect future noise.
3. Predictors are not linear derivations of each other.

To use this technique, a researcher would need to decide on the method of inference/estimation of the hemodynamic response. As mentioned above, many fNIRS studies assume the shape of the hemodynamic response with canonical gamma functions. Different convolutions of gamma functions are used to assume the shape of the canonical hemodynamic response (Tak and Ye 2014). While this method of the GLM is useful if the shape of the response is already known, assuming the shape could potentially lead to modelling errors as the response can change between recordings (Hoshi 2007). Another potential method is deconvolution (Monti 2011), which instead estimates the shape of the hemodynamic response. After the method is chosen, the predictors are put into the GLM, which then estimates the

weights of each of the predictors (i.e. how much they contribute to variability), and if they are significantly different from zero (Monti 2011). Some programs, like Homer2, have additional parameters to control such as the option to include short-separation channels as predictors or the option to change the GLM solving method (Huppert et al., 2009).

An additional consideration for the GLM is that the researcher can avoid the uncertainty of the DPF (Tak and Ye 2014), a term used to correct for the extra distance that NIR light travels in the cortex due to light scatter from biological tissues (Kamran et al., 2018). The DPF is a highly variable parameter because it can change between different ages and populations of participants (Duncan et al., 1996), as well as between brain regions (Zhao et al., 2002). Group-analysis of fNIRS data can also be easily completed using a multi-level GLM analysis (Tak and Ye 2014). However, fNIRS data seems to violate many of the GLM assumptions, particularly regarding the contents of the noise (Monti 2011). Motion artifacts and systematic physiological noise violate the assumption that noise is independent (Barker et al., 2013), and thus lead to biased results from the GLM. Specifically, noise comes from multiple distributions, and is not independently distributed (Huppert 2017).

To summarize, the GLM is a statistical technique used to model the cortical signal recorded with fNIRS. It is simple and effective, as it assumes the recording is simply the linear combination of multiple regressors, representing task-related cortical signal and task-unrelated noise. The GLM also has multiple assumptions, of which fNIRS violates many. However, with proper removal of noise-related artifacts, assumptions can be met and therefore the true hemodynamic response can be assessed.

3.3.4 Wavelet Filter

Wavelet filters are used to filter out different types of noise, but mostly spike motion artifacts (Molavi and Dumont 2012). Wavelet filtering is based on the premise that cortical signal is comprised of different frequencies than motion artifacts (Molavi and Dumont 2012). Wavelet filtering begins with the base mother wavelet, which is scaled and translated to create daughter wavelets (Gurley and Kareem 1999). The fNIRS recording is then decomposed using these daughter wavelets. Wavelet coefficients (expressions) then describe how well the wavelet transform describes the fNIRS recording. The greater the number of wavelet coefficients, the better the wavelet transform can represent the full signal. These wavelet coefficients are organized into a distribution, associated with the scaling and translation parameters (Gurley and Kareem 1999). Motion artifacts are considered to be outliers in this distribution because of their differences when compared to cortical signal, and can be removed as such (Molavi and Dumont 2012).

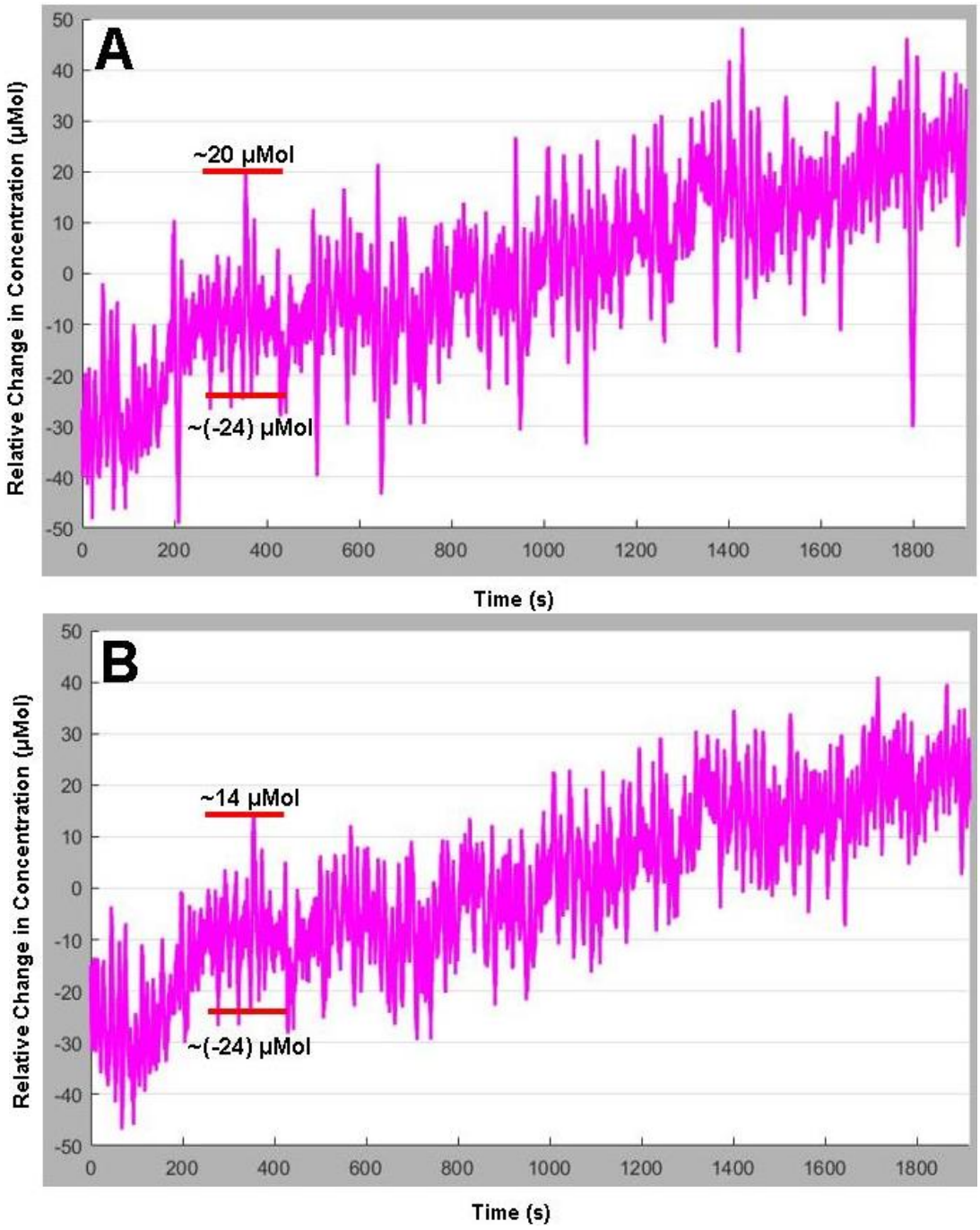

Figure 4: A comparison between unprocessed oxygenated hemoglobin concentration data (**A**) and data filtered with a discrete wavelet transform (IQR = 1.5; Molavi and Dumont 2012). The x-axis represents time in seconds, and the y axis represents relative change in oxygenated hemoglobin concentration in micromolar. A positive spike at ~350 s is first at an amplitude of ~20 µMol in graph **A**, however once filtered it was reduced to an amplitude of ~14 µMol in graph **B**. Additionally, the negative spike very close to the positive spike doesn't seem to change from **A** to **B**, however the signals producing this spike may be inside the IQR of 1.5.

There are different types of wavelet transforms, including the discrete wavelet transform (DWT; Robertson et al., 2010), the continuous wavelet transform (CWT; Sato et al., 2006b), and the minimum-description-length wavelet (wavelet-MDL), which is a specific DWT for reducing global physiological trends (Jang et al., 2009). All wavelet transforms are derived from a mother wavelet, which is scaled and translated to produce the daughter wavelets (Ifeachor and Jervis 2002). The difference between the CWT and the DWT lies in the manner that daughter wavelets are derived from the mother wavelet.

Daughter wavelets in the DWT are derived based on specific methods, in other words by *discretizing* the scale, translation, time, and setting parameters of the mother wavelet (Ifeachor and Jervis 2002). For example, powers of 2 could be used to scale and translate a mother wavelet (Robertson et al., 2010). In DWTs, the number of wavelet coefficients required for full representation of the original signal is the same as the number of time points in the dataset. The discrete wavelet-MDL detrending algorithm can be used to remove spike motion artifacts, as well as global trends in the data related to physiological activity (Jang et al., 2009). It does this by estimating the number of wavelet coefficients required to fit the wavelet transform to the data, and then using the minimum number. In other words, if there are many different but viable ways to describe the data, use the simplest way (Jang et al., 2009).

In the CWT, there is less of a restriction on scaling and time shifting factors for the daughter wavelets than in the DWT (Ifeachor and Jervis 2002). The daughter wavelets can consist of any combination of dilations and translations of the mother wavelet. This means that redundancies may arise from CWTs due to oversampling, however the flexibility of the scaling and translation parameters can make small changes in the data easier to interpret if used to greater extents (Gurley and Kareem 1999). Consequently, the number of wavelet coefficients

that may be used to describe the full signal in the CWT is much greater than the number of time points in the signal.

Generally, the utilization of the wavelet technique requires the researcher to not only choose which type of wavelet transform to apply (Discrete, Continuous), but also which mother wavelet to use and the scaling and translation parameters for the daughter wavelets. There are many different mother wavelets to choose from. For example, the wavelet transform described in Molavi and Dumont (2012) designed specifically for fNIRS data uses the Daubechies mother wavelet (Daubechies 1988). Once the scaling and transformation parameters are chosen for all wavelets, the wavelets are compared to the fNIRS data, and the data is decomposed into wavelet coefficients using the daughter wavelets. The decomposition allows for different frequencies in the original signal to be seen at different times, at which point frequency components relating to motion can be removed (Robertson et al., 2010). The wavelet coefficients, formed from the different daughter wavelets and their interactions with the data, are assumed to form a gaussian probability distribution (Brigadoi et al., 2014). In this distribution, wavelet coefficients around the zero mean with low variability are assumed to represent the slow frequency hemodynamic response, while those around the edges describe the highly variable, high frequency motion artifacts. The probability threshold, α, is then set by the researcher to know which wavelet coefficients to remove from the distribution; i.e. if a coefficient does not meet the probability threshold, then it is labeled an artifact and is decreased in signal amplitude (Brigadoi et al., 2014). After the outliers are reduced in signal amplitude, the rest of the coefficients are combined to form the original waveform, without artifacts (Molavi and Dumont 2012).

This method of filtering relies on the assumption that motion artifacts oscillate much faster in time than fNIRS hemodynamic signals (Molavi and Dumont 2012). As such, motion

artifacts that result from slower movements over time are not identified by this filter. As well, the type of motion artifact present in the researcher's fNIRS data may depend on the population. For example, young infants are known to move even in their sleep and cannot be instructed to keep still (Sato et al., 2006b). Additionally, infants are known to make spontaneous movements if the duration of the stimulus is longer (Aslin and Mehler 2005). These spontaneous movements are likely to result in fast changes of the hemodynamic signal, in the form of baseline shifts or spike artifacts. Adults, on the other hand, may be less likely to produce motion artifacts considering the simple fact that they can be instructed not to move outside the confines of the task presentation. Wavelet transforms are useful in that they can localize fast signal changes and can separate the signal into different frequencies at different times, which allows for the removal of solely motion-related components. However, they are not good for removing artifacts with slower oscillations (Robertson et al., 2010). With improper usage, motion artifacts are not removed efficiently from the data. Specifically, if the threshold criterion is too strong or weak for motion artifact removal, the researcher risks removing too much signal or too little artifact.

In summary, wavelet filters involve the decomposition of an fNIRS recording into its constituents. This technique is useful for removing motion artifacts and physiological noise, depending on the type of wavelet filter used. The two types of wavelets are continuous and discrete wavelet transforms, which decompose the fNIRS recording based on non-discretized or discretized wavelet parameters, respectively.

3.3.5 Smoothing Filters

This technique is most frequently used to decrease the presence of high-frequency noise in fNIRS data. Smoothing filters can thus be considered to be a type of low-pass filter. However, the difference is the method by which smoothing filters reduce high-frequency noise. For example, the moving average filter smooths signals by averaging neighboring points and using that average as the new value of a point (Kawala-Sterniuk et al., 2020). In the low-pass filter, however, lower frequencies are passed and higher frequencies are specifically attenuated. There are many different types of smoothing algorithms, some of the most common in our search being the moving average (ex. Amemiya et al., 2010, Button et al., 2015, Groff et al., 2019, etc.), Gaussian smoothing (ex. Chacaroun et al., 2019, Funane et al., 2014, Kim et al., 2017, etc.), and Savitzky-Golay smoothing filters (ex. Holper and Wolf 2010, Shin et al., 2014).

Signals can be smoothed in different ways, some being in the time domain, and some being spatial smoothing. Time domain smoothing reduces the contribution of high-frequency noise in the data, whereas spatial smoothing averages signals from poor channels with the surrounding fNIRS channels, reducing the effect of the noisy channel while still preserving some of its signal (Wriessnegger et al., 2018). The moving average type of smoothing works by averaging a number of data points together, reducing high-frequency fluctuations (Mivule and Turner 2014). Gaussian smoothing involves a Gaussian weighting function, which multiplies the value of each point according to where it is on the distribution. The center of the Gaussian is set on one point, which is weighted along with the neighboring points. The distribution is then moved to the next point and the process is repeated (Ye et al., 2009, Khan et al., 2018). Savitsky-Golay smoothing is mostly employed to smooth over spike motion artifacts (Savitzky and Golay 1964). It can also be used to smooth physiological noise in data, however the reasons for why

this filter is appropriate are unclear in this circumstance (Rahman et al., 2019). This type of filter uses a least-squares polynomial to fit the fNIRS data within a certain window, while preserving some higher frequencies (Nguyen et al., 2013). For more detail on the specific mathematics of this filter, see Savitzky and Golay 1964.

To smooth fNIRS data, the type of smoothing filter needs to be chosen. This choice will depend on the specific requirements for the filter. The moving average filter replaces values based on the average of neighboring data points (Kawala-Sterniuk et al., 2020). This is the 'classic' smoothing filter. To use this filter, one needs to decide on a window around the point they wish to average. Many fNIRS studies (ex. Button et al., 2015, Groff et al., 2019, Harrison et al., 2018, Herold et al., 2017, etc.) appear to use a five second window to smooth data. It is unclear why these studies use specifically five seconds, as no reasons were given for the chosen parameter. Once the window is chosen, applying the filter requires computational processing for each data point. Gaussian smoothing is implemented much like the moving average filter, only the neighboring points around the point of interest are weighted according to a Gaussian distribution, instead of merely averaged (Khan et al., 2018, Ye et al., 2009). The Savitzky-Golay filter uses a polynomial fitting function to approximate the values of the fNIRS waveform within a specific time window (Savitzky and Golay 1964). The fitting is performed with a least-squares fitting function of $2n + 1$, where n is the number of neighboring samples in the window and can be equal or greater than the order of the polynomial (Jahani et al., 2018). Jahani et al. (2018) suggest choosing an n less than the number of samples (time points) of the hemodynamic response, otherwise the response may be smoothed itself.

There is not much information regarding considerations for smoothing techniques; however, these techniques are similar to low-pass filtering in that they "smooth over" high-

frequency spikes in the data. In contrast, smoothing techniques do not account for the frequency components of the noise like low-pass filters – they operate in the time or spatial domains. In this sense, smoothing techniques do not account for particular frequency-related aspects of the signal and noise. However, this may be seen as a positive aspect of smoothing algorithms, as they do not assume certain frequencies only represent noise. As learned from the implementation of smoothing filters in Electroencephalography (EEG), smoothing a signal too strongly can have adverse effects (Kawala-Sterniuk et al., 2020). In the case of fNIRS, the hemodynamic response may become distorted and less obvious in the time course of the experiment.

3.4 Discussion

The purpose of this chapter was to identify the most common fNIRS processing techniques in the motor control field, and to describe them in terms of their uses, methodologies, and methodological considerations. The most common techniques were identified as band-pass, low- and high-pass filtering, wavelet filtering, the GLM, and smoothing filters. The following topics will be discussed below: considerations regarding the development of a processing stream, and basic descriptions of less common techniques that may be useful.

When choosing techniques for a processing stream, it is important to always take the specific characteristics of the fNIRS dataset into account. For example, if the dataset does not include spike motion artifacts, utilizing a wavelet filtering technique is illogical as it specifically removes those artifacts (Molavi and Dumont 2012). Further, both physiological and motion characteristics can change between individuals, populations, tasks, and brain regions (Duncan et al., 1996; Zhao et al., 2002; Duan et al., 2018, Sato et al., 2006b). Therefore, the processing

stream should be personalized for each dataset to account for differences in physiological, motion, and instrumental noise, and variation in fNIRS responses to different tasks.

The improper use of a technique results in the distortion of the fNIRS response (ex. Over-smoothing fNIRS data; Kawala-Sterniuk et al., 2020), or the incomplete removal of noise (ex. Low-pass filtering with a high cutoff frequency). The creation of a processing stream particular to the researcher's dataset thus requires an in-depth knowledge of the different processing techniques available, as well as their parameters and methodologies. Additionally, knowledge of the different techniques is important for the assessment of other studies in the field. For example, the researcher can assess the validity of other studies based on their processing stream. This particular aspect is important for the progression of the field, as it ensures that high-quality research is being done, in both the researcher's own work and others.

There are many different fNIRS processing techniques available to use, and the most common techniques may not be the best to use. For example, band-pass, low and high-pass filters could be replaced with short-separation channel regression which has been shown to be effective in reducing physiological noises (Saager and Berger 2005; Yamada et al., 2009). This technique is used to regress physiological noises from the scalp and cerebrospinal fluid out from channels containing physiological noises and hemodynamic activity, so that the only signals left correspond to actual hemodynamic activity. Short-separation channel measurements are available with many devices, such as those from Artinis, Hitachi, TechEn, and other companies. Another relatively uncommon technique is prewhitening. Barker et al. (2013) describe an autoregressive prewhitening filter that can be applied to data as a part of the GLM. In this method, the frequency composition of the noise term is estimated, and a prewhitening filter is then designed specifically for that noise. This process is then repeated until the noise has been

whitened, meaning that no one frequency is represented over any others in the noise – all frequencies have similar power. Finally, a replacement technique for wavelet or smoothing filters may be something like spline interpolation in combination with a Savitzky-Golay filter (Jahani et al., 2018). This technique was found to reduce the contributions of baseline shifts and spikes in fNIRS data better than some other motion correction techniques like wavelet filtering and CBSI, with a lower processing time.

3.5 Conclusions

In this chapter, some common and uncommonly used fNIRS processing techniques were reviewed in terms of methodology, and considerations for usage. Processing was mostly limited to the use of a few common techniques (i.e. band-pass filtering), although these techniques may not be the best to use for all researchers. FNIRS contains different types of noise in comparison to other neuroimaging modalities, requiring the implementation of specific techniques to process such noise. As well, processing should account for differences in the noise due to time, ROI, and population. The information in this chapter may benefit the field by providing some insight on the usage of common techniques, and some replacements for those techniques to new fNIRS researchers. In the future, the information in this chapter may help to provide a basis for choosing standard fNIRS processing techniques.

Chapter 4: General Discussion and Conclusions

There were two goals of this thesis. The first goal was to explore lower limb complexity modulation using fNIRS. The second goal was to develop the use of fNIRS technology in the Neurophysiology and Neuroimaging lab. To attain the first goal, I performed an experiment in which fNIRS was recorded while participants engaged in ankle dorsiflexion force-tracking. The second goal was pursued through performing a comprehensive review on processing techniques in fNIRS. This general discussion will explore the implications, significance, limitations, and future directions of the work.

4.1 Experiment 1

4.1.1 Experiment 1 Summary

I conducted a study to investigate the effects of a complexity-modulated lower limb force tracking motor task on hemodynamic activity, particularly in the TA motor representation. No statistically significant activations except one were found over the TA motor representation when participants engaged in a simple versus complex force tracking task. This was possibly due to the depth of the TA representation within the central sulcus. Complexity-modulated upper limb tasks elicit differential activations in the motor cortices (Leff et al., 2011), however, the question of whether complexity modulated lower limb tasks can alter cortical hemodynamic responses thus remains unanswered. However, channels overlying areas thought to be preSMA/SMA and STG/SII produced significant increases in HbO activity. These areas, and thus the associated activations, are thought to be related to motor learning (Hatakenaka et al., 2007) and sensory integration (Tachibana et al., 2011), respectively.

4.1.2 Implications

There are many implications for this thesis in the field of fNIRS. The lack of hemodynamic activity in the TA motor region for most participants potentially indicates that fNIRS is incapable of detecting activity from this area, unlike activity induced by upper limb tasks. Consequently, this result may drive researchers to consider the results of their own lower limb fNIRS studies more closely. Specifically, similar studies such as Pittaccio et al. (2013) and Koenraadt et al. (2012) reported fNIRS activations from the medial motor cortices during lower limb tasks, but did not statistically evaluate these activations. To overcome this limitation, lower limb fNIRS studies must recruit greater numbers of participants to allow for a true statistical evaluation of lower limb hemodynamic signals. However, if these lower limb signals cannot be identified after this assessment, researchers may look to other avenues for study, or may study the TA motor representation with different neuroimaging methods. The present study is also important for basic knowledge regarding complex and simple motor tasks. This area of research is mostly dominated by upper limb studies, with few lower limb studies. As such, it is not known if complex and simple lower limb tasks induce activation in the same way as activations induced by the upper limb. This information would be vital for future research involving lower limb neurorehabilitation, as the same principles applied to upper limb neurorehabilitation may be insubstantial in this circumstance.

4.2 Processing Review

4.2.1 Processing Review Summary

I conducted a review of fNIRS processing techniques to investigate the current state of the literature and to provide a processing guide for new fNIRS researchers. The most common fNIRS processing techniques were identified from 100 fNIRS motor studies and were subsequently explained in terms of their methodologies and considerations for usage. Common techniques were identified as low-pass, band-pass, and high-pass filters, wavelet filters, smoothing filters, and the GLM. Less common alternatives to these techniques were also provided.

4.2.2 Implications

The processing review has one main implication for fNIRS. Processing streams are very important for the outcome of a study, as they can completely change the results. Some fNIRS researchers thus have completed studies comparing and contrasting different processing techniques (for example, Brigadoi et al., 2014; Jahani et al., 2018). However, these studies do not usually explain the techniques in a way that newer researchers would understand. Further, few of these studies provide in-depth information on how to use the techniques, which is very important for newer fNIRS researchers. In this review, many common techniques were identified from the literature. Importantly, these techniques, although common, were not necessarily the most appropriate options. As such, researchers should take care to choose techniques to use not because they were used by other labs, but because they are appropriate for their dataset.

4.3 Limitations and Challenges

This thesis has provided important information regarding complexity modulated force-tracking in the lower limb, however it is not without its limitations. Anatomical variations can contribute to variability within fNIRS data, as well can human error in the positioning of the cap. No MRI data was collected from participants, therefore anatomical differences between participants were not recorded except for differences in head circumference. This data would have allowed me to personalize certain characteristics of the fNIRS processing stream for each participant, potentially reducing variability in results. As well, the machinery available to us was limited in that it was not capable of short-separation channel measurements. Short-separation channel regression is thought to be the current gold standard for removal of physiological noises from fNIRS data as the noise is directly measured (Saager and Berger 2005; Zhou et al., 2020). As such, the machine's incapability of providing this data for us affected our choices for elements of the processing stream. However, the processing stream we developed for the present study was unbiased, as it utilized an autoregressive prewhitening procedure that utilized statistics to remove physiological noise, along with an iterative reweighted least squares estimation to remove motion noise (Huppert 2016). Another limitation of this work was that the "Random" waveforms were handmade, and as such were not truly random, but instead pseudorandom. Thus, some waveforms may have been more difficult/easier to track than others. However, there will always be a degree of subjectivity when creating the waveforms, as truly random waveforms may be extremely difficult to track. Future research may involve creating an algorithm that chooses characteristics of the waveform at random within certain bounds. For example, a waveform may be created to have an average frequency of 2 Hz with a certain level of variance around that frequency. This work may have also been limited in that twitch interpolation was not

used, and as such there was no objective confirmation that participants were fully activating their TA muscle during the MVF recording. This may have introduced additional variability into the data as participants may not have been attempting the task to the fullest extent of their ability. Another potential limitation is that different participants may have become fatigued at different rates, and thus this may have affected the signals obtained from the task by providing different relative levels of difficulty between participants. Regarding statistics, p-values were not Bonferroni-corrected due to the exploratory nature of the experiment. Consequently, the family-wise error rate may have been inflated. A final limitation of this work is the small sample size of five participants. Further data collection could not proceed due to the Covid-19 pandemic. This limits the data in that group statistics may not be performed, and the data collected may not convey the true activity present within the healthy population. Nonetheless, the exploratory nature of the present study provides a glimpse into not only lower limb complexity modulation, but also general lower limb fNIRS studies.

4.4 Future Directions

The investigation of similar lower limb tasks may be warranted using fNIRS due to the results of the present study, as the question of fNIRS detecting lower limb complexity modulation remains unanswered. Some previous lower limb fNIRS studies investigating similar muscles to the present study have not statistically analyzed their data, and thus this information would help to clarify whether the lack of TA motor activation in the present study is a true result. Additionally, future studies may investigate lower limb muscles with motor representations closer to the surface of the scalp. Consequently, this information may change the way lower limb fNIRS research is conducted, in that lower limb fNIRS research may become limited to certain

tasks or muscles. Another future direction of this work lies in adding other control conditions to elucidate activations from purely perceptual components of the task, and activations from purely motor components. These control conditions could be called “Motor Only” and “Visual Only”, and could also be implemented in a pseudorandom order like the present study.

The force-tracking task created in the present study has many applications. Namely, this task could be used for diagnostic and/or neurorehabilitation purposes. For diagnostics, muscular function could be analyzed with the participant’s performance on the task while changing different aspects, including fine motor control, muscular endurance, and muscle power. However, the diagnostic assessment may be more valuable to connect with neuroimaging measures, as changes in motor cortex organization may not translate to changes in task performance (Shadmehr and Holcomb 1997). As such, the utility of the task may depend on the manner in which it is used, or its combination with neuroimaging methods like fNIRS.

More importantly, this force-tracking task could potentially be used in neurorehabilitation due to the wide range of characteristics that can be altered to change the difficulty and the motor control elements required to complete the task. For example, the difficulty of the task could be slowly increased as an SCI patient regains muscular function. Difficulty may be increased in a number of ways, including providing more unpredictable waveforms, increasing the intensity or frequency of the waveforms, or possibly by changing the wave shapes. As well, altering these characteristics in certain ways may change with the goal of the task. For example, the amount of time that participants perform the task may be increased to train muscular endurance. Additionally, participants may be required to perform underneath a certain error threshold to train fine motor control. This may be a more space efficient and less expensive method than using some other neurorehabilitation equipment, while also being safer for the patient since they

do not need to stand. To improve upon the task, future researchers may develop a waveform generator to objectively produce waveforms for participants to complete. This waveform generator would have multiple characteristics for a researcher to change, such as the frequency of the waveform, amplitude range, and the variability of the peaks and troughs. This development would allow researchers to continuously and effortlessly produce reliably different waveforms while preserving control over aspects like difficulty.

Regarding processing techniques, developing a true comprehensive guide for researchers may be essential, as there is no one-size-fits-all technique at the moment that can address all noise issues with fNIRS data. Such a technique or set of techniques would address not only physiological and motion noise, but also variability between different populations of participants and recordings within participants. Further, future researchers should be encouraged to examine all processing techniques when choosing a processing stream, as many uncommon techniques may provide better-suited processing for their dataset than some more common techniques. This small change in the way researchers conduct their processing may benefit the field enormously by ensuring the production of high-quality science.

More studies are required to compare the efficacies of fNIRS processing techniques, especially more uncommon processing techniques. These studies would provide future researchers with the background needed to make informed decisions about their processing streams. As well, the creation of new techniques and the improvement of older techniques is constantly needed to ensure that fNIRS is optimized for future research.

4.5 Conclusions

This thesis has explored the potential for complexity modulation research in the lower limb. Due to a limited dataset, no conclusions can be made at this time. Nonetheless, the present study has shown that fNIRS may not be capable of detecting hemodynamic activations from the TA motor representation using specific lower limb motor tasks.

References

Amemiya, K., Ishizu, T., Ayabe, T., & Kojima, S. (2010). Effects of motor imagery on intermanual transfer: a near-infrared spectroscopy and behavioural study. *Brain research*, *1343*, 93-103.

Anson, M. L., & Mirsky, A. E. (1930). Hemoglobin, the heme pigments, and cellular respiration. *Physiological Reviews*, *10*(3), 506-546.

Anwar, A. R., Muthalib, M., Perrey, S., Galka, A., Granert, O., Wolff, S., ... & Muthuraman, M. (2013, July). Comparison of causality analysis on simultaneously measured fMRI and NIRS signals during motor tasks. In *2013 35th Annual International Conference of the IEEE Engineering in Medicine and Biology Society (EMBC)* (pp. 2628-2631). IEEE.

Anwar, A. R., Muthalib, M., Perrey, S., Galka, A., Granert, O., Wolff, S., ... & Muthuraman, M. (2016). Effective connectivity of cortical sensorimotor networks during finger movement tasks: a simultaneous fNIRS, fMRI, EEG study. *Brain topography*, *29*(5), 645-660.

Asahara, R., & Matsukawa, K. (2018). Decreased prefrontal oxygenation elicited by stimulation of limb mechanosensitive afferents during cycling exercise. *American Journal of Physiology-Regulatory, Integrative and Comparative Physiology*, *315*(2), R230-R240.

Asahara, R., Endo, K., Liang, N., & Matsukawa, K. (2018). An increase in prefrontal oxygenation at the start of voluntary cycling exercise was observed independently of exercise effort and muscle mass. *European journal of applied physiology*, *118*(8), 1689-1702.

Aslin, R. N., & Mehler, J. (2005). Near-infrared spectroscopy for functional studies of brain activity in human infants: promise, prospects, and challenges. *Journal of biomedical optics*, *10*(1), 011009.

Banville, H., Gupta, R., & Falk, T. H. (2017). Mental task evaluation for hybrid NIRS-EEG brain-computer interfaces. *Computational intelligence and neuroscience*, *2017*.

Barak, O. F., Ovcin, Z. B., Jakovljevic, D. G., Lozanov-Crvenkovic, Z., Brodie, D. A., & Grujic, N. G. (2011). Heart rate recovery after submaximal exercise in four different recovery protocols in male athletes and non-athletes. *Journal of sports science & medicine*, *10*(2), 369.

Barker, J. W., Aarabi, A., & Huppert, T. J. (2013). Autoregressive model based algorithm for correcting motion and serially correlated errors in fNIRS. *Biomedical optics express*, *4*(8), 1366-1379.

Batula, A. M., Kim, Y. E., & Ayaz, H. (2017a). Virtual and actual humanoid robot control with four-class motor-imagery-based optical brain-computer interface. *BioMed research international*, *2017*.

Batula, A. M., Mark, J. A., Kim, Y. E., & Ayaz, H. (2017b). Comparison of brain activation during motor imagery and motor movement using fNIRS. *Computational intelligence and neuroscience*, *2017*.

Beurskens, R., Helmich, I., Rein, R., & Bock, O. (2014). Age-related changes in prefrontal activity during walking in dual-task situations: a fNIRS study. *International journal of psychophysiology*, *92*(3), 122-128.

Brigadoi, S., Cutini, S., Scarpa, F., Scatturin, P., & Dell'Acqua, R. (2012). Exploring the role of primary and supplementary motor areas in simple motor tasks with fNIRS. *Cognitive processing*, *13*(1), 97-101.

Brigadoi, S., Ceccherini, L., Cutini, S., Scarpa, F., Scatturin, P., Selb, J., ... & Cooper, R. J. (2014). Motion artifacts in functional near-infrared spectroscopy: a comparison of motion correction techniques applied to real cognitive data. *Neuroimage*, *85*, 181-191.

Bruno, J. L., Baker, J. M., Gundran, A., Harbott, L. K., Stuart, Z., Piccirilli, A. M., ... & Reiss, A. L. (2018). Mind over motor mapping: Driver response to changing vehicle dynamics. *Human brain mapping*, *39*(10), 3915-3927.

Buccino, A. P., Keles, H. O., & Omurtag, A. (2016). Hybrid EEG-fNIRS asynchronous brain-computer interface for multiple motor tasks. *PloS one*, *11*(1), e0146610.

Button, C., Croft, J. L., Cotter, J. D., Graham, M. J., & Lucas, S. J. (2015). Integrative physiological and behavioural responses to sudden cold-water immersion are similar in skilled and less-skilled swimmers. *Physiology & behavior*, *138*, 254-259.

Chacaroun, S., y Gonzalez, I. V. E., Flore, P., Doutreleau, S., & Verges, S. (2019). Physiological responses to hypoxic constant-load and high-intensity interval exercise sessions in healthy subjects. *European journal of applied physiology*, *119*(1), 123-134.

Chance, B., Zhuang, Z., UnAh, C., Alter, C., & Lipton, L. (1993). Cognition-activated low-frequency modulation of light absorption in human brain. *Proceedings of the National Academy of Sciences*, *90*(8), 3770-3774.

Chen, M., Pillemer, S., England, S., Izzetoglu, M., Mahoney, J. R., & Holtzer, R. (2017). Neural correlates of obstacle negotiation in older adults: an fNIRS study. *Gait & posture*, *58*, 130-135.

Chiang, T. C., Vaithianathan, T., Leung, T., Lavidor, M., Walsh, V., & Delpy, D. T. (2007). Elevated haemoglobin levels in the motor cortex following 1 Hz transcranial magnetic stimulation: a preliminary study. *Experimental brain research*, *181*(4), 555-560.

Choi, D. S., Lee, H. J., Shin, Y. I., Lee, A., Kim, H. G., & Kim, Y. H. (2019). Modulation of cortical activity by high-frequency whole-body vibration exercise: An fnirs study. *Journal of sport rehabilitation*, *28*(7), 665-670.

Colier, W. N., Quaresima, V., Baratelli, G., Cavallari, P., van der Sluijs, M. C., & Ferrari, M. (1997, August). Detailed evidence of cerebral hemoglobin oxygenation changes in

response to motor cortical activation revealed by a continuous-wave spectrophotometer with 10-Hz temporal resolution. In *Optical Tomography and Spectroscopy of Tissue: Theory, Instrumentation, Model, and Human Studies II* (Vol. 2979, pp. 390-396). International Society for Optics and Photonics.

Crivelli, D., Rueda, M. S., & Balconi, M. (2018). Linguistic and motor representations of everyday complex actions: an fNIRS investigation. *Brain Structure and Function*, *223*(6), 2989-2997.

Cui, X., Bray, S., Bryant, D. M., Glover, G. H., & Reiss, A. L. (2011). A quantitative comparison of NIRS and fMRI across multiple cognitive tasks. *Neuroimage*, *54*(4), 2808-2821.

Dassonville, P., Lewis, S., Zhu, X. H., Uğurbil, K., Kim, S. G., & Ashe, J. (1998). Effects of movement predictability on cortical motor activation. *Neuroscience research*, *32*(1), 65-74.

Daubechies, I. (1988). Orthonormal bases of compactly supported wavelets. *Communications on pure and applied mathematics*, *41*(7), 909-996.

Davis, T. L., Kwong, K. K., Weisskoff, R. M., & Rosen, B. R. (1998). Calibrated functional MRI: mapping the dynamics of oxidative metabolism. *Proceedings of the National Academy of Sciences*, *95*(4), 1834-1839.

de Lima-Pardini, A. C., Morais, G. A. Z., Balardin, J. B., Coelho, D. B., Azzi, N. M., Teixeira, L. A., & Sato, J. R. (2017). Measuring cortical motor hemodynamics during assisted stepping–An fNIRS feasibility study of using a walker. *Gait & Posture*, *56*, 112-118.

Delpy, D. T., & Cope, M. (1997). Quantification in tissue near–infrared spectroscopy. *Philosophical Transactions of the Royal Society of London. Series B: Biological Sciences*, *352*(1354), 649-659.

Delpy, D. T., Cope, M., van der Zee, P., Arridge, S., Wray, S., & Wyatt, J. S. (1988). Estimation of optical pathlength through tissue from direct time of flight measurement. *Physics in Medicine & Biology*, *33*(12), 1433.

Derosiere, G., Alexandre, F., Bourdillon, N., Mandrick, K., Ward, T. E., & Perrey, S. (2014). Similar scaling of contralateral and ipsilateral cortical responses during graded unimanual force generation. *Neuroimage*, *85*, 471-477.

Dresler, M., Koch, S. P., Wehrle, R., Spoormaker, V. I., Holsboer, F., Steiger, A., ... & Czisch, M. (2011). Dreamed movement elicits activation in the sensorimotor cortex. *Current Biology*, *21*(21), 1833-1837.

Duan, L., Zhao, Z., Lin, Y., Wu, X., Luo, Y., & Xu, P. (2018). Wavelet-based method for removing global physiological noise in functional near-infrared spectroscopy. *Biomedical Optics Express*, *9*(8), 3805-3820.

Duncan, A., Meek, J. H., Clemence, M., Elwell, C. E., Fallon, P., Tyszczuk, L., ... & Delpy, D. T. (1996). Measurement of cranial optical path length as a function of age using phase resolved near infrared spectroscopy. *Pediatric research*, *39*(5), 889-894.

Ferrari, M., & Quaresima, V. (2012). A brief review on the history of human functional near-infrared spectroscopy (fNIRS) development and fields of application. *Neuroimage*, *63*(2), 921-935.

Ferrari, M., Bisconti, S., Spezialetti, M., Moro, S. B., Di Palo, C., Placidi, G., & Quaresima, V. (2014). Prefrontal cortex activated bilaterally by a tilt board balance task: a functional near-infrared spectroscopy study in a semi-immersive virtual reality environment. *Brain topography*, *27*(3), 353-365.

Fox, P. T., Raichle, M. E., Mintun, M. A., & Dence, C. (1988). Nonoxidative glucose consumption during focal physiologic neural activity. *Science*, *241*(4864), 462-464.

Franceschini, M. A., Fantini, S., Thompson, J. H., Culver, J. P., & Boas, D. A. (2003). Hemodynamic evoked response of the sensorimotor cortex measured noninvasively with near-infrared optical imaging. *Psychophysiology*, *40*(4), 548-560.

Freund, P., Weiskopf, N., Ward, N. S., Hutton, C., Gall, A., Ciccarelli, O., ... & Thompson, A. J. (2011). Disability, atrophy and cortical reorganization following spinal cord injury. *Brain*, *134*(6), 1610-1622.

Fu, Y., Xiong, X., Jiang, C., Xu, B., Li, Y., & Li, H. (2016). Imagined hand clenching force and speed modulate brain activity and are classified by NIRS combined with EEG. *IEEE Transactions on Neural Systems and Rehabilitation Engineering*, *25*(9), 1641-1652.

Funane, T., Atsumori, H., Katura, T., Obata, A. N., Sato, H., Tanikawa, Y., ... & Kiguchi, M. (2014). Quantitative evaluation of deep and shallow tissue layers' contribution to fNIRS signal using multi-distance optodes and independent component analysis. *Neuroimage*, *85*, 150-165.

Gagnon, L., Cooper, R. J., Yücel, M. A., Perdue, K. L., Greve, D. N., & Boas, D. A. (2012). Short separation channel location impacts the performance of short channel regression in NIRS. *Neuroimage*, *59*(3), 2518-2528.

Gagnon, L., Yücel, M. A., Dehaes, M., Cooper, R. J., Perdue, K. L., Selb, J., ... & Boas, D. A. (2012). Quantification of the cortical contribution to the NIRS signal over the motor cortex using concurrent NIRS-fMRI measurements. *Neuroimage*, *59*(4), 3933-3940.

Girouard, H., & Iadecola, C. (2006). Neurovascular coupling in the normal brain and in hypertension, stroke, and Alzheimer disease. *Journal of applied physiology*, *100*(1), 328-335.

Gratton, G., Maier, J. S., Fabiani, M., Mantulin, W. W., & Gratton, E. (1994). Feasibility of intracranial near-infrared optical scanning. *Psychophysiology*, *31*(2), 211-215.

Gratton, G., Brumback, C. R., Gordon, B. A., Pearson, M. A., Low, K. A., & Fabiani, M. (2006). Effects of measurement method, wavelength, and source-detector distance on the fast optical signal. *Neuroimage*, *32*(4), 1576-1590.

Groff, B. R., Antonellis, P., Schmid, K. K., Knarr, B. A., & Stergiou, N. (2019). Stride-time variability is related to sensorimotor cortical activation during forward and backward walking. *Neuroscience letters*, *692*, 150-158.

Gurley, K., & Kareem, A. (1999). Applications of wavelet transforms in earthquake, wind and ocean engineering. *Engineering structures*, *21*(2), 149-167.

Harrison, S. J., Hough, M., Schmid, K., Groff, B. R., & Stergiou, N. (2018). When Coordinating Finger Tapping to a Variable Beat the Variability Scaling Structure of the Movement and the Cortical BOLD Signal are Both Entrained to the Auditory Stimuli. *Neuroscience*, *392*, 203-218.

Hatakenaka, M., Miyai, I., Mihara, M., Sakoda, S., & Kubota, K. (2007). Frontal regions involved in learning of motor skill—a functional NIRS study. *Neuroimage*, *34*(1), 109-116.

Heinze, R. A., Vanzella, P., Morais, G. A. Z., & Sato, J. R. (2019). Hand motor learning in a musical context and prefrontal cortex hemodynamic response: a functional near-infrared spectroscopy (fNIRS) study. *Cognitive processing*, *20*(4), 507-513.

Herold, F., Orlowski, K., Börmel, S., & Müller, N. G. (2017). Cortical activation during balancing on a balance board. *Human movement science*, *51*, 51-58.

Herold, F., Aye, N., Hamacher, D., & Schega, L. (2019). Towards the Neuromotor Control Processes of Steady-State and Speed-Matched Treadmill and Overground Walking. *Brain topography*, *32*(3), 472-476.

Hoge, R. D., Atkinson, J., Gill, B., Crelier, G. R., Marrett, S., & Pike, G. B. (1999). Linear coupling between cerebral blood flow and oxygen consumption in activated human cortex. *Proceedings of the National Academy of Sciences*, *96*(16), 9403-9408.

Holper, L., & Wolf, M. (2010). Motor imagery in response to fake feedback measured by functional near-infrared spectroscopy. *Neuroimage*, *50*(1), 190-197.

Holper, L., & Wolf, M. (2011). Single-trial classification of motor imagery differing in task complexity: a functional near-infrared spectroscopy study. *Journal of neuroengineering and rehabilitation*, *8*(1), 34.

Holper, L., Biallas, M., & Wolf, M. (2009). Task complexity relates to activation of cortical motor areas during uni-and bimanual performance: a functional NIRS study. *Neuroimage*, *46*(4), 1105-1113.

Holper, L., Muehlemann, T., Scholkmann, F., Eng, K., Kiper, D., & Wolf, M. (2010). Testing the potential of a virtual reality neurorehabilitation system during performance of observation, imagery and imitation of motor actions recorded by wireless functional near-infrared spectroscopy (fNIRS). *Journal of neuroengineering and rehabilitation*, *7*(1), 57.

Holper, L., Kobashi, N., Kiper, D., Scholkmann, F., Wolf, M., & Eng, K. (2012). Trial-to-trial variability differentiates motor imagery during observation between low versus high responders: a functional near-infrared spectroscopy study. *Behavioural Brain Research*, *229*(1), 29-40.

Holper, L., Scholkmann, F., & Wolf, M. (2014). The relationship between sympathetic nervous activity and cerebral hemodynamics and oxygenation: a study using skin conductance measurement and functional near-infrared spectroscopy. *Behavioural brain research*, *270*, 95-107.

Holtzer, R., Mahoney, J. R., Izzetoglu, M., Izzetoglu, K., Onaral, B., & Verghese, J. (2011). fNIRS study of walking and walking while talking in young and old individuals. *Journals of Gerontology Series A: Biomedical Sciences and Medical Sciences*, *66*(8), 879-887.

Holtzer, R., Yuan, J., Verghese, J., Mahoney, J. R., Izzetoglu, M., & Wang, C. (2017). Interactions of subjective and objective measures of fatigue defined in the context of brain control of locomotion. *The Journals of Gerontology: Series A*, *72*(3), 417-423.

Holtzer, R., Kraut, R., Izzetoglu, M., & Ye, K. (2019). The effect of fear of falling on prefrontal cortex activation and efficiency during walking in older adults. *GeroScience*, *41*(1), 89-100.

Hong, K. S., & Naseer, N. (2016). Reduction of delay in detecting initial dips from functional near-infrared spectroscopy signals using vector-based phase analysis. *International Journal of Neural Systems*, *26*(03), 1650012.

Horovitz, S. G., & Gore, J. C. (2003, September). Studies of the sensitivity of near infrared spectroscopy to detect changes in levels of brain activation due to manipulations of motor tasks. In *Proceedings of the 25th Annual International Conference of the IEEE Engineering in Medicine and Biology Society (IEEE Cat. No. 03CH37439)* (Vol. 2, pp. 1106-1108). IEEE.

Hoshi, Y. (2007). Functional near-infrared spectroscopy: current status and future prospects. *Journal of biomedical optics*, *12*(6), 062106.

Hoshi, Y., & Tamura, M. (1993). Detection of dynamic changes in cerebral oxygenation coupled to neuronal function during mental work in man. *Neuroscience letters*, *150*(1), 5-8.

Hu, X. S., Hong, K. S., & Ge, S. S. (2013). Reduction of trial-to-trial variability in functional near-infrared spectroscopy signals by accounting for resting-state functional connectivity. *Journal of Biomedical Optics*, *18*(1), 017003.

Hund-Georgiadis, M., & Von Cramon, D. Y. (1999). Motor-learning-related changes in piano players and non-musicians revealed by functional magnetic-resonance signals. *Experimental Brain Research*, *125*(4), 417-425.

Huppert, T. J. (2016). Commentary on the statistical properties of noise and its implication on general linear models in functional near-infrared spectroscopy. *Neurophotonics*, *3*(1), 010401.

Huppert T. J. (2017). *Data Analysis Methods in fNIRS – I*. Retrieved from: http://huppertlab.net/publications-2/lab-videos/.

Huppert, T. J., Diamond, S. G., Franceschini, M. A., & Boas, D. A. (2009). HomER: a review of time-series analysis methods for near-infrared spectroscopy of the brain. *Applied optics*, *48*(10), D280-D298.

Huppert, T., Schmidt, B., Beluk, N., Furman, J., & Sparto, P. (2013). Measurement of brain activation during an upright stepping reaction task using functional near-infrared spectroscopy. *Human brain mapping*, *34*(11), 2817-2828.

Ifeachor, E. C., and Jervis, B. W. (2002). *Digital Signal Processing: a Practical Approach*. Harlow; New York, NY: Pearson Education; Prentice Hall.

Irani, F., Platek, S. M., Bunce, S., Ruocco, A. C., & Chute, D. (2007). Functional near infrared spectroscopy (fNIRS): an emerging neuroimaging technology with important applications for the study of brain disorders. *The Clinical Neuropsychologist*, *21*(1), 9-37.

Ishii, K., Liang, N., Asahara, R., Takahashi, M., & Matsukawa, K. (2018). Feedforward-and motor effort-dependent increase in prefrontal oxygenation during voluntary one-armed cranking. *The Journal of Physiology*, *596*(21), 5099-5118.

Jacques, S. L. (2013). Optical properties of biological tissues: a review. *Physics in Medicine & Biology*, *58*(11), R37.

Jahani, S., Setarehdan, S. K., Boas, D. A., & Yücel, M. A. (2018). Motion artifact detection and correction in functional near-infrared spectroscopy: a new hybrid method based on spline interpolation method and Savitzky–Golay filtering. *Neurophotonics*, *5*(1), 015003.

Jang, K. E., Tak, S., Jung, J., Jang, J., Jeong, Y., & Ye, Y. C. (2009). Wavelet minimum description length detrending for near-infrared spectroscopy. *Journal of biomedical optics*, *14*(3), 034004.

Jang, S. H., Jang, W. H., Chang, P. H., Lee, S. H., Jin, S. H., Kim, Y. G., & Yeo, S. S. (2014). Cortical activation change induced by neuromuscular electrical stimulation during hand movements: a functional NIRS study. *Journal of NeuroEngineering and Rehabilitation*, *11*(1), 29.

Jin, H., Li, C., & Xu, J. (2018). Pilot study on gait classification using fNIRS signals. *Computational Intelligence and Neuroscience*, *2018*.

Jobsis, F. F. (1977). Noninvasive, infrared monitoring of cerebral and myocardial oxygen sufficiency and circulatory parameters. *Science*, *198*(4323), 1264-1267.

Kamran, M. A., Mannann, M., & Jeong, M. Y. (2018). Differential Path-Length Factor's Effect on the Characterization of Brain's Hemodynamic Response Function: A Functional Near-Infrared Study. *Frontiers in neuroinformatics*, *12*, 37.

Karim, H., Schmidt, B., Dart, D., Beluk, N., & Huppert, T. (2012). Functional near-infrared spectroscopy (fNIRS) of brain function during active balancing using a video game system. *Gait & posture*, *35*(3), 367-372.

Kato, T., Kamei, A., Takashima, S., & Ozaki, T. (1993). Human visual cortical function during photic stimulation monitoring by means of near-infrared spectroscopy. *Journal of Cerebral Blood Flow & Metabolism*, *13*(3), 516-520.

Kawala-Sterniuk, A., Podpora, M., Pelc, M., Blaszczyszyn, M., Gorzelanczyk, E. J., Martinek, R., & Ozana, S. (2020). Comparison of smoothing filters in analysis of EEG data for the medical diagnostics purposes. *Sensors*, *20*(3), 807.

Khan, R. A., Naseer, N., Qureshi, N. K., Noori, F. M., Nazeer, H., & Khan, M. U. (2018). fNIRS-based Neurorobotic Interface for gait rehabilitation. *Journal of neuroengineering and rehabilitation*, *15*(1), 7.

Kim, H. Y., Kim, E. J., & You, J. S. H. (2017). Adaptive locomotor network activation during randomized walking speeds using functional near-infrared spectroscopy. *Technology and Health Care*, *25*(S1), 93-98.

Kleinschmidt, A., Obrig, H., Requardt, M., Merboldt, K. D., Dirnagl, U., Villringer, A., & Frahm, J. (1996). Simultaneous recording of cerebral blood oxygenation changes during human brain activation by magnetic resonance imaging and near-infrared spectroscopy. *Journal of cerebral blood flow & metabolism*, *16*(5), 817-826.

Kobashi, N., Holper, L., Scholkmann, F., Kiper, D., & Eng, K. (2012). Enhancement of motor imagery-related cortical activation during first-person observation measured by functional near-infrared spectroscopy. *European Journal of Neuroscience*, *35*(9), 1513-1521.

Koehler, S., Egetemeir, J., Stenneken, P., Koch, S. P., Pauli, P., Fallgatter, A. J., & Herrmann, M. J. (2012). The human execution/observation matching system investigated with a complex everyday task: a functional near-infrared spectroscopy (fNIRS) study. *Neuroscience letters*, *508*(2), 73-77.

Koenraadt, K. L. M., Duysens, J., Smeenk, M., & Keijsers, N. L. W. (2012). Multi-channel NIRS of the primary motor cortex to discriminate hand from foot activity. *Journal of Neural Engineering*, *9*(4), 046010.

Koenraadt, K. L., Duysens, J., Meddeler, B. M., & Keijsers, N. L. (2013). Hand tapping at mixed frequencies requires more motor cortex activity compared to single frequencies: an fNIRS study. *Experimental brain research*, *231*(2), 231-237.

Koenraadt, K. L., Roelofsen, E. G., Duysens, J., & Keijsers, N. L. (2014). Cortical control of normal gait and precision stepping: an fNIRS study. *Neuroimage*, *85*, 415-422.

Koren, Y., Parmet, Y., & Bar-Haim, S. (2019). Treading on the unknown increases prefrontal activity: A pilot fNIRS study. *Gait & Posture*, *69*, 96-100.

Kuboyama, N., Nabetani, T., Shibuya, K. I., Machida, K., & Ogaki, T. (2004). The effect of maximal finger tapping on cerebral activation. *Journal of physiological anthropology and applied human science*, *23*(4), 105-110.

Kuboyama, N., Nabetani, T., Shibuya, K., Machida, K., & Ogaki, T. (2005). Relationship between cerebral activity and movement frequency of maximal finger tapping. *Journal of physiological anthropology and applied human science*, *24*(3), 201-208.

Kurz, M. J., Wilson, T. W., & Arpin, D. J. (2012). Stride-time variability and sensorimotor cortical activation during walking. *Neuroimage*, *59*(2), 1602-1607.

Lachert, P., Janusek, D., Pulawski, P., Liebert, A., Milej, D., & Blinowska, K. J. (2017). Coupling of Oxy-and Deoxyhemoglobin concentrations with EEG rhythms during motor task. *Scientific Reports*, *7*(1), 1-9.

Leff, D. R., Orihuela-Espina, F., Elwell, C. E., Athanasiou, T., Delpy, D. T., Darzi, A. W., & Yang, G. Z. (2011). Assessment of the cerebral cortex during motor task behaviours in adults: a systematic review of functional near infrared spectroscopy (fNIRS) studies. *Neuroimage*, *54*(4), 2922-2936.

Limanowski, J., & Friston, K. (2020). Attentional modulation of vision versus proprioception during action. *Cerebral Cortex*, *30*(3), 1637-1648.

Lin, P. Y., Lin, S. I., & Chen, J. J. J. (2012). Functional near infrared spectroscopy study of age-related difference in cortical activation patterns during cycling with speed feedback. *IEEE Transactions on Neural Systems and Rehabilitation Engineering*, *20*(1), 78-84.

Lin, T. Y., Wu, J. S., Lin, L. L., Ho, T. C., Lin, P. Y., & Chen, J. J. J. (2016). Assessments of muscle oxygenation and cortical activity using functional near-infrared spectroscopy in healthy adults during hybrid activation. *IEEE Transactions on Neural Systems and Rehabilitation Engineering*, *24*(1), 1-9.

Lu, C. F., Teng, S., & Wu, Y. T. (2013, July). Dynamics of hemoglobin states in the sensorimotor cortex during motor tasks: A functional near infrared spectroscopy study. In *2013 35th Annual International Conference of the IEEE Engineering in Medicine and Biology Society (EMBC)* (pp. 1803-1806). IEEE.

Lu, C. F., Liu, Y. C., Yang, Y. R., Wu, Y. T., & Wang, R. Y. (2015). Maintaining gait performance by cortical activation during dual-task interference: a functional near-infrared spectroscopy study. *PloS one*, *10*(6), e0129390.

Lu, F. M., Wang, Y. F., Zhang, J., Chen, H. F., & Yuan, Z. (2017). Optical mapping of the dominant frequency of brain signal oscillations in motor systems. *Scientific reports*, *7*(1), 1-13.

Lucas, M., Wagshul, M. E., Izzetoglu, M., & Holtzer, R. (2019). Moderating effect of white matter integrity on brain activation during dual-task walking in older adults. *The Journals of Gerontology: Series A*, *74*(4), 435-441.

Maidan, I., Shustak, S., Sharon, T., Bernad-Elazari, H., Geffen, N., Giladi, N., ... & Mirelman, A. (2018). Prefrontal cortex activation during obstacle negotiation: What's the effect size and timing?. *Brain and cognition*, *122*, 45-51.

Mandrick, K., Derosiere, G., Dray, G., Coulon, D., Micallef, J. P., & Perrey, S. (2013). Prefrontal cortex activity during motor tasks with additional mental load requiring attentional demand: a near-infrared spectroscopy study. *Neuroscience research*, *76*(3), 156-162.

Matcher, S. J., & Cooper, C. E. (1994). Absolute quantification of deoxyhaemoglobin concentration in tissue near infrared spectroscopy. *Physics in Medicine & Biology*, *39*(8), 1295.

McCormick, P. W., Stewart, M., Lewis, G., Dujovny, M., & Ausman, J. I. (1992). Intracerebral penetration of infrared light. *Journal of neurosurgery*, *76*(2), 315-318.

Mehnert, J., Brunetti, M., Steinbrink, J. M., Niedeggen, M., & Dohle, C. (2013). Effect of a mirror-like illusion on activation in the precuneus assessed with functional near-infrared spectroscopy. *Journal of Biomedical Optics*, *18*(6), 066001.

Mehta, R. K., & Rhee, J. (2017). Age-specific neural strategies to maintain motor performance after an acute social stress bout. *Experimental Brain Research*, *235*(7), 2049-2057.

Metzger, F. G., Ehlis, A. C., Haeussinger, F. B., Schneeweiss, P., Hudak, J., Fallgatter, A. J., & Schneider, S. (2017). Functional brain imaging of walking while talking–An fNIRS study. *Neuroscience*, *343*, 85-93.

Millikan, G. A. (1942). The oximeter, an instrument for measuring continuously the oxygen saturation of arterial blood in man. *Review of scientific Instruments*, *13*(10), 434-444.

Mirelman, A., Maidan, I., Bernad-Elazari, H., Nieuwhof, F., Reelick, M., Giladi, N., & Hausdorff, J. M. (2014). Increased frontal brain activation during walking while dual tasking: an fNIRS study in healthy young adults. *Journal of neuroengineering and rehabilitation*, *11*(1), 85.

Mirelman, A., Maidan, I., Bernad-Elazari, H., Shustack, S., Giladi, N., & Hausdorff, J. M. (2017). Effects of aging on prefrontal brain activation during challenging walking conditions. *Brain and cognition*, *115*, 41-46.

Mivule, K., & Turner, C. (2014). Applying moving average filtering for non-interactive differential privacy settings. *Procedia Computer Science*, *36*, 409-415.

Miyai, I., Tanabe, H. C., Sase, I., Eda, H., Oda, I., Konishi, I., ... & Kubota, K. (2001). Cortical mapping of gait in humans: a near-infrared spectroscopic topography study. *Neuroimage*, *14*(5), 1186-1192.

Molavi, B., & Dumont, G. A. (2012). Wavelet-based motion artifact removal for functional near-infrared spectroscopy. *Physiological measurement*, *33*(2), 259.

Monti, M. M. (2011). Statistical analysis of fMRI time-series: a critical review of the GLM approach. *Front. Hum. Neurosci*. *5*:28. doi: 10.3389/fnhum.2011.00028

Moro, S. B., Carrieri, M., Avola, D., Brigadoi, S., Lancia, S., Petracca, A., ... & Quaresima, V. (2016). A novel semi-immersive virtual reality visuo-motor task activates ventrolateral prefrontal cortex: a functional near-infrared spectroscopy study. *Journal of neural engineering*, *13*(3), 036002.

Muthalib, M., Re, R., Zucchelli, L., Perrey, S., Contini, D., Caffini, M., ... & Torricelli, A. (2015). Effects of increasing neuromuscular electrical stimulation current intensity on cortical sensorimotor network activation: a time domain fNIRS study. *PLoS One*, *10*(7), e0131951.

Muthalib, M., Besson, P., Rothwell, J., Ward, T., & Perrey, S. (2016). Effects of anodal high-definition transcranial direct current stimulation on bilateral sensorimotor cortex activation during sequential finger movements: an fNIRS study. In *Oxygen Transport to Tissue XXXVII* (pp. 351-359). Springer, New York, NY.

Muthalib, M., Ferrari, M., Quaresima, V., Kerr, G., & Perrey, S. (2018). Functional near-infrared spectroscopy to probe sensorimotor region activation during electrical stimulation-evoked movement. *Clinical Physiology and Functional Imaging*, *38*(5), 816-822.

Naseer, N., & Hong, K. S. (2013). Classification of functional near-infrared spectroscopy signals corresponding to the right-and left-wrist motor imagery for development of a brain–computer interface. *Neuroscience letters*, *553*, 84-89.

Naseer, N., & Hong, K. S. (2015). fNIRS-based brain-computer interfaces: a review. *Frontiers in human neuroscience*, *9*, 3.

Nguyen, H. T., Ngo, C. Q., Truong Quang Dang, K. H. O. A., & Vo, V. T. (2013). Temporal hemodynamic classification of two hands tapping using functional near—infrared spectroscopy. *Frontiers in human neuroscience*, *7*, 516.

Obrig, H., Hirth, C., Junge-Hulsing, J. G., Doge, C., Wolf, T., Dirnagl, U., & Villringer, A. (1996). Cerebral oxygenation changes in response to motor stimulation. *Journal of applied physiology*, *81*(3), 1174-1183.

Oldfield, R. C. (1971). The assessment and analysis of handedness: the Edinburgh inventory. *Neuropsychologia*, *9*(1), 97-113.

Perutz, M. F. (1978). Hemoglobin structure and respiratory transport. *Scientific American*, *239*(6), 92-125.

Pfurtscheller, G., Klobassa, D. S., Altstatter, C., Bauernfeind, G., & Neuper, C. (2011). About the stability of phase shifts between slow oscillations around 0.1 Hz in cardiovascular and cerebral systems. *IEEE transactions on biomedical engineering*, *58*(7), 2064-2071.

Piantadosi, C. A. (2007). Early development of near-infrared spectroscopy at Duke University. *Journal of biomedical optics*, *12*(6), 062102.

Pinti, P., Scholkmann, F., Hamilton, A., Burgess, P., & Tachtsidis, I. (2019). Current status and issues regarding pre-processing of fNIRS neuroimaging data: an investigation of diverse signal filtering methods within a general linear model framework. *Frontiers in human neuroscience*, *12*, 505.

Pinti, P., Tachtsidis, I., Hamilton, A., Hirsch, J., Aichelburg, C., Gilbert, S., & Burgess, P. W. (2020). The present and future use of functional near-infrared spectroscopy (fNIRS) for cognitive neuroscience. *Annals of the New York Academy of Sciences*, *1464*(1), 5.

Pittaccio, S., Garavaglia, L., Molteni, E., Guanziroli, E., Zappasodi, F., Beretta, E., ... & Passaretti, F. (2013, July). Can passive mobilization provide clinically-relevant brain stimulation? A pilot EEG and NIRS study on healthy subjects. In *2013 35th Annual International Conference of the IEEE Engineering in Medicine and Biology Society (EMBC)* (pp. 3547-3550). IEEE.

Plichta, M. M., Herrmann, M. J., Baehne, C. G., Ehlis, A. C., Richter, M. M., Pauli, P., & Fallgatter, A. J. (2006). Event-related functional near-infrared spectroscopy (fNIRS): are the measurements reliable?. *Neuroimage*, *31*(1), 116-124.

Plichta, M. M., Herrmann, M. J., Baehne, C. G., Ehlis, A. C., Richter, M. M., Pauli, P., & Fallgatter, A. J. (2007). Event-related functional near-infrared spectroscopy (fNIRS) based on craniocerebral correlations: reproducibility of activation?. *Human Brain Mapping*, *28*(8), 733-741.

Propper, R. E., Dodd, K., Christman, S. D., & Brunyé, T. T. (2017). Relationship between sustained unilateral hand clench, emotional state, line bisection performance, and prefrontal cortical activity: A functional near-infrared spectroscopy study. *Laterality: Asymmetries of Body, Brain and Cognition*, *22*(6), 671-689.

Rahman, M. A., Rashid, M. A., & Ahmad, M. (2019). Selecting the optimal conditions of Savitzky–Golay filter for fNIRS signal. *Biocybernetics and Biomedical Engineering*, *39*(3), 624-637.

Rao, S. M., Binder, J. R., Bandettini, P. A., Hammeke, T. A., Yetkin, F. Z., Jesmanowicz, A., Lisk, L. M., Morris, G. L., Mueller, W. M., and Estkowski, L. D. 1993. Functional magnetic resonance imaging of complex human movements. *Neurology 43*: 2311–2318.

Rao, S. M., Bandettini, P. A., Binder, J. R., Bobholz, J. A., Hammeke, T. A., Stein, E. A., & Hyde, J. S. (1996). Relationship between finger movement rate and functional magnetic resonance signal change in human primary motor cortex. *Journal of Cerebral Blood Flow & Metabolism*, *16*(6), 1250-1254.

Rasmussen, P., Dawson, E. A., Nybo, L., Van Lieshout, J. J., Secher, N. H., & Gjedde, A. (2007). Capillary-oxygenation-level-dependent near-infrared spectrometry in frontal lobe of humans. *Journal of Cerebral Blood Flow & Metabolism*, *27*(5), 1082-1093.

Robertson, F. C., Douglas, T. S., & Meintjes, E. M. (2010). Motion artifact removal for functional near infrared spectroscopy: a comparison of methods. *IEEE Transactions on Biomedical Engineering*, *57*(6), 1377-1387.

Rosner, A. O., & Barlow, S. M. (2016). Hemodynamic changes in cortical sensorimotor systems following hand and orofacial motor tasks and pulsed pneumotactile stimulation. *Somatosensory & motor research*, *33*(3-4), 145-155.

Rosso, A. L., Cenciarini, M., Sparto, P. J., Loughlin, P. J., Furman, J. M., & Huppert, T. J. (2017). Neuroimaging of an attention demanding dual-task during dynamic postural control. *Gait & posture*, *57*, 193-198.

Rushworth, M. F., Krams, M., & Passingham, R. E. (2001). The attentional role of the left parietal cortex: the distinct lateralization and localization of motor attention in the human brain. *Journal of cognitive neuroscience*, *13*(5), 698-710.

Saager, R. B., & Berger, A. J. (2005). Direct characterization and removal of interfering absorption trends in two-layer turbid media. *JOSA A*, *22*(9), 1874-1882.

Sagari, A., Iso, N., Moriuchi, T., Ogahara, K., Kitajima, E., Tanaka, K., ... & Higashi, T. (2015). Changes in cerebral hemodynamics during complex motor learning by character entry into touch-screen terminals. *Plos one*, *10*(10), e0140552.

Santosa, H., Zhai, X., Fishburn, F., & Huppert, T. (2018). The NIRS brain AnalyzIR toolbox. *Algorithms*, *11*(5), 73.

Santosa, H., Fishburn, F., Zhai, X., & Huppert, T. J. (2019). Investigation of the sensitivity-specificity of canonical-and deconvolution-based linear models in evoked functional near-infrared spectroscopy. *Neurophotonics*, *6*(2), 025009.

Sato, H., Kiguchi, M., Maki, A., Fuchino, Y., Obata, A., Yoro, T., & Koizumi, H. (2006a). Within-subject reproducibility of near-infrared spectroscopy signals in sensorimotor activation after 6 months. *Journal of biomedical optics*, *11*(1), 014021.

Sato, H., Tanaka, N., Uchida, M., Hirabayashi, Y., Kanai, M., Ashida, T., ... & Maki, A. (2006b). Wavelet analysis for detecting body-movement artifacts in optical topography signals. *Neuroimage*, *33*(2), 580-587.

Savitzky, A., & Golay, M. J. (1964). Smoothing and differentiation of data by simplified least squares procedures. *Analytical chemistry*, *36*(8), 1627-1639.

Schürholz, M., Rana, M., Robinson, N., Ramos-Murguialday, A., Cho, W., Rohm, M., ... & Sitaram, R. (2012). Differences in hemodynamic activations between motor imagery and upper limb FES with NIRS. In *2012 Annual International Conference of the IEEE Engineering in Medicine and Biology Society* (pp. 4728-4731). IEEE.

Seidel, O., Carius, D., Kenville, R., & Ragert, P. (2017). Motor learning in a complex balance task and associated neuroplasticity: a comparison between endurance athletes and nonathletes. *Journal of neurophysiology*, *118*(3), 1849-1860.

Seidel, O., Carius, D., Roediger, J., Rumpf, S., & Ragert, P. (2019). Changes in neurovascular coupling during cycling exercise measured by multi-distance fNIRS: a comparison

between endurance athletes and physically active controls. *Experimental brain research*, *237*(11), 2957-2972.

Shadmehr R, Holcomb HH (1997) Neural correlates of motor memory consolidation. *Science 277*:821–825.

Shibuya, K. (2011). The activity of the primary motor cortex ipsilateral to the exercising hand decreases during repetitive handgrip exercise. *Physiological measurement*, *32*(12), 1929.

Shibuya, K., Kuboyama, N., & Tanaka, J. (2014). Changes in ipsilateral motor cortex activity during a unilateral isometric finger task are dependent on the muscle contraction force. *Physiological measurement*, *35*(3), 417.

Shibuya, K., Kuboyama, N., & Yamada, S. (2016). Complementary activation of the ipsilateral primary motor cortex during a sustained handgrip task. *European journal of applied physiology*, *116*(1), 171-178.

Shin, J., & Jeong, J. (2014). Multiclass classification of hemodynamic responses for performance improvement of functional near-infrared spectroscopy-based brain–computer interface. *Journal of biomedical optics*, *19*(6), 067009.

Solodkin, A., Hlustik, P., Noll, D. C., & Small, S. L. (2001). Lateralization of motor circuits and handedness during finger movements. *European Journal of Neurology*, *8*(5), 425-434.

Strangman, G., Culver, J. P., Thompson, J. H., & Boas, D. A. (2002). A quantitative comparison of simultaneous BOLD fMRI and NIRS recordings during functional brain activation. *Neuroimage*, *17*(2), 719-731.

Strangman, G., Franceschini, M. A., & Boas, D. A. (2003). Factors affecting the accuracy of near-infrared spectroscopy concentration calculations for focal changes in oxygenation parameters. *Neuroimage*, *18*(4), 865-879.

Strangman, G., Goldstein, R., Rauch, S. L., & Stein, J. (2006). Near-infrared spectroscopy and imaging for investigating stroke rehabilitation: test-retest reliability and review of the literature. *Archives of physical medicine and rehabilitation*, *87*(12), 12-19.

Streletz, L. J., Belevich, J. K., Jones, S. M., Bhushan, A., Shah, S. H., & Herbison, G. J. (1995). Transcranial magnetic stimulation: cortical motor maps in acute spinal cord injury. *Brain topography*, *7*(3), 245-250.

Stuart, S., Alcock, L., Rochester, L., Vitorio, R., & Pantall, A. (2019). Monitoring multiple cortical regions during walking in young and older adults: dual-task response and comparison challenges. *International journal of psychophysiology*, *135*, 63-72.

Sukal-Moulton, T., de Campos, A. C., Alter, K. E., & Damiano, D. L. (2020). Functional near-infrared spectroscopy to assess sensorimotor cortical activity during hand squeezing and ankle dorsiflexion in individuals with and without bilateral and unilateral cerebral palsy. *Neurophotonics*, *7*(4), 045001.

Tachibana, A., Noah, J. A., Bronner, S., Ono, Y., & Onozuka, M. (2011). Parietal and temporal activity during a multimodal dance video game: an fNIRS study. *Neuroscience letters*, *503*(2), 125-130.

Tak, S., & Ye, J. C. (2014). Statistical analysis of fNIRS data: a comprehensive review. *Neuroimage*, *85*, 72-91.

Tempest, G. D., & Reiss, A. L. (2019). The Utility of Functional Near-infrared Spectroscopy for Measuring Cortical Activity during Cycling Exercise. *Medicine and science in sports and exercise*, *51*(5), 979-987.

Turner, J. R., & Carroll, D. (1985). Heart rate and oxygen consumption during mental arithmetic, a video game, and graded exercise: Further evidence of metabolically-exaggerated cardiac adjustments?. *Psychophysiology*, *22*(3), 261-267.

Vaalto, S., Julkunen, P., Säisänen, L., Könönen, M., Määttä, S., & Karhu, J. (2013). Long-term plasticity may be manifested as reduction or expansion of cortical representations of actively used muscles in motor skill specialists. *Neuroreport*, *24*(11), 596-600.

van Melick, N., Meddeler, B. M., Hoogeboom, T. J., Nijhuis-van der Sanden, M. W., & van Cingel, R. E. (2017). How to determine leg dominance: The agreement between self-reported and observed performance in healthy adults. *PloS one*, *12*(12), e0189876.

Vasta, R., Cerasa, A., Gramigna, V., Augimeri, A., Olivadese, G., Pellegrino, G., ... & Quattrone, A. (2017). The movement time analyser task investigated with functional near infrared spectroscopy: An ecologic approach for measuring hemodynamic response in the motor system. *Aging Clinical and Experimental Research*, *29*(2), 311-318.

Veesa, J. D., & Dehghani, H. (2019). Functional near infrared spectroscopy using spatially resolved data to account for tissue scattering: A numerical study and arm-cuff experiment. *Journal of biophotonics*, *12*(10), e201900064.

Verstynen, T., Diedrichsen, J., Albert, N., Aparicio, P., & Ivry, R. B. (2005). Ipsilateral motor cortex activity during unimanual hand movements relates to task complexity. *Journal of neurophysiology*, *93*(3), 1209-1222.

Villringer, A., Planck, J., Stodieck, S., Bötzel, K., Schleinkofer, L., Dirnagl, U., 1994. Noninvasive assessment of cerebral hemodynamics and tissue oxygenation during activation of brain cell function in human adults using near infrared spectroscopy. *Adv. Exp. Med. Biol. 345*, 559–565.

Villringer, A., Planck, J., Hock, C., Schleinkofer, L., & Dirnagl, U. (1993). Near infrared spectroscopy (NIRS): a new tool to study hemodynamic changes during activation of brain function in human adults. *Neuroscience letters*, *154*(1-2), 101-104.

Waldert, S., Tüshaus, L., Kaller, C. P., Aertsen, A., & Mehring, C. (2012). fNIRS exhibits weak tuning to hand movement direction. *PLoS One*, *7*(11), e49266.

Watanabe, E., Yamashita, Y., Maki, A., Ito, Y., Koizumi, H., Mayanagi, Y., 1994. Infrared spectroscopy as noninvasive functional mapping of human brain. *Neurosci. Res. Suppl. 19*, 2501.

Willis, S. J., Borrani, F., & Millet, G. P. (2019). Leg-vs arm-cycling repeated sprints with blood flow restriction and systemic hypoxia. *European journal of applied physiology*, *119*(8), 1819-1828.

Winter, D. A. (2009). *Biomechanics and motor control of human movement*. John Wiley & Sons.

Wolf, U., Toronov, V., Choi, J. H., Gupta, R., Michalos, A., Gratton, E., & Wolf, M. (2011). Correlation of functional and resting state connectivity of cerebral oxy-, deoxy-, and total hemoglobin concentration changes measured by near-infrared spectrophotometry. *Journal of biomedical optics*, *16*(8), 087013.

Woorons, X., Dupuy, O., Mucci, P., Millet, G. P., & Pichon, A. (2019). Cerebral and muscle oxygenation during repeated shuttle run sprints with hypoventilation. *International journal of sports medicine*, *40*(06), 376-384.

Wriessnegger, S. C., Kirchmeyr, D., Bauernfeind, G., & Müller-Putz, G. R. (2017). Force related hemodynamic responses during execution and imagery of a hand grip task: A functional near infrared spectroscopy study. *Brain and Cognition*, *117*, 108-116.

Wriessnegger, S. C., Bauernfeind, G., Kurz, E. M., Raggam, P., & Müller-Putz, G. R. (2018). Imagine squeezing a cactus: Cortical activation during affective motor imagery measured by functional near-infrared spectroscopy. *Brain and cognition*, *126*, 13-22.

Yamada, T., Umeyama, S., & Matsuda, K. (2009). Multidistance probe arrangement to eliminate artifacts in functional near-infrared spectroscopy. *Journal of biomedical optics*, *14*(6), 064034.

Ye, J. C., Tak, S., Jang, K. E., Jung, J., & Jang, J. (2009). NIRS-SPM: statistical parametric mapping for near-infrared spectroscopy. *Neuroimage*, *44*(2), 428-447.

Yeo, S. S., Chang, P. H., & Jang, S. H. (2013). The cortical activation differences between proximal and distal joint movements of the upper extremities: a functional NIRS study. *NeuroRehabilitation*, *32*(4), 861-866.

Yin, X., Xu, B., Jiang, C., Fu, Y., Wang, Z., Li, H., & Shi, G. (2015). NIRS-based classification of clench force and speed motor imagery with the use of empirical mode decomposition for BCI. *Medical engineering & physics*, *37*(3), 280-286.

Yokoyama, N., Ohtaka, C., Kato, K., Kubo, H., & Nakata, H. (2019). The difference in hemodynamic responses between dominant and non-dominant hands during muscle contraction and relaxation: An fNIRS study. *Plos one*, *14*(7), e0220100.

Yozu, A., Obayashi, S., Nakajima, K., & Hara, Y. (2016). Hemodynamic response of the supplementary motor area during locomotor tasks with upright versus horizontal postures in humans. *Neural plasticity*, *2016*.

Yu, J., Ang, K. K., Yang, H., & Guan, C. (2014, August). Cortical activation of passive hand movement using Haptic Knob: A preliminary multi-channel fNIRS study. In *2014 36th Annual International Conference of the IEEE Engineering in Medicine and Biology Society* (pp. 2097-2100). IEEE.

Zhao, H., Tanikawa, Y., Gao, F., Onodera, Y., Sassaroli, A., Tanaka, K., & Yamada, Y. (2002). Maps of optical differential pathlength factor of human adult forehead, somatosensory motor and occipital regions at multi-wavelengths in NIR. *Physics in Medicine & Biology*, *47*(12), 2075.

Zhou, X., Sobczak, G., McKay, C. M., & Litovsky, R. Y. (2020). Comparing fNIRS signal qualities between approaches with and without short channels. *Plos one*, *15*(12), e0244186.

Zimmermann, R., Marchal-Crespo, L., Edelmann, J., Lambercy, O., Fluet, M. C., Riener, R., ... & Gassert, R. (2013). Detection of motor execution using a hybrid fNIRS-biosignal BCI: a feasibility study. *Journal of neuroengineering and rehabilitation*, *10*(1), 4.

Appendices

Appendix A

Table 1: Processing Methodologies of Recent fNIRS Motor Control Studies

Author/Date	Equipment Hardware	Processing Software	Montage (ROIs)	Participant Demographics	Task (s)	Processing Techniques	Reported HRFs?	Type of task
Amemiya et al. 2010	Hitachi ETG-7000 Continuous wave	Not reported	4x4 optode arrangement, 24 channels located over bilateral pre-SMA, SMA, PMC, SMC, DLPFC	n = 33 (18F, avg age 21.4 yrs)	ME, MI, and control. ME - Finger tapping for 30s, alternated with 30s rest (counting task). MI – imagined finger-tapping for 30s, alternated with 30s rest (counting) Control – counting for 30s.	Applied moving average to data smoothing factor of 5	Yes	Finger tapping ME + MI
Anwar et al. 2013	Artinis Oxymon Mk-III Continuous wave	Not reported	15 channels located over contralateral MC, PMC, and PFC	n = 6 (5F, avg age 25 yrs)	Finger tapping (1 digit) – Repeated at 2-5 Hz for 30s, alternating with 30s rest. Finger tapping sequence (simple) – 30s of sequential tapping against the thumb alternated with 30s rest.	Bandpass filtered between 0.01-0.5 Hz, smoothed time series with window length of 25 points	No	Finger tapping ME
Anwar et al. 2016	Artinis Oxymon Mk-III Continuous wave	Not reported	15 channels located over SMC, PMC, and DLPFC	n = 9 (5F, avg age 27 yrs)	Finger tapping – Single digit tapping at 2-5 Hz for 30s, alternated with 30s rest. Simple sequence – Sequential finger tapping against the thumb for 30s alternated with 30s rest. Complex sequence – Sequential finger tapping against the thumb for 30s,	Removed mean time series from time series, no filtering applied	No	Finger tapping ME

					alternated with 30s rest.			
Asahara and Matsukawa 2018	Hamamatsu NIRO 200 Continuous wave	Not reported	Two channels located over bilateral PFC	n = 19 (7F, avg age 24 yrs)	Passive cycling for 1 minute with either both legs or 1 leg, performed at 35, 50, and 65 rpm.	Averaged data for every 5 seconds	Yes	Cycling
Asahara et al. 2018	Hamamatsu NIRO 200 Continuous wave	BIOPACK Systems	Two channels located over bilateral PFC	n = 13 (5F, avg age 25 yrs)	Active and passive one and two-legged cycling for 1 minute, and MI of active cycling for 1 minute, each trial separated by rest time of 5 minutes.	Sequentially averaged data for every 1 s	Yes	Cycling
Banville et al. 2017	NIRx NIRScout Continuous wave	HOMER2	60 channels located over frontal, central, temporal, and parietal lobes	n = 12 (5F, avg age 24.6 yrs)	Motor imagery of finger tapping for 15s, alternated with 10-15s of rest.	Bandpass filtered 0.8-1.2 Hz, rejected channels with nonsignificant correlation across all epochs, bandpass filtered again 0.01-0.3 Hz	Yes	Finger Tapping MI
Batula et al. 2017a	Hitachi ETG-4000 Continuous wave	Not reported	Two 3x3 arrays, 24 channels located over bilateral motor cortices (centered over Cz)	n = 13 (sex not reported, aged 18-35)	15s motor imagery or execution task of RH, RF, LH, LF, 4s rest after task.	Applied 20^{th}-order low-pass filter (FIR, 0.1 Hz), any channels with very high gain removed, CAR	Yes	U+L ME+MI
Batula et al. 2017b	Hitachi ETG-4000 Continuous wave	Not reported	2 3x3 arrays, 24 channels located over bilateral motor cortices (centered over Cz)	n = 13 (sex not reported, aged 18-35)	15s motor imagery or execution, with 4s rest. LH and RH clenching (ME or MI), LF and RF tapping (ME or MI), and rest.	100^{th} order low-pass FIR filter (0.1 Hz), CAR, CBSI	Yes	U+L ME+MI
Beurskens et al. 2014	NIRx DYNOT Continuous wave	NIRS-SPM	14 channels overlying the bilateral frontal lobe	N = 25, n_1 = 15 (sex not reported, avg age 24.5 ± 3.3 yrs) and n_2 = 10 (sex not reported, avg	NW + visual checking or alphabet recall demands (active 30s).	Visually inspected, applied moving standard deviation and spline interpolation, baseline-corrected, applied pre-coloring	Yes	Dual-task Walking

				age 71.0 ± 3.8 yrs)		filter, applied wavelet-MDL de-trending algorithm, applied wavelet transform		
Brigadoi et al. 2012	ISS Imagent Frequency domain	Not reported	10 channels located over bilateral M1 and SMA	n = 7 (0F, avg age 29.3 yrs)	1s or 3s finger tapping alternated with 15 s rest.	Applied bandpass filter (0.01-0.3 Hz), applied algorithm (Scarpa et al 2011) to reduce global physiological noise, applied non-parametric Bayesian approach (Scarpa et al 2010) to reduce further	Yes	Finger tapping ME
Bruno et al. 2018	NIRx NIRSport Continuous wave	HOMER2	40 channels located over bilateral parietal cortices and PFC	n = 21 (10F, avg age 23.48 yrs)	Driving (straight, turning) with congruent (normal steering), and incongruent (reversed steering) trials. Task was ~30s with ~14.5s "rest" (autonomous driving).	Applied motion artifact correction with wavelet filter, applied bandpass filter (0.01-0.5 Hz), applied GLM	Yes	Driving
Buccino et al. 2016	NIRx NIRScout Continuous wave	Not reported	34 channels located over bilateral motor cortices	n = 15 (0F, avg age 27.4 yrs)	R and L arm raising, R and L hand grasping for 6s, with 6s rest	Applied 4th order IIR Butterworth bandpass filter (0.01-0.2 Hz)	No	Arm task
Button et al. 2015	Hamamatsu NIRO-200 Continuous wave	MATLAB	1 channel located over right PFC	n = 32 (16F, aged 18-45 yrs)	Tread water for 150s, 60s rest OR 150s tread water and watch video + 120s swim at 60% V_{max} + swimming time at 90% $V_{max.}$	Applied moving average (5.0s)	No	Swimming
Chacaroun et al. 2019	Artinis Oxymon Mk-III Continuous wave	Not reported	Montage placed over left PFC	n = 21 (12F, avg age 29 yrs)	CL exercise (30 min) or HII exercise (15 1min exercise alternated with 1min rest).	Applied Gaussian smoothing algorithm (2s width)	No	Cycling

Chen et al. 2017	fNIR Devices fNIR Imager 1000 Continuous wave	Not reported	16 channels located over bilateral PFC	n = 90 (46F, avg age 78.1 yrs)	NW, WWT, ON + NW, or ON +WWT for 3 consecutive loops at their "normal pace".	Applied low-pass filter (FIR, 0.14 Hz)	No	Dual-task Walking
Choi et al. 2019	NIRx NIRScout Continuous wave	Not reported	31 channels located over bilateral M1, PMC, SMA, prefrontal, and somatosensory cortices	n = 18 (0F, avg age 25.3 yrs)	WBVe with 4 different conditions (0, 10, 20, 27 Hz vibration) while in a half-squat position for 30s alternated with 30s rest.	Applied low-pass filter (FIR, 0.2 Hz)	No	Balance task
Crivelli et al. 2018	NIRx NIRScout Continuous wave	Not reported	16 channels located over bilateral vPMC, and somatosensory cortices	n = 20 (10F, avg age 24.15 yrs)	Five conditions – OBS, LIS, OBS-LIS, EXE, EXE-LIS for 6s, alternated with 10s rest. Tasks were taken from a set of 22 transitive actions (ex. "light a lighter", "pour some wine").	Applied bandpass filter (0.01-0.3 Hz)	Yes	Upper Limb Tasks (22 actions)
De Lima Pardini et al. 2017	NIRx NIRSport Continuous wave	nirsLAB v201605	23 channels located over bilateral SMA	n = 8 (0F, avg age 23.63 yrs)	Single step with a walker and without for 2 s, alternated with rest of 10-13 s.	Downsampled (2 Hz), applied bandpass filter (FIR, 0.02-0.2 Hz), applied GLM (canonical boxcar function), applied precoloring	Yes	Walking
Derosiere et al. 2014	Artinis Oxymon Mk-III Continuous wave	Artinis Oxysoft	10 channels located over bilateral SM1 and rostral PFC	n = 15 (sex not reported, avg age 28 yrs)	Isometric handgrip at different levels of MVC (5, 10, 20, 30, 40, and 50% MVC) for 30s, alternated with 60s of rest.	Applied low-pass filter (0.7 Hz), detrended	No	Hand grasping/clenching ME
Dresler et al. 2011	Custom built Continuous wave	Not reported	22 channels located over right central sensorimotor areas	n = 6 (0F, avg age 29.6 yrs)	Dreamed hand clenching, 10 s LH alternated with 10 s RH, regular hand clenching, and imagined hand clenching.	Applied low-pass 3rd order Butterworth filter (0.3 Hz), applied GLM (canonical boxcar function, cosine-filter)	Yes	Dreamed Hand Clenching

Ferrari et al. 2014	Hamamatsu NIRO-200 Continuous wave	MATLAB	8 channels located over bilateral PFC	n = 22 (0F, avg age 26.5 yrs)	Balance (ITBBT or Constant TBBT) for 5 min, 2 min rest afterwards.	Detrended, applied low-pass filter (0.1 Hz)	No	Balance task
Fu et al. 2017	Hitachi ETG-4000 Continuous wave	NIRS-SPM	24 channels located over central and sensorimotor areas	n = 6 (3F, avg age 26.8 yrs)	Imagined hand clenching at different speeds (0.5, 1, and 2 Hz) and different forces (20, 50, and 80% MVGF) for 10s, alternated with 18-20s rest.	Applied low-pass filter (0.1 Hz), linearly detrended	Yes	Hand grasping/clenching MI
Funane et al. 2014	Hitachi ETG-7100 Continuous wave	Not reported	84 channels located over the left motor area	n = 14 (0F, avg age 40 yrs)	Finger-tapping task for 15s, alternated with 25s rest.	Applied low-pass filter (0.5 Hz), and high-pass filter (0.0125 Hz), applied Gaussian smoothing (FWHM: 2s)	Yes	Finger tapping ME
Gagnon et al. 2012	Techen CW6 Continuous wave	Not reported	21 channels located over the left motor cortex	n = 6 (sex not reported, age not reported)	Finger tapping for 30s, alternated with 30s rest.	Applied bandpass filter (0.01-1.25 Hz), applied Kalman filter to regress SS channels and recover HRF, applied Rauch-Tung-Striebel smoother, further applied low-pass filter (0.5 Hz), applied GLM	Yes	Finger tapping ME
Groff et al. 2019	Hitachi ETG-4000 Continuous wave	Not reported	4x4 array centered on Cz, 24 channels located over bilateral SMA, PreCG, PostCG, and SPL	n = 10 (4F, avg age 22.1 yrs)	Walking for 30s, alternated with 30s of rest (standing).	Applied moving average (5.0s), applied high-pass filter (0.01 Hz)	No	Walking
Harrison et al. 2018	Hitachi ETG-4000 Continuous wave	Not reported	4x4 centered over Cz, 16 channels located over bilateral motor and	n = 17 (7F, aged 19-36 yrs)	Finger tap/no-tap (30s task, 30s rest), self-paced finger tapping for 15 minutes, and coordinated finger	Applied moving average (5.0s), applied high-pass filter (0.01 Hz), applied PCA	No	Finger tapping ME

			sensorimotor cortices		tapping for 15 minutes.			
Heinze et al. 2019	NIRx NIRSport Continuous wave	nirsLAB v201605	20 channels located over bilateral PFC	n = 15 (5F, avg age 21.5 yrs)	Learning piano chords for 30s, alternated with 22s of rest.	Applied bandpass filter (0.01-0.2 Hz)	Yes	Learning Piano Chords
Herold et al. 2017	Hitachi ETG-4000 Continuous wave	Device-intern software	4x4 array overlying bilateral SMA, PreCG, and Post-CG	n = 10 (sex not reported, aged 21-47 yrs)	Standing and balance on board task (active 30s, rest 30s).	Applied a moving average (5.0 s), applied low-pass filter (0.5 Hz)	No	Balance task
Herold et al. 2019	NIRx NIRSport Continuous wave	HOMER2	10 channels located over bilateral PFC, PMC, and SMA	n = 13 (sex not reported, age not reported)	Walking for 40s, alternated with rest (standing) for 40s.	Applied wavelet (IQR = 1.219) and bandpass filters (0.01-0.5 Hz)	No	Walking
Holper and Wolf 2010	MCP-II (custom built) Continuous wave	MATLAB	10 channels located over left primary motor cortex	n = 15 (9F, avg age 29 yrs)	Motor imagery (with (positive or negative) and without feedback) for 20s, or finger tapping for 20s, alternated with 20s rest.	Applied low-pass filter (0.1 Hz), smoothed with 1st order Savitzky-Golay filter (501 points)	No	Finger tapping ME + MI
Holper and Wolf 2011	Custom built wireless miniaturized NIRS Continuous wave	MATLAB	4 channels located over left PMC and SMA, centered over F3	n = 12 (6F, avg age 29 yrs)	Simple finger tapping (pressing '0' key) or complex finger tapping (finger tapping sequence), or imagined finger tapping (MI-simple, MI-complex) for 15s, alternated with 20s rest.	Applied low-pass 7th order Chebyshew filter (20dB attenuation @ 5 Hz), downsampled to 10 Hz	Yes	Finger tapping ME + MI
Holper et al. 2010	Custom built wireless miniaturized NIRS Continuous wave	MATLAB	4/8 channels located over either contralateral (unilateral group) or bilateral (bilateral group) secondary motor areas,	n = 23 (sex not reported, age not reported)	RH OBS, RH OBS + MI, MI, or IM of ball-catching for 20s alternated with 30s rest.	Applied low-pass 7th order Chebyshew filter (20dB attenuation @ 5 Hz), downsampled to 10 Hz	Yes	Observation/VR/VMT + MI

			centered over F3/F4					
Holper et al. 2012	Custom built wireless miniaturized NIRS Continuous wave	MATLAB	4/8 channels located over bilateral secondary motor areas (PMC, SMA), centered over F3/F4	n = 17 (10F, avg age 25.6 yrs)	IM ball grasping, mirrored IM, MI + OBS, or MI + OBS mirrored for 15s, alternated with 20s rest.	Applied low-pass 7th order Chebyshew filter (20dB attenuation @ 5 Hz), downsampled to 10 Hz, applied spline interpolation for motion artifacts	No	Observation/VR/VMT + MI
Holper et al. 2014	Custom built wireless miniaturized NIRS Continuous wave	MATLAB	4 channels located over right PMC	n = 17 (7F, avg age 30.7 yrs)	Finger tapping for 10s, alternated with rest of 10-12s.	Applied low-pass 7th order Chebyshew filter (20dB attenuation @ 5 Hz), downsampled to 10 Hz, applied spline interpolation for motion artifacts	No	Finger tapping ME
Holtzer et al. 2011	Drexel custom built fNIRS sensor Continuous wave	Not reported	16 channels located over bilateral PFC	N = 22, n_1 = 11 older adults (7F, aged 69-88 yrs) and n_2 = 11 younger adults (7F, aged 19-29 yrs)	NW (15 ft), WWT (15 ft) – minimum time was ~3.5-4 s for task.	Applied low-pass filter (FIR, 0.14 Hz), applied combined ICA/PCA	No	Dual-task Walking
Holtzer et al. 2017	fNIRS Devices fNIRS Imager 1000 Continuous wave	Not reported	4x10 overlying bilateral PFC	n = 314 (56F, avg age 76.8 ± 6.7 yrs)	Continuous straight walks under NW and WWT conditions (3 loops around track, 30s active dual task).	Visually inspected, applied low-pass filter (FIR, 0.14 Hz)	Yes	Dual-task Walking
Holtzer et al. 2019	fNIRS Devices fNIRS Imager 1100 Continuous wave	Not reported	4x10 overlying bilateral PFC	N = 75, n_1 = 19 with fear of falling (13F, avg age 79.84 ± 6.01 yrs) and n_2 = 56 without fear of falling (25F, avg age 76.73 ± 6.39 yrs)	NW and WWT (alphabet recital) for 3 loops around track (30s active dual task).	Visually inspected, applied low-pass filter (FIR, 0.14 Hz)	No	Dual-task Walking

Hong and Naseer 2016	NIRx DYNOT Continuous wave	Not reported	12 channels located over left MC	n = 2 (0F, age not reported)	RH clenching for 20s, rest for 1min.	Applied low-pass filter (0.3 Hz), applied high-pass filter (0.01 Hz)	Yes	Hand grasping/clenching ME
Hu et al. 2013	NIRx DYNOT Continuous wave	MATLAB	34 channels located over bilateral motor cortices (centered over Cz)	n = 5 (0F, aged 24-31 yrs)	Finger tapping for 24s, alternating with 20s rest.	Applied bandpass filter (0.01-0.08 Hz, Butterworth), applied GLM	Yes	Finger tapping ME
Huppert et al. 2013	Techen CW6 Continuous wave	MATLAB	15 channels located over left prefrontal, frontal, motor, peri-insular vestibular and premotor cortices	n = 10 (5F, aged 21-47 yrs)	Stepping in response to a directional cue, 4-8s rest between steps.	Applied GLM (canonical gamma functions, discrete cosine transform (0-1/120 Hz)), prewhitened data (2^{nd} order autoregressive)	Yes	Walking
Ishii et al. 2018	Shimadzu FOIRE Continuous wave	Not reported	44 channels located over bilateral frontal, and frontoparietal areas (MC, somatosensory, SMA, PM, PFC)	n = 22 (11F, avg age 25 yrs)	Voluntary (30 or 60% MVC) or passive one arm cranking exercise for 1 min.	Downsampled to 1Hz, block averaged trials	Yes	Arm task
Jang et al. 2014	Shimadzu FOIRE-3000 Continuous wave	NIRS-SPM	49 channels located over bilateral (but mostly left) frontal and frontoparietal areas (MC, somatosensory, SMA, PM, PFC)	n = 12 (5F, avg age 29 yrs)	RH grasping movements for 20s, alternated with 20s rest, pre- and post-NMES.	Applied Gaussian smoothing (FWHM = 2s), applied wavelet-MDL based detrending, applied GLM (canonical HRF)	Yes	Hand grasping/clenching ME
Jin et al. 2018	Shimadzu FOIRE-3000 Continuous wave	Not reported	22 channels located over bilateral PFC, FEC, PMC, SMA	n = 22 (5F, avg age 22 yrs)	Walking with 3 conditions – SL, SM, + ML, alternated with rest for 30s.	Applied wavelet decomposition	No	Walking
Karim et al. 2012	Techen CW6	MATLAB	32 channels located over	n = 9 (4F, aged 18-42 yrs)	Wii balance board task for 37.6s	Applied GLM (canonical boxcar	Yes	Balance task

	Continuous wave		bilateral PFC, frontal cortex, and STG		(beginner), 63.1s (advanced), alternated with 30s rest.	function, discrete cosine transform 0-1/120 Hz), prewhitening (2nd order autoregressive)		
Khan et al. 2018	NIRx DYNOT Continuous wave	NIRS-SPM	12 channels located over left motor cortex	n = 9(0F, avg age 30 yrs)	Walking for 10s, alternated with 20s rest.	Applied low-pass filter (0.5 Hz), applied high-pass filter (0.01 Hz), compared different filters (Butterworth, Kalman, HRF, FIR, Wiener, Gaussian)	No	Walking
Kim et al. 2017	Shimadzu LABNIRS Continuous wave	NIRS-SPM	31 channels located over bilateral PFC, SMA, PMC, SMC, and SAC	n = 1 (1F, aged 30 yrs)	Walking at different speeds (1.5, 2, 2.5, and 3 km/h) for 30s, alternated with 30s rest.	Applied Gaussian smoothing (FWHM = 2s), used wavelet detrending for motion artifacts, applied GLM (canonical)	No	Walking
Kobashi et al. 2012	Custom built miniaturized wireless fNIRS sensor Continuous wave	MATLAB	Centered on F3/F4, 8 channels located over bilateral secondary motor areas including PMC	n = 12 (13F, avg age 25.6 yrs)	MI + OBS of ball-grasping, or IM of ball-grasping, in both first-person and mirrored views for 15s, alternated with 20s rest.	Applied spline interpolation to reduce motion artifacts, low-pass filter (7th order Chebyshew with 20dB attenuation @ 5 Hz), downsamples to 10 Hz	Yes	Observation/VR/VMT + MI
Koehler et al. 2012	Hitachi ETG-4000 Continuous wave	MATLAB	3x11 array, 52 channels located over left frontal, central, and parietal areas	n = 39 (25F, avg age 21.8 yrs)	ME or OBS (allocentric or egocentric) of a table-setting task for 12s, alternated with12s of rest.	Applied moving average (5s)	Yes	Observation/VR/VMT ME
Koenraadt et al. 2012	Artinis Oxymon Continuous wave	Oxymon software	8 channels located over left motor cortex	n = 13 (11F, avg age 24 yrs)	Hand and foot rhythmic and discrete movements for 20s, alternated with 20-30s of rest.	Applied low-pass filter (Butterworth, 1 Hz)	No	Hand + Foot Tapping
Koenraadt et al. 2013	Artinis Oxymon Mk-III	Not reported	8 channels located over left motor cortex	n = 11 (9F, avg age 30 yrs)	Hand tapping at different frequencies	Applied low-pass filter (2nd order Butterworth, 1 Hz)	No	Finger tapping ME

	Continuous wave				for 25-35s, alternated with rest for 25-35s.			
Koenraadt et al. 2014	Artinis Oxymon Continuous wave	Oxymon software	9 channels located over left sensorimotor cortex, SMA, and prefrontal cortex	n = 11 (8F, avg age 23 yrs)	Walking or precision stepping for 35s, alternated with rest for 25-35s.	Applied low-pass filter (2^{nd} order Butterworth, 1.25 Hz), applied high-pass filter (2^{nd} order Butterworth, 0.01 Hz), regressed SS channels, applied low-pass filter again (2^{nd} order Butterworth, 1 Hz)	Yes	Walking
Koren et al. 2019	Artinis PortaLight Continuous wave	HOMER2	6 channels located over bilateral PFC	n = 20 (sex not reported, aged 18-30 yrs)	Walking (ON or NW) around 20m long course, alternating with 30s rest.	Applied spline interpolation to correct motion artifacts (p = 0.99), applied wavelet correction as needed for motion artifacts (IQR = 0.1), applied bandpass filter (0.01-0.2 Hz)	Yes	Obstacle Negotiation
Kurz et al. 2012	Hitachi ETG-4000 Continuous wave	Not reported	24 channels located over medial aspects of M1, SMA, and paracentral lobule	n = 13 (sex not reported, avg age 23.7 yrs)	Walking at 0.45 m/s for 30s, alternated with rest for 30s.	Applied high-pass filter (0.01 Hz), applied 5s moving average, applied PCA on all channels	Yes	Walking
Lachert et al. 2017	Custom built fNIRS sensor Time domain	Not reported	8 channels located over bilateral motor cortices	n = 10 (5F, avg age 28.1 yrs)	Tapping a computer mouse for 20s, alternated with 30s rest.	Detrended via linear approximation, smoothed with a moving average (10 points), applied low-pass filter (0.4 Hz)	Yes	Finger tapping ME
Lin et al. 2012	ISS Imagent Frequency domain	HOMER	20 channels located over bilateral SMC, SMA, and PMC	N = 25, n_1 = 12 younger (4F, avg age 23.4 yrs) and n_2 = 13 elderly (6F, avg age 67.6 yrs)	Cycling for 20s, alternated with 30s rest	Applied 3^{rd} order IIR Butterworth bandpass filter (0.002-0.5 Hz), applied PCA	No	Cycling
Lin et al. 2016	ISS Imagent	HOMER	20 channels located over	n = 19 (0F, avg age 23.7 yrs)	Knee extension tasks (VOL, ES, HA @ 10,	Applied 3^{rd} order IIR Butterworth	Yes	Knee Extension

	Frequency domain		bilateral SMC, and PMC		30, and 50 mA) for 20s, alternated with 30s of rest.	bandpass filter (0.0016-0.8 Hz)		
Lu et al. 2013	NIRx DYNOT Continuous wave	NAVI (NIRx)	5x6 array, located over left SMC	n = 10 (5F, avg age 22.7 yrs)	Hand grasping for 20s, alternated with 20s rest.	Applied low-pass filter (0.5 Hz), applied GLM	Yes	Hand grasping/clenching ME
Lu et al. 2015	NIRx NIRSport Continuous wave	HOMER2	14 channels located over bilateral PFC, PMC, and SMA	n = 17 (8F, avg age 23.1 yrs)	NW, WCT, or WMT for 60s, alternated with 60s rest.	Applied bandpass filter (0.01-0.2 Hz), applied PCA and spike rejection	Yes	Dual-task Walking
Lu et al. 2017	Techen CW6 Continuous wave	HOMER2	13 channels located over right motor cortex, PMC, PFC, and SMA	n = 29 (15F, avg age 24.2 yrs)	Serial finger-tapping for 5s, alternated with 4.9s of rest.	Applied bandpass filter (0.1-0.8 Hz)	Yes	Finger tapping ME
Lucas et al. 2019	fNIRS Devices fNIRS Imager 1000 Continuous wave	Not reported	4x10 overlying bilateral PFC	n = 55 (27F, avg age 74.76 yrs)	Continuous straight walks under NW or WWT conditions (3 loops around track).	Visually inspected, applied low-pass filter (0.14 Hz)	Yes	Dual-task Walking
Maidan et al. 2018	Artinis PortaLite Continuous wave	MATLAB	6 channels located over bilateral DLPFC, and anterior PFC	n = 20 (sex not reported, aged 20-50 yrs)	ON while walking along a 50m elliptical pathway, alternated with 20s rest.	Applied bandpass (0.01-0.14 Hz), applied wavelet filter, applied CBSI	Yes	Obstacle Negotiation
Mandrick et al. 2013	Hamamatsu NIRO-300 Continuous wave	MATLAB	PFC (at the midpoint between Fp2-F4)	n = 15 (0F, avg age 28.3 ± 6 yrs)	Grasping tasks with non-dominant hand. 60s at two submaximal workloads (15% and 30% MVC).	Applied low-pass filter (0.1 Hz), utilized time series analysis technique (amplitude-based approach)	Yes	Hand grasping/clenching ME
Mehnert et al. 2013	NIRx NIRScout Continuous wave	MATLAB	16x16 overlying bilateral occipito-parietal and precentral areas	n = 20 (5F, avg age 27.7 yrs)	Normal or mirrored finger movements (80 trials per hand, 15s active, 10s rest).	Linearly interpolated data to correct for motion artifacts, applied 3rd order Butterworth band-pass filter (0.016-0.2 Hz),	Yes	Hand/finger movements ME

						applied GLM		
Mehta and Rhee 2017	TechEn CW6 Continuous wave	HOMER2	PFC (Fp1 and Fp2)	n = 9 (6F, aged 65 yrs or older) n = 10 (6F, aged 20–35 yrs)	6 arm force control trials, (10s at 30% MVC, 20s rest).	Applied low-pass filter (3 Hz), used wavelet-based method (1.5 IQR), applied low-pass filter again (0.5 Hz), applied high-pass filter (0.016 Hz)	No	Arm task
Metzger et al. 2017	Hitachi ETG-4000 Continuous wave	MATLAB	Frontal, temporal and parietal cortex of both hemispheres using two large 4x4 probe-sets with 24 channels	n = 12 (8F, avg age 27.6 yrs)	NW at 3km/h or 5km/hr for 45s, rest 15 s, as well as a WWT condition.	Applied moving average within a time window of five seconds, baseline corrected (10s), linear fit (consisting of 10-s baseline, 45-s activation task, and 15-s rest), applied CBSI	Yes	Dual-task Walking
Mirelman et al. 2014	Artinis system Continuous wave	Not reported	Two separate pairs of NIRS probes each 6 channels overlying left (Fp1) and right (Fp2)	n = 23 (13F, avg age 30.9 ± 3.7 yrs)	Speed walking while counting forward, walking while serially subtracting or standing while serially subtracting (30 m walking, 20 s rest).	Applied low-pass filter with a finite impulse response filter (0.14 Hz), applied Continuous Wavelet transform	Yes	Dual-task Walking
Mirelman et al. 2017	Artinis PortaLite Continuous wave	MATLAB	Two probes overlying left and right Brodmann's areas 10, the dorsolateral and anterior prefrontal cortex (PFC)	N = 43, n_1 = 23 young adults (13F, avg age 30.9 ± 3.7 yrs) and n_2 = 20 older adults (10F, avg age 69.7 ± 5.8 yrs)	Walking at self-selected comfortable speed, walking while serially subtracting, and NW + ON (30 s active, 20 s rest).	Applied bandpass filter (0.01–0.14 Hz), applied wavelet filter, applied CBSI	No	Dual-task Walking
Moro et al. 2016	Artinis Oxymon Mk-III Continuous wave	HOMER2	20 channels located over bilateral DLPFC, frontopolar cortex, VLPFC	n = 21 (0F, avg age 26.1 yrs)	2 min VMT, with baseline and rest of 1 min. VMT was moving a virtual sphere over a virtual path.	Applied wavelet filter (iqr = 1) for motion artifact correction, applied a deconvolution GLM (temporal basis =	Yes	Observation/VR/VMT ME

						gaussian (2s apart, SD = 3s)) which also used SS channels to regress physiological signal, then IWLS method to solve GLM		
Muthalib et al. 2015	Custom built Time domain	NIRS-SPM	Full topographic map from 32 optical channels	n = 9 (0F, avg age 39.2 ± 13 yrs)	10 voluntary wrist extension contractions (active 1s, rest 1s).	Applied GLM (gamma functions), detrending filter (Wavelet-MDL), and Time series (O2Hb or HHb time course) modeled as a linear combination of L regressors	No	Wrist Extension ME
Muthalib et al. 2016	Artinis Oxymon MkIII Continuous wave	Not reported	12x4 (16 channels) overlying left and right SMC	n = 8 (sex not reported, avg age 30.4 ± 10.6 yrs)	Finger tapping task with RH or LH (active 30s, rest 30s), before (Pre), during (Online), and after (Offline) anodal HD-tDCS (2 mA, 20 min) targeting left SMC.	Applied low-pass filter (0.1 Hz), baseline corrected (last 5 seconds of rest), sample-to-sample averaged (10 samples/s)	Yes	Finger tapping ME
Muthalib et al. 2018	Artinis Oxymon Mk III Continuous wave	Not reported	8x2 overlying bilateral SMC	n = 8 (0F, avg age 25.9 ± 4.3 yrs)	NMES evoked wrist extension and voluntary wrist extension (10 blocks of 10 wrist extensions, 1s active, 1s rest).	Applied low-pass filter (0.1 Hz), visually inspected	Yes	Wrist Extension ME
Naseer and Hong 2013	NIRx DYNOT Continuous wave	Not reported	12x12 (17 channels each hemisphere) overlying left and right primary motor cortices	n = 10 (0F, avg age 28.5 ± 4.8 yrs)	MI for LW or RW upwards 4 or 5 times (10s active, 20s rest).	Baseline corrected, applied low-pass filter using 4th order Butterworth filter (0.1 Hz)	Yes	Wrist Extension MI
Pfurtscheller et al. 2011	Custom built Continuous wave	Not reported	1x1 overlying frontal cortex (FP1)	n = 26 (14F, avg age 23 ± 2.8 yrs)	Finger movements (active 40 s, rest 5 min).	Applied 5th-order Butterworth filter (0.9 Hz)	No	Hand/finger movements ME

Pittaccio et al. 2013	Commercial fNIRS device Continuous wave	Not reported	32 channels overlying the motor and somatosensory brain areas	n = 2 (0F, avg age 32 ± 7.1 yrs)	Active, passive, and assisted foot dorsiflexion conditions (5min. each, 7s of dorsiflexion, 30s of rest).	Visually inspected, applied low pass filter (0.030 Hz), segmented continuous tracks into epochs, applied GLM	No	Ankle Dorsiflexion
Propper et al. 2017	Biopac Systems fNIR400 Continuous wave	Not reported	16 channels overlying left and right dorsolateral prefrontal cortex	n = 39 (0F, ages not reported)	Sustained unilateral hand clenching (active 30s, rest 20s).	Applied finite impulse response filter, applied cut-off between 400 mV - 4000 mV	No	Hand grasping/clenching ME
Rosner and Barlow 2016	TechEn CW6 Continuous wave	HOMER2	4x12 overlying face and hand sensorimotor cortices	n = 22 (17F, avg age 23.16 ± 1.76 yrs)	Repetitive hand grip task at 10% MVC (20s active, 20s rest).	Applied low-pass filter (0.3 Hz), applied automated detection algorithm based on standard deviation, block averaged from -10s to +30s	Yes	Hand grasping/clenching ME
Rosso et al. 2017	TechEn CW6 Continuous wave	Not reported	15x15 overlying the prefrontal, temporal, and motor cortices of the left hemisphere	N = 16, n_1 = 10 (7F, aged 66–81 yrs), n_2 = 6 (2F, aged 22–30 yrs)	Balance task on a dynamic posturography platform, auditory choice reaction time task while seated, and postural control with attention tasks (active 121s, rest 30s).	Applied GLM (canonical)	Yes	Balance task
Sagari et al. 2015	Hitachi ETG-4000 Continuous wave	Not reported	24 channels overlying right and left PFC, presupplementary motor area, supplementary motor area, dorsal premotor cortex, and sensorimotor cortex	n = 20 (11F, avg age 27.5 ± 5.5 yrs)	Character entry into a touch-screen terminal (active 15s, rest 25s).	Applied moving average (window: 5 s), analyzed in integral mode	No	Character Entry

Schurholz et al. 2012	Shimadzu FOIRE-3000 Continuous wave	NIRS-SPM	4x4 overlying bilateral motor cortex, primary motor cortex, premotor cortex and somatosensory cortex	n = 8 (6F, avg age 24.8±2.4 yrs)	RH MI, or passive RH movement by FES (active 10s).	Detrended (of global trends and of noise components) using wavelet-MDL, utilized precoloring	No	Wrist Flexion/Extension MI
Seidel et al. 2017	NIRx NIRSport Continuous wave	nirsLAB	15 optodes overlying the sensorimotor system	n = 43 (20F, avg age 25 yrs)	Static balance task (20s rest), MBT training 20 min	Signal quality checked by CV (15% cutoff) applied baseline correction (10s of rest), applied bandpass filter (0.01 Hz to 0.2 Hz), applied time series analysis, applied GLM	No	Balance task
Seidel et al. 2019	NIRx NIRSport Continuous wave	HOMER2	15 optodes overlying bilateral sensorimotor system	n = 42 (16F, avg age 26.81 yrs)	Cycled five trials at 20, 40, and 60% PPO (active 30 s)	Signal quality checked by CV (15% cutoff), applied wavelet filtering (1.219 IQR), applied band-pass filter (0.01-0.5 Hz), applied short separation regression	No	Cycling
Shibuya 2011	Hamamatsu NIRO-300L Continuous wave	Not reported	Overlying the C3 and C4 hand motor areas	n = 12 (0F, avg age 24.08 ± 0.18 yrs)	5 sets static-handgrip at 60% MVC (active 10s, rest 75s)	Baseline corrected (30s), applied high-pass filter (0.02 Hz)	Yes	Hand grasping/clenching ME
Shibuya et al. 2014	NIRS: NIRO-300L Continuous wave	Chart software	Overlying M1 areas of both hemispheres	n = 10 (0F, avg age 21.1 ± 0.84 yrs)	Unilateral finger movement task at 20, 40, and 60% MVC (10s active)	Applied visual inspection, applied low-pass filter (0.7 Hz), baseline corrected (60s)	Yes	Hand/finger movements ME

Shibuya et al. 2016	Shimadzu NIRStation OMM3000 Continuous wave	Not reported	Overlying M1 areas of both hemispheres	n = 10 (0F, avg age 22.2 ± 0.2 yrs)	Handgrip task at 30-60% MVC (active 180s)	Applied CAR, projected onto CSP	Yes	Hand grasping/clenching ME
Shin et al. 2014	Custom built Continuous wave	Not reported	8 channels overlying bilateral M1	n = 8 (1F, avg age 26.8 ± 1.6 yrs)	L and R arm lifting and knee extension with various active and rest periods	Normalized, applied zero-phase distortion filter (third-order Chebyshev I with a ripple factor of 0.5 dB; 0.03-0.07 Hz), applied CBSI, applied third-order Savitzky–Golay smoothing filter	Yes	Arm Lifting + Knee Extension
Stuart et al. 2019	Shimadzu LABNIRS Continuous wave	NIRS-SPM	Overlying bilateral frontal lobes	N = 35, n_1 = 17 (9F, avg age 20.3 ± 1.2 yrs), n_2 = 18 (9F, avg age 72.6 ± 8.0 yrs)	Single and dual-task conditions (active 30s, rest 30s). Standing or NW on a treadmill, or WCT.	Applied low-pass filter (0.15 Hz), applied wavelet-minimum description length algorithm, applied baseline correction	No	Dual-task Walking
Tempest et al. 2019	NIRx NIRSport Continuous wave	HOMER2	16x16 overlying prefrontal, parietal, and motor regions	n = 13 (7F, avg age 29.8 ± 3.9 yrs)	Handgrip squeezing (active 10s, rest 20s).	Pruned channels with poor signal quality, applied wavelet-based motion correction, applied bandpass filter (0.01-0.5 Hz), applied GLM	No	Hand grasping/clenching ME
Vasta et al. 2017	Hitachi ETG-4000 Continuous wave	NIRS-SPM	22 channels overlying premotor cortex, primary motor cortex and the supplementary motor area	n = 11 (5F, aged 27–64 yrs)	Hand MTA tasks (60s active, 60s rest).	Applied visual inspection, applied moving average with a window width of 5 s, applied bandpass filter (0.005-0.5 Hz)	No	Hand/finger movements ME
Waldert et al. 2012	NIRx DYNOT-932	Not reported	23 detectors and 9 sources overlying C3 and C4	n = 17 (7F, avg age 26.8 ± 5.6 yrs)	Periodic (0.25 Hz) hand movements causing the finger tips to alternate	Applied low-pass filter using a 3rd order Butterworth filter, applied	Yes	Hand/finger movements ME

	Continuous wave				between the outer and home position for 10s in each trial	acausal filtering (zero phase shift) with 0.12 Hz cutoff		
Willis et al. 2019	Artinis PortaLite Continuous wave	Not reported	Overlying prefrontal cortex	n = 7 (2F, avg age 26.6 ± 2.9 yrs)	Maximal sprints (active 10s, rest 20s).	Applied fourth-order low-pass zero-phase Butter-worth filter (0.2 Hz)	No	Sprinting
Wolf et al. 2011	Omnia ISS Frequency domain	Not reported	10 channels overlying dominant motor area for each individual	n = 12 (1F, avg age 28.8 ± 12.7 yrs)	Palm-squeezing (active 21s or 10s, rest 20s or 17s).	Applied DPF-method, applied low-pass filter (0.1 Hz)	No	Hand grasping/clenching ME
Woorons et al. 2019	Artinis PortaLite Continuous wave	Not reported	Overlying left prefrontal cortex	n = 10 (3F, avg age 19.2 ± 2.3 yrs)	Back-and-forth sprints at maximal velocity (active 6s).	Applied low-pass filter (0.1 Hz)	Yes	Sprinting
Wriessnegger et al. 2017	NIRx NIRScout Continuous wave	MATLAB	61 channels overlying parietal and motor cortical areas	n = 13 (5F, avg age 25 ± 3 yrs)	ME or MI hand grip task (active 10s, 10-14 rest).	Applied visual inspection, applied high pass filter (0.01 Hz), applied low pass filter (0.8 Hz), utilized TF models	Yes	Hand grasping/clenching ME + MI
Wriessnegger et al. 2018	NIRx NIRScout Continuous wave	MATLAB	61 channels overlying frontal left, central left, parietal left, frontal right, central right parietal right brain regions	n = 20 (10F, avg age 24.8 ± 2.5 yrs)	MI of hand squeezing (active 10s).	Applied visual inspection, applied high pass filter (0.01 Hz), applied low pass filter (0.8 Hz), utilized TF models, applied spatial smoothing	No	Hand grasping/clenching MI
Yeo et al. 2013	Shimadzu FOIRE-3000 Continuous wave	NIRS-SPM	49 channels overlying primary sensory-motor cortex, premotor cortex, and prefrontal cortex	n = 9 (2F, avg age 27.4 ± 3.2 yrs)	Flexion-extension movements of the right shoulder or hand (active 30s, rest 60s).	Applied Gaussian smoothing (FWHM = 2s), applied wavelet-MDL based detrending algorithm	No	Arm task

Yin et al. 2015	Hitachi ETG-4000 Continuous wave	Not reported	24 channels overlying primary motor area and the supplementary motor area	n = 6 (3F, avg age 26.8 ± 3.3 yrs)	Hand clenching MI speed task and hand clenching force task.	Applied linear-detrending filter, applied low-pass 5th-order Chebyshev II filter (0.1 Hz), downsampled to 1 Hz	Yes	Hand grasping/clenching ME + MI
Yokoyama et al. 2019	Shimadzu FOIRE-3000 Continuous wave	Not reported	31 channels overlying PM, M1, and PPC of both hemispheres	n = 20 (20F, avg age 21.6 yrs)	Hand grip task (active 10s).	Applied moving average (smoothing factor of 25 points), applied baseline normalization (-5s to 0s)	Yes	Hand grasping/clenching ME
Yozu et al. 2016	Hitachi ETG-4000 Continuous wave	Not reported	24 channels overlying Fz	n = 10 (5F, avg age 32.0 ± 7.7 yrs)	Hand-knee quadrupedal crawling, upright quadrupedal using crutches and typical upright bipedalism (active 30s, rest 40s).	Applied baseline drift correction, applied first-degree baseline fit, averaged across channels over SMA	Yes	Quadrapedalism + Walking
Yu et al. 2014	NIRx DYNOT Continuous wave	NIRS-SPM	122 channels located over bilateral primary motor, and somatosensory cortices	n = 8 (sex not reported, age not reported)	Hand grasping MI or passive hand movement (active 5s), alternated with 10s rest.	Applied low-pass filter, applied GLM	Yes	Hand grasping/clenching MI
Zimmermann et al. 2013	ISS Oxiplex TS Continuous wave	Not reported	Two probes overlying left M1 and left PMv	n = 7 (1F, avg age 26.0 ± 2.2 yrs)	Finger pinching task (active 20s, rest 15 to 24 s).	Downsampled to 5 Hz, applied 5-point median filter, used inverse z-score of the raw intensity signals to identify MA	Yes	Hand/finger movements ME